Jessica de Jonge - 4021878

Heave reduction of the crane tip of a J-class vessel by inducing a roll moment using active ballast systems

TUDelft

This page is intentionally left blank.

Master Thesis Maritime Technology

In partial fulfilment of obtaining the degree of Master of Science
at the Delft University of Technology

Heave reduction of the crane tip of a J-class vessel by inducing a roll moment using active ballast systems

By

Jessica de Jonge

4021878

Graduation date	: February 6th, 2017
Student number	: 4021878
Professor	: Prof. Dr. Ir. R.H.M. Huijsmans
Daily company supervisor	: Ir. K.T. van der Heiden
TU Delft supervisor	: Dr. Ing. C.H. Thill
Committee member	: Ir. K. Visser

A digital version of this thesis is available at http://repository.tudelft.nl/

This page is intentionally left blank.

Preface

This report is written to represent the research done for the MSc Thesis of the Master of Maritime Technology at the Technical University of Delft, in order to obtain the degree of Master of Science. This research was provided by, and done in collaboration with Jumbo, located in Schiedam, The Netherlands.

I would like to take the opportunity to thank Jumbo for the possibility to graduate at the company, as well as the opportunity to start a student job there 7 years ago when I was at the start of the Bachelor study of Maritime Technology. I got to know the company quite well, for which I would like to thank those who showed me around the company throughout all these years. I would like to thank my supervisor, Kasper van der Heiden, for providing me with the interesting graduation subject, as well as the possibility (and budget) to do model tests (although these did not entirely go as planned). I would also like to thank Jasper van den Broek, who has provided me with the necessary data when I would need something. Furthermore, I would like to thank former colleagues Sander van der Vooren and Eveline Dijkers, who have given me lots of mental support at Jumbo.

Outside of Jumbo I would like to thank my TU Delft supervisor Cornel Thill, who was nearly always available to answer the many questions I had concerning model tests, and Vincent Wegener and Piet from the RDM Campus, who have helped me with the (preparations for the) model tests performed at the Aqualab. I would like to thank Monique Gazendam, secretary at the Maritime Technology department, for answering the enormous amount of questions concerning a graduation thesis, and my graduation professor René Huijsmans, for making me push hard to finish in time, but still continue to dig deeper into theory and execution.

Lastly, I would like to thank my mother and grandparents, my brothers, my friends, and especially Ruben and Jules for constantly supporting me during the project, and pushing me back up when I was at a low point because 'stuff just wouldn't work'.

Abstract

Jumbo is a shipping and offshore company, with nearly 50 years of operating their own fleet for transport and installation of heavy loads. Jumbo owns and operates in total 12 heavy lift vessels, amongst which two are equipped with offshore installation equipment such as DP2, a deep-water installation winch and two 900 tons Huisman cranes. Jumbo is already an experienced offshore installation contractor, but wishes to become even more competitive in an already competitive market.

One of the problems Jumbo encounters during offshore installation, is substantial heave amplitudes in swell waves, which reduces the workability of the vessels. The heave amplitudes of the vessel cause heaving of the load that must be installed in deep water. Too large heave amplitudes of the load cause the offshore operation to become difficult or not possible. To improve the workability of the vessels, the heave amplitude of the load must be reduced. Currently this is being done by installing a passive heave compensator between the hook of the crane and the load. This however comes with its downsides such as that it reduces the maximum load that can be installed. Therefore, a new concept for the compensation of the heave of the load is investigated in this research.

The heaving motion of the load is caused, amongst others, by the heave amplitude of the crane from which it hangs. It is believed that by reducing the vertical amplitude of the crane tip, the heave amplitude of the load will also reduce. The concept for the reduction of this heave amplitude of the crane tip, is by means of actively rolling the vessel, as the heave motion of an eccentric point on-board a vessel is a superposition of the heave, roll and pitch motions of a vessel.

To obtain a roll moment, active ballasting is investigated. From the existing active ballasting systems two concepts are chosen: displacing a solid mass transversely over the deck, and pumping ballast water from portside tanks to starboard tanks, and vice versa. Both systems tested at two different ballast velocities: the maximum velocity in which the COG of the mass can be displaced in y-direction.

To investigate the influence of these active ballast system on the motions of the vessel and the heave amplitude of the crane tip, a Simulink model is built. This model simulates a wave pattern in which the vessel is placed, calculates the responses of the vessel based on hydrodynamic coefficients obtained using Ansys AQWA, and calculates the motions of the crane tip. It then calculates how much roll the vessel must experience to compensate the vertical offset of the crane tip. This then is the input for the control system controlling the ballast system; it determines where the COG of the ballast must be, the size of the error between the current COG location and the necessary COG location, and acts accordingly by increasing or decreasing the ballasting speed. As such, a roll moment is induced by the ballast, rolling the vessel, and influencing the heave amplitude of the crane.

The simulations are performed for both regular waves, as well as JONSWAP wave spectra. The output of the model is processed by calculating the Fourier transforms to obtain the motion spectra. From this the significant heave amplitude of the crane tip can be calculated and compared to the significant heave amplitude of the crane tip without an active ballast system. This was done for waves with longer (peak) periods, as the main wave profile of importance were swell type waves.

The results from the simulations showed that all four ballast systems and settings decreased the significant heave amplitude of the crane tip. The ballast tanks showed averaged decreases over all scenarios up to 90% for the faster system, and over 65% for the slower system. The solid mass system showed averaged decreases, respectively. Comparing both systems at equal ballast velocity showed that the ballast tank outperformed the solid mass system, mainly due to the vertical location of the COG of the ballast.

From the results, it can be concluded that installing an active ballasting system will reduce the heave amplitude of the crane tip significant, improving the workability. From this research, it also can be concluded that a ballasting system which moves the COG of the ballast at a maximum velocity of 1 m/s transversely, is the most viable solution for further research and possible implementation.

Nomenclature

Abbreviations

AHC	Active heave compensator
ART	Anti roll tank
CFD	Computational fluid dynamics
COB	Centre of buoyancy
COG	Centre of gravity
CT	Crane Tip
DDS	Deepwater Deployment System
DOF	Degrees of freedom
DP	Dynamic Positioning
HLV	Heavy lift vessel
JONSWAP	Joint North Sea Wave Project
PHC	Passive heave compensator
RAO	Response amplitude operator
RMS	Root Mean Square

Greek symbols

γ	[-]	Peakedness factor of JONSWAP spectrum
ε_i	[rad]	Phase angle for motion i
ζ	[m]	Wave elevation
ζ_a	[m]	Wave amplitude
λ	[m]	Wave length
μ	[°]	Wave heading
ρ	[kg/m³]	Density
σ	[m]	RMS of wave elevation
ϕ_R	[rad]	Induced roll amplitude by the ballast
ϕ_n	[rad]	Necessary roll amplitude for heave reduction
$\phi(t), \dot{\phi}(t), \ddot{\phi}(t)$	[rad], [rad/s], [rad/s²]	Roll displacement, velocity, acceleration, at time t
$\theta(t), \dot{\theta}(t), \ddot{\theta}(t)$	[rad], [rad/s], [rad/s²]	Pitch displacement, velocity, acceleration, at time t
$\psi(t), \dot{\psi}(t), \ddot{\psi}(t)$	[rad], [rad/s], [rad/s²]	Yaw displacement, velocity, acceleration, at time t
ω	[rad/s]	Wave frequency
Φ	[-]	Total potential
Φ_d	[-]	Diffraction potential
Φ_r	[-]	Radiation potential
Φ_w	[-]	Wave velocity potential

Capital Latin symbols

A_{WL}	[m²]	Waterline area
$\overline{BM}$	[m]	Distance between COB and metacentre
$\overline{BN_\phi}$	[m]	$\overline{BM}$, corrected for roll
$\bar{F}$	[N]	Force vector
$\overline{GM_T}, \overline{GM_L}$	[m]	Transverse, and longitudinal metacentric height
$\overline{GN\phi}$	[m]	$\overline{GM}$, corrected for roll
H_s	[m]	Significant wave height
I_x, I_y, I_z	[kgm²]	Mass moment of inertia about the x-, y-, and z-axis
I_T	[m⁴]	Transverse area moment of inertia
$\overline{KB}$	[m]	Distance between keel and COB
$\overline{KG}$	[m]	Distance between keel and COG
$\bar{M}$	[N/m]	Moment vector
$S_\zeta(\omega), S_{x_i}(\omega)$	[m²s]	Wave, and motion spectrum
S_{WL}	[m²]	First order waterline moment
T	[s]	Period
T_p	[s]	Peak period

Small Latin symbols

$a_{i,j}$	[kg] or [kgm²]	Components of the added mass matrix
$b_{i,j}$	[kg/s] or kgm²/s]	Components of the damping matrix
$c_{i,j}$	[kg/s²] or [kgm²/s²]	Components of the hydrostatic matrix
d	[m]	Transverse ballast shift distance
g	[m/s²]	Gravitational acceleration
h	[m]	Water depth
k	[rad/m]	Wave number
k_{xx}, k_{yy}, k_{zz}	[m]	Radii of inertia about the x-, y-, and z-axis
$m_{i,j}$	[kg] or [kgm²]	Components of the mass matrix
m_0	[m²]	Area under spectral curve
t	[s]	Time
v	[m/s]	Velocity
x, y, z	[m]	Coordinates of a point
$x_{CT}(t), y_{CT}(t), z_{CT}(t)$	[m]	Surge, sway, heave amplitude of the crane tip, at time t
$x(t), \dot{x}(t), \ddot{x}(t)$	[m], [m/s], [m/s²]	Surge displacement, velocity, acceleration, at time t
$y(t), \dot{y}(t), \ddot{y}(t)$	[m], [m/s], [m/s²]	Sway displacement, velocity, acceleration, at time t
$z(t), \dot{z}(t), \ddot{z}(t)$	[m], [m/s], [m/s²]	Heave displacement, velocity, acceleration, at time t

Table of Contents

1 Introduction

The seas and oceans in our world harbour many discovered and undiscovered resources and usable features. One may think of subsea oil- and gas fields, but also thermal differences and heave currents. These are a few of many different approaches to extract energy from these waters. To do so, all sorts of equipment and structures need to be installed either on the surface, sub-surface or at the bottom of the ocean.

Jumbo is a Dutch company that owns and operates a fleet of twelve heavy lift vessels, of which two are outfitted with (amongst others) a dynamic positioning system (class 2, or DP-II). This makes these two vessels capable for offshore installation work, as for example the installation of subsea templates for oil- and gas field development. These vessels, the *HLV Fairplayer* and *HLV Jumbo Javelin*, have the possibility to install structures in a water depth up to 3,000 m with the help of the in-house developed Deepwater Deployment System (DDS). Appendix A gives the specifications of the *Fairplayer* concerning its offshore capabilities.

The offshore installation consists of a number of phases:

1) Loading of the offshore structure onto the vessel
2) Sailing to the installation site
3) Switching to dynamic positioning
4) Lifting the offshore structure from deck
5) Shifting the offshore structure from inboard to outboard
6) Lowering the offshore structure through the splash zone
7) Lowering the offshore structure towards the installation depth
8) Touch-down on the sea bottom
9) Unhooking of the load

Between these phases, other phases also could occur, for instance shifting loads on deck, or the transfer of loads from other floating objects.

Every phase has its own difficulties to overcome. The installation phases, phase 6 through 9, are the phases of focus in this report. This will be referred to as the (offshore) installation process.

1.1   Problem definition

During the offshore installation process of a structure, a vessel experiences many motions in all six degrees of freedom (DOF) due to being subjected to, amongst others, wave forces. Whereas in port the waves are shielded by quays and the motions of the vessel thus are very small, out on the ocean these waves (and therewith, motions) can become much larger.

The six DOFs in which a vessel can move, are visualised in Figure 1.1, and can be split up into translations and rotations about the x-, y- and z-axis of the ship-bound coordinate system. The origin is located in the ship's centre of gravity (COG). The coordinate system is described in the North-East-Down manner. This is the standard setting of the Simulink model that is used as a basis during the project. The translations in this project (in the time domain) are:

- Surge $(x(t))$: translation in x-direction   (positive when moving forward)
- Sway $(y(t))$: translation in y-direction   (positive when moving to starboard)
- Heave $(z(t))$: translation in z-direction   (positive when moving downward)

The rotations (in the time domain) are defined as:

- Roll $(\phi(t))$: rotation about the x-axis   (positive when rolling to starboard)
- Pitch $(\theta(t))$: rotation about the y-axis   (positive when bow pitching upward)
- Yaw $(\psi(t))$: rotation about the z-axis   (positive when turning to starboard)

The motions surge, sway and yaw are being compensated with help op the on-board DP-system. To compensate for the motions roll, pitch and heave other measures are to be taken, to keep these motions within set bounds. For example, to reduce the roll motions of a vessel, anti-roll systems can be installed.

One of the difficulties that occurs during the installation phase of an offshore structure, is heave. When an offshore structure is lifted overboard with an on-board crane, the motions of the vessel will have an influence on the motions of the load in the crane. When the load is lowered to the seabed, the vessel motions may cause the load to experience large heaving motions, which will create difficult situations during the touch-down phase. One can imagine that when the load has large heave amplitudes, it may slam into the bottom of the sea. This may cause damage to the structure. Also, the structure might be lifted off from the sea bed again, which of course is also unfavourable.
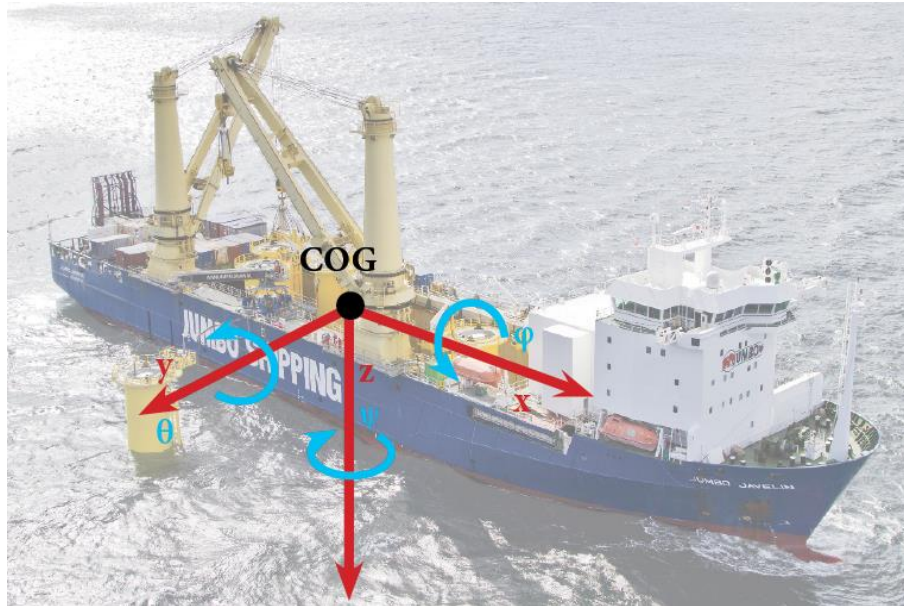
Figure 1.1 Definition of the 6 DOF ship motions in this project

Another interesting fact: currently Jumbo is not yet in the field of demobilisation of for instance old oil fields. Would Jumbo want to start in this market, one hurdle to overcome would be to attach the hook to the structure that must be lifted from the sea bed again. When the heave amplitudes of, in this case, the crane hook is very large, it may be nearly impossible to (safely) attach the hook to the structure.

To reduce the amplitudes of the crane hook and/or load, the offshore installation can only take place during certain so-called 'weather windows'. During these windows, the waves will not cause the vessel to move out of certain set boundaries. These of course are very specific to each project and location. To enlarge this window, and with that the workability of the vessel, some options are available, such as passive or active heave compensators. An elucidation on this is given in Chapter 2.

Summarized
During the touch-down phase of an (deep water) offshore installation procedure, the heaving motions of the structure that must be installed caused by, amongst others, the motions of the vessel are a limiting factor in operability. The heave motion of the load must be reduced in order to increase the operability of the vessel.

1.2 Factors of influence

There are many factors that cause the crane load near the seabed to move in the vertical direction. For instance, when looking at a Jumbo J-class vessel (Figure 1.2), it can be seen that the crane tips have an eccentricity with respect to the ship's COG in all three directions: the tips are located on the starboard side, several tens of meters above the ship's COG and also both forward and aft of the COG. The location of the crane tip of the forward crane is listed in Table 1.1. The crane is pointed outward perpendicular to the x-axis, under an angle of 32°.

The location of the crane tip, the eccentricities, means that the vertical displacement, the heave motion, of the crane tips is composed of the motions heave, roll and pitch.

x-coordinate	17.1 m
y-coordinate	27.5 m
z-coordinate	-41.7 m
Boom angle	32°

Table 1.1 Coordinates of the forward crane tip w.r.t. the vessel's COG
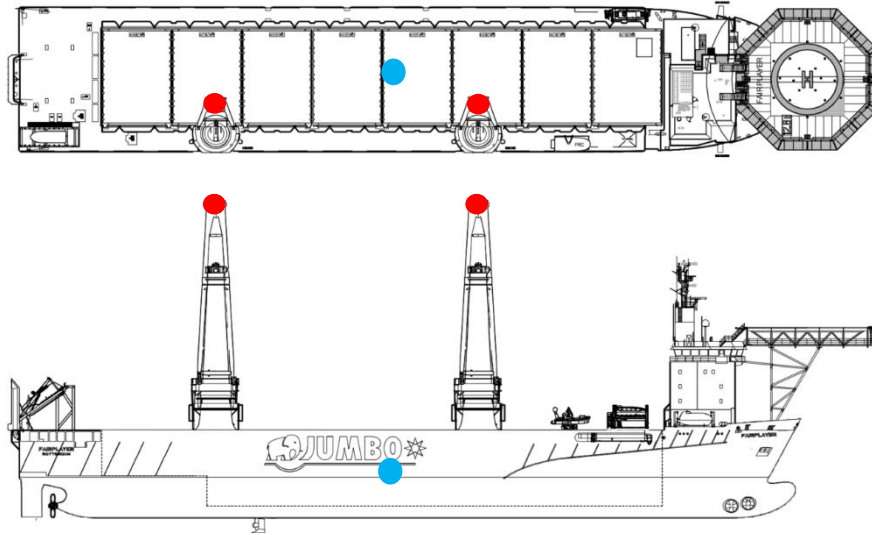
Figure 1.2 General arrangements of the Fairplayer *and location of the crane tips (red dots) and COG (blue dots)*

These three motions are caused and influenced by, amongst others:

- Waves
- Wind
- Cable resonance
- Moving fluids in tanks (ballasting or sloshing)
- Load distribution in the hold or on deck
- Currents
- Other external forces, such as thruster impulses from the DP system
- Proximity of the sea bed

An explanation on the influences will be given in Chapter 3.

1.3 Proposed solutions

Jumbo currently uses passive heave compensators that must be put between a load and the crane hook, but would like to have other options to compensate the heave motion of the offshore structure during the installation phase. At this moment, a graduate student is working on a feasibility check of the installation of an active heave compensator, but this still seems a very expensive solution to the heave problem.

Therefore, and several other reasons, Jumbo wishes to consider another (new and rather unconventional) type of heave compensation: reducing the crane tip vertical motions by imposing countering roll moments on the vessel by means of a ballast system.

As mentioned, the heave motions of the crane tips are composed of the vessel motions heave, roll and pitch. During deep-water offshore installations, often only one of the two cranes is used to lift the structure to the desired depth and install it there. Figure 1.3 gives a representation of a cross-section of the vessel located at the forward crane.

1.3.1 Combined motion equation

Under some restrictions, the heave motion of the tip of the crane can be described by equation (1.2).

$$z_{CT}(t) = -x \cdot \theta(t) + y \cdot \phi(t) + z(t) \tag{1.1}$$

Where:

- $z_{CT}(t)$ = heave motion of the crane tip
- x, y = x- and y coordinate of the crane tip
- $\phi(t)$ = roll motion of the vessel
- $z(t)$ = heave motion of the vessel
- $\theta(t)$ = pitch motion of the vessel

By adding an extra term to this equation, the countering roll motion, the equation changes into equation (1.2).

$$z_{CT}(t) - z \cdot \phi_R(t) = -x \cdot \theta(t) + y \cdot \phi(t) + z(t) \qquad (1.2)$$

Where:

- $\phi_R(t)$ = roll motion of the vessel, induced actively by means of ballasting
- z = z-coordinate of the crane tip

The goal is that the left-hand side of the equation must be kept as close to zero as possible.
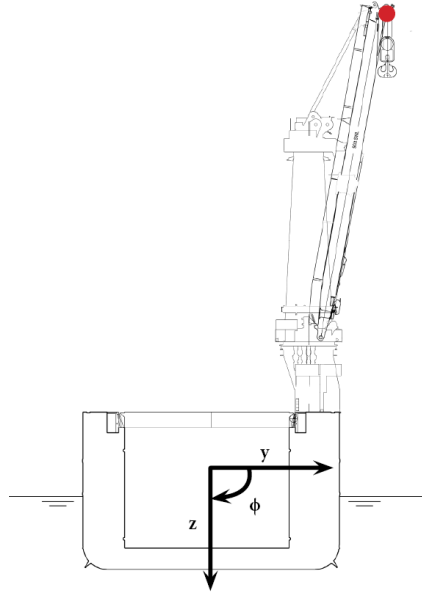
Figure 1.3 Cross-section of the vessel at the forward crane (x = 17.1m w.r.t. the COG)

1.3.2   Concept explanation

To visualize how this concept works, a simplified two-dimensional representation is given in Figure 1.4. In this figure, the vessel is only subjected to the heave motion due to the waves, to clarify the explanation. This figure consists of three parts:

1) The initial situation
2) A positive crane tip heave amplitude
3) A negative crane tip heave amplitude

The distance between the still water plane (SW) (red dotted line) and the initial crane tip height (blue dotted line) will need to be kept constant throughout the offshore installation. This is set to be the reference height. This reference plane (here the SW) can of course be any plane.

In the second situation, the vessel experiences a positive heave amplitude, causing a positive heave amplitude in the crane tip. To compensate for this displacement, the vessel must roll in negative direction, towards portside. In the third situation, the vessel experiences a negative heave amplitude, thus a negative crane tip heave amplitude. To compensate this, the vessel must be rolled towards starboard.

By constantly repeating this process of verifying whether the crane tip is above or below the reference height and imposing roll amplitudes on the vessel, the heaving motion of the crane tip will be reduced and ideally be reduced to zero.

To create these roll amplitudes, the easiest solution is to look into active ballasting systems, or (anti-) roll systems. By reinterpreting the current active anti-roll systems, several options can be considered:

- Shifting a weight from side to side
- Actively 'over-ballasting' with the use of ballast- or anti-roll tanks
- Create extra buoyancy alternatingly on starboard- and portside
- Gyro stabilizers

An explanation on the different systems is given in Chapter 2.
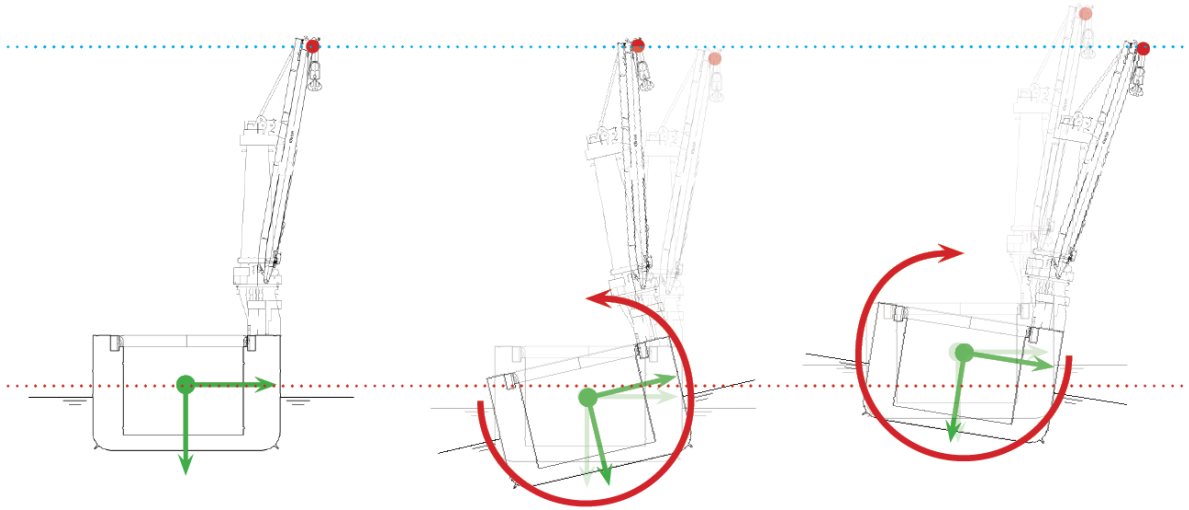
Figure 1.4 Visualization of the concept (roll amplitudes are exaggerated for clarification)

Summarized

By actively rolling the vessel, based on the heave amplitude of the crane tip, using an active ballasting – or active anti-roll system, ideally, the heave amplitude of the crane tip can be reduced to zero.

1.3.3 Expected maximum roll angles

To create an insight in what the necessary roll angles must be, the plot in Figure 1.5 is used. The roll amplitude is, according to geometry, dependent on the angle between the boom and the crane tower. The smaller the angle, the higher the crane tip will be, and the larger the angle must be to compensate a vertical motion. Figure 1.5 shows the positive and negative roll angles for different boom angles and different heave amplitudes.
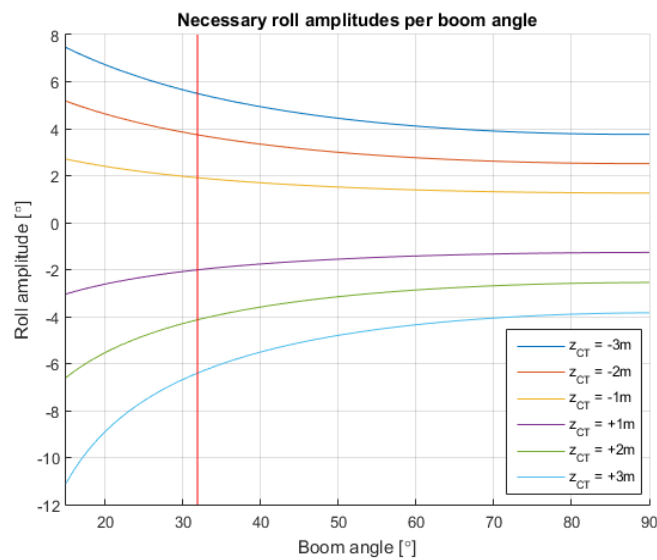
Figure 1.5 ϕ_R to compensate $-3\text{m} \leq z_{CT} \leq +3\text{m}$

The minimum boom angle is 15°. Smaller boom angles are practically impossible. The boom angle chosen for this project is 32°, as listed in Table 1.1. What this means for the necessary roll amplitudes, is visualized by the red line in Figure 1.5.

1.4 Objective

With the problem description mentioned, the following research objective is set for this thesis project:

The goal of this project is to improve the workability in swell waves of a Jumbo J-class vessel by reducing the heave amplitude of the crane tip by imposing a roll amplitude created by an actively controlled ballasting system.

The goal will be achieved by creating a computer simulation model using Simulink. This simulation model will be validated by means of performed MARIN towing tank tests. The purpose of the computer simulation model is to verify how and under what conditions such a system will work.

1.5 Approach

To attain the research goal, several steps must be set. The approach of the research, and there with the structure of this report, is illustrated in Figure 1.6.
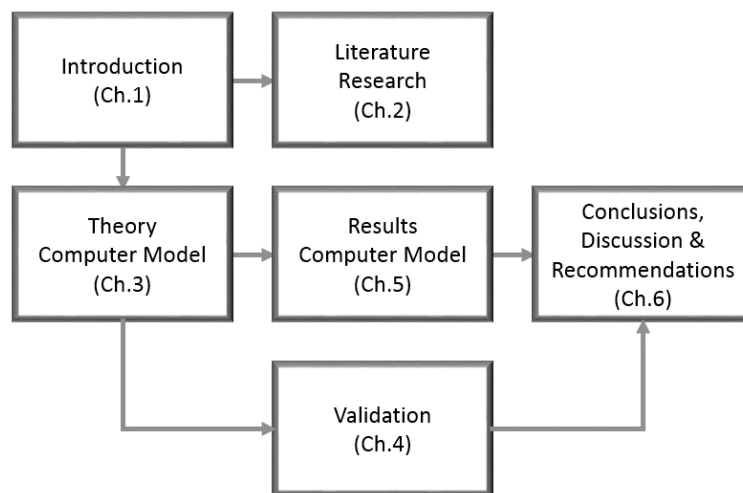
Figure 1.6 Structure of the report

The first chapter describes the problem that will be countered in this research. The first definitions are given, the influences on the problem, as well as the proposed solution to the problem. The second chapter states the conventional systems that are currently being used to solve the problem, as well as systems that are listed to be applicable for the proposed solution. The third chapter describes the underlying principles that are used for the development of the computer model. In chapter 4 the validation of the computer model will be explained and performed, followed by the results in chapter 5. Finally, conclusions are drawn and discussed in chapter 6, accompanied with recommendations for further research. Furthermore, in the appendices a complete description of physical model tests is given, as well as the used parameters and specifications of the vessel.

1.6 Framework

To solve the problem and attain the goal set for this project, both computer simulations and model tests will be performed. As both are a representation of reality, and due to the fact that the time available for the project is limited, some simplifications and boundary conditions need to be determined and set beforehand. This paragraph explains what boundary conditions are used.

1.6.1 Computer Model & Simulations

The program that will be used to create the computer model in, will be Matlab. The simulations then will be performed using an add-on of Matlab called Simulink. Matlab is a well-known program by students of the Technical University of Delft, and has very good mathematical performances. Simulink can, amongst others, be used very well for the simulations of dynamic systems, and is very easy to use due to the graphical user interface.

The computer model will be a mathematical description of reality, and will be based on the Simulink model developed at the Norwegian University of Science and Technology (NTNU) in Trondheim, Norway. This model is called the Marine Systems Simulator (MSS), and is used to simulate vessel motions in the six DOF of a vessel. For more information on this, please refer to (Perez, et al., 2005).

Using predetermined hydrodynamic coefficients of the J-class vessel obtained using ANSYS AQWA, known fixed parameters of the vessel, and a control system that regulates the ballasting, the simulations will be performed for situations with both the system switched on and off. The complete framework of the computer model and the simulations is explained in Chapter 3.

1.6.2 Real boundaries

Apart from the abovementioned simplifications and boundaries, there are some real boundaries that are to be taken into account. These boundaries hold for both the computer simulations and the towing tank tests.

1.6.2.1 *Maximum allowable roll angles*

Due to the rolling of the vessel, the cable will 'swing' towards the hull. The hull of the ship may not be touched by the cable, this could either cause damage to either the cable with a potential breaking hazard, or could damage the hull. To do so, a minimal clearance of 1 meter must be kept between the cable and the hull. Depending on the boom angle, a maximum roll angle is determined. This is visualized in Figure 1.7. It is important to keep these boundaries in mind; when looking at Figure 1.5, it can be noted that for the smaller boom angles larger roll angles are necessary to compensate the higher heave amplitudes. In the case of a boom angle of 32°, the maximum roll amplitude that the vessel can make is approximately 16° towards portside. For crane tip heave amplitudes of 3 meters the necessary roll amplitude is only 6.4°.
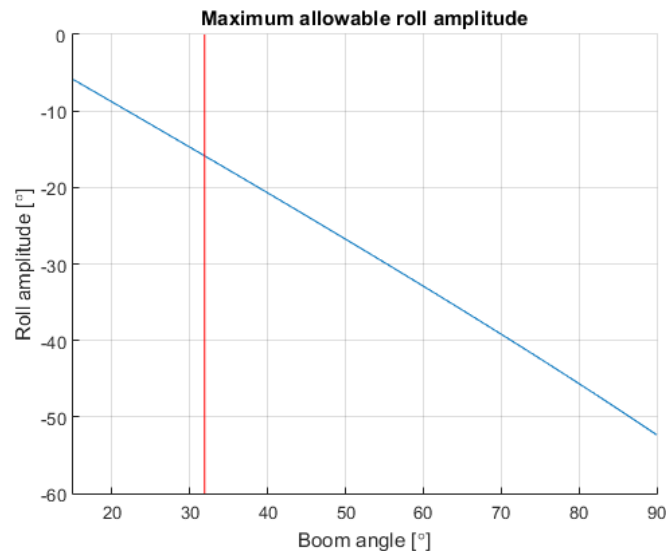
Figure 1.7 Maximum allowable roll amplitude

1.6.2.2 *Ballasting system*

The goal of the project is not to actually develop the ballasting system, it merely verifies the applicability of it. Therefor the results from both the computer simulations and the towing tank tests will not fully be based on existing equipment.

1.6.2.3 *Motion influences*

As mentioned earlier, there are many different influences on the motions of the vessel. For simplification in both the simulations and the model tests several influences are left out of the equations. The motions of the vessel are the results of the incoming waves. Wind and current for instance are not taken into account. More on this in Chapter 3.

2 Conventional systems & research overview

Improving the performance of vessels and systems during any type of offshore installation is an ongoing and innovative process. In this chapter a short overview of the development of the heave reduction systems through the years and at this moment is given. Furthermore, roll reduction systems are elucidated, and a choice of systems is made that will be used for the solution of the problem stated in Chapter 1.

2.1 Heave compensation systems

The development of heave compensation systems started around the 1970s. Since then it has been developed and redeveloped multiple times. Figure 2.1 gives an approximate timeline of the developments throughout the years.
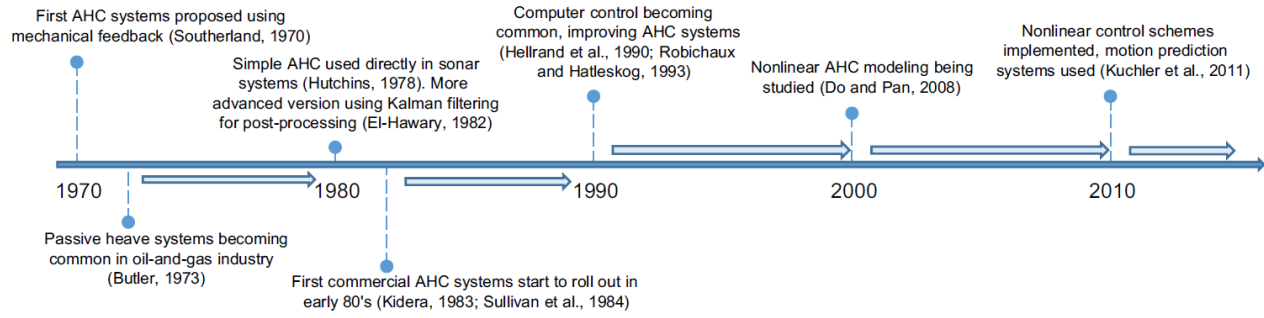
Figure 2.1 An approximated timeline of the development in heave compensation systems (Woodacre, et al., 2015)

Nowadays there are three types of heave compensation, or reduction, systems:

- Passive heave compensation systems (PHC systems)
- Active heave compensation systems (AHC systems)
- Hybrid active-passive heave compensation systems

The difference between an active and a passive compensation system can be described by the means of controlling the system. A passive system is a system that functions without the interference of any external control. The system is set up beforehand for the environment it will be used, and after that will operate on its own. Furthermore, a passive heave compensator requires no energy input to operate.

On the contrary, an active heave compensation system functions with the help of sensors and controllers to actively compensate the motion. To attain this, it also requires the input of energy. And a hybrid system is a combination of a passive system and a heave system either in series or parallel.

In the following sub paragraphs these system types will be explained, giving their underlying principles, as well as their advantages and disadvantages.

2.1.1 Passive heave compensation systems

A passive heave system is, simply said, a motion absorber with an open-loop system; the motion of the vessel is the input, and the reduced amplitude of the suspended load is the output. Jumbo owns two passive heave compensators, of which one is shown in Figure 2.2. A PHC is usually put between the crane and the suspended load, but could in fact be installed in series anywhere along the load-carrying line.

A passive heave compensator is more or less a parallel spring and damper system. By changing the spring constant k and the damping coefficient c of the system, the compensator can be used for many different (wave) frequencies. Figure 2.3 shows a Bode plot of the occurring wave frequencies and the heave amplitude (in decibels) for an uncompensated system (red dotted line) and a PHC system. By adding a PHC to the system, the resonance frequency, or Eigen frequency of the ship (ω_n), is shifted to a wave frequency outside the wave frequency spectrum.

To determine the needed spring constant and damping, the equations (2.1) and (2.2) can be used (Woodacre, et al., 2015).

$$\omega_c = \omega_n \cdot \sqrt{1 - \left(\frac{b}{2\omega_n}\right)^2} \tag{2.1}$$

$$\omega_n = \sqrt{\frac{c}{m_L}} \tag{2.2}$$

Here, ω_c is the compensated Eigen frequency, and m_L the mass of the suspended load. The total damping is defined by, but not restricted to, the weight of the submerged cable, drag in heave direction caused by the load and mechanical friction in the compensator itself.

As mentioned, not only has the weight of the load be taken into account, but also the weight of the cable. Especially in deep water this will be a significant part of the total weight hanging in the crane. It also might cause resonance effects in the cable, creating larger heave motions than the ship initiates.

Figure 2.2 One of Jumbo's passive heave compensators during the North Amethyst Project
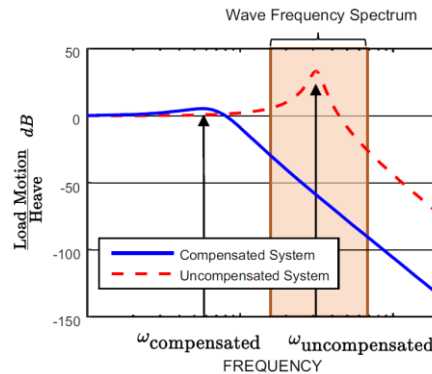
Figure 2.3 Bode plot of the compensated and uncompensated system (Woodacre, et al., 2015)

(Driscoll, et al., 1998) has made a comparison between a ship-mounted PHC and a PHC at the crane hook, and found that the heave compensation was more effective when mounted near the load. A downside to this, is that the settings of the heave compensator must be pre-determined for the installation depth, and cannot be altered anymore while at this depth.

There are some great advantages to a passive heave compensation system. For example, it requires no power input to function. Next to this, a passive heave compensator such as shown in Figure 2.2 can be implemented in the existing system without the need to perform (complex) modifications. If heave reduction of 80% maximum is sufficient, this system is very interesting. For a more extensive explanation and examples of PHC systems, reference is made to (Woodacre, et al., 2015).

2.1.2   Active heave compensation systems
If heave reduction of about 80% is not sufficient for the installation, or relative heave compensation is needed (for instance between two floating objects), the better option would be to use active heave compensation.

An active heave reduction system is, in contradiction to the passive system, a closed-loop system. The heave motion of the ship is measured and relayed to a controller. This controller than processes the motion and determines the motions the actuator needs to make in order to compensate for the heave motion. One of the greatest advantages of an AHC system is that the motion feedback is not limited to that of the vessel itself, but can also be in comparison with for instance another vessel or the elevation of the water surface. In comparison to the passive system, the active system settings can also be altered whilst in operation.

On the downside, the implementation of an active heave compensation system implies that an extensive infrastructure must be designed, produced and installed. This also means that specialized training for the use, troubleshoot, maintenance and repair is needed. The system will also require quite some power for operation, which would be something to take into consideration. Again, for a more detailed explanation and examples of AHC systems is referred to (Woodacre, et al., 2015).

2.1.3   Hybrid systems

If the power consumption of an active system is the limitation for its implementation, a hybrid system might be the solution. A hybrid system consists of both passive and active parts built into its heave compensation system. These can either be set up in a parallel set-up, or in series, although the parallel set-up has preference. When in series, both the active as the passive system need to be able to hold the full load, where in the parallel set-up the active portion only needs to be able to hold about 10% of the load, when the passive portion is able to hold the full 100%, as is presented by (Hatleskog & Dunnigan, 2007) and (Robichaux & Hatleskog, 1993). A hybrid system is able to be as precise as the active system, only in this case it will need much smaller forces and can be physically smaller than the AHC system. This means it needs less fluids, flow, pressure and power and thus it will be less expensive in operational costs. However, the increased complexity and needed infrastructure may not be worth the additional cost when compared to a strictly passive or active system (Woodacre, et al., 2015).

2.2   Current heave compensation research

Most of the current heave compensation research done by researchers is not focussed on new designs of these devices, but more on the improvement of the already existing systems and their underlying control system of it. Nowadays the computer and control systems of active and hybrid heave compensation systems are much faster than some years ago, and also simulations are much more precise. This makes it possible to improve the current systems by for instance reducing power consumption and response time. An example of such a research is done by (Liu, et al., 2015) for a hybrid heave compensator.

Apart from this, heave compensation system builders, such as Bosch Rexroth, Cranemaster and Innovative Input continue to create, extend or improve their already known designs in-house. Of these researches usually nothing is published until a new design is brought to the market for rent or sale in the offshore industry.

2.3   Current active roll reduction systems

To create a countering roll motions on the vessel, a weight must be shifted over the breadth of the vessel to create a rolling moment. This is equal to what happens in an active roll reduction system, only in this case the roll is not reduced to zero, but controlled to the needed roll angle to compensate the crane tip's heave motion. Nowadays, the most commonly used devices to control roll motions of a vessel are water- or ballast tanks, gyrostabilizers, stabilizer fins and the ship's rudder.

There are many types of roll reduction systems on the market. In this case, specifically is searched for a controllable system, or active system, to induce the needed roll moments. A short description of the most conventional active systems is given in this paragraph.

2.3.1   Roll reduction tanks

The most commonly used system to reduce roll on board a vessel, is the use of roll reduction tanks (RRT). These can either be used passively or actively. Here only the active anti roll tanks are considered. The common concept is the displacement of a fluid in horizontal direction, creating a roll moment about the roll axis.

The active RRTs can be divided into two main types: the free-flooding tank, and the U-tank. The main advantage of these tanks is that, depending on the power of the pumps, the shifting of the water, and with that the weight needed for the roll moment, can be achieved rather quick. Also, since most vessels have already got ballast tanks on board, the extra space needed for this system is minimal. A short explanation between U-tanks and free-flooding tanks is given in the following sub paragraphs.

2.3.1.1   *U-tanks*

The name U-tank is derived from its shape compared to the letter U, as can be seen from Figure 2.4. It connects two (ballast-) tanks by a water duct at the base of the tanks. The water is actively transported from one side to the other by means of a pump. This pump can either transport water, as visualized in the right drawing, or it can transport air. By doing so, the pressure above the water is changed, causing the water to flow to the opposite tank.
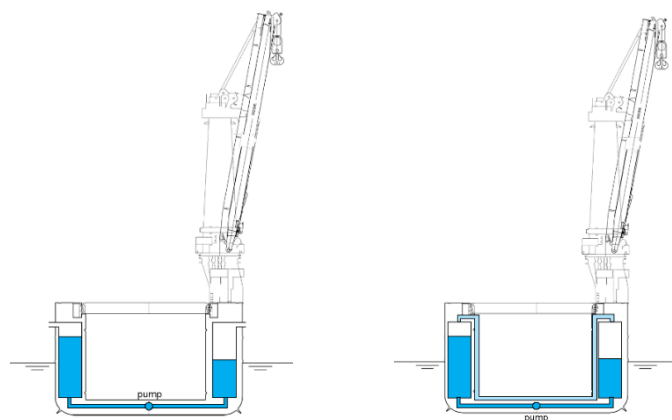
Figure 2.4 Visual representation of active U-tank configurations on board a J-class vessel

2.3.1.2   *Free-flooding tanks*

The free-flooding tanks, also known as n-tanks (again because of the resemblance in shape compared to the letter n), is visualized in Figure 2.5. The free-flooding tank is not the same as the (passive) free-flowing tank, which will not be described in this report as it is not applicable here. The free-flooding tank works similar to the U-tank, apart from the fact that the water duct at the base has been removed and the in- and outflow water needed for the roll reduction comes directly from the sea through inlets at the bottom. A downside to the free-flooding tanks in comparison with the U-tanks, is that the holes in the hull create an extra drag during sailing, depending on size and location.
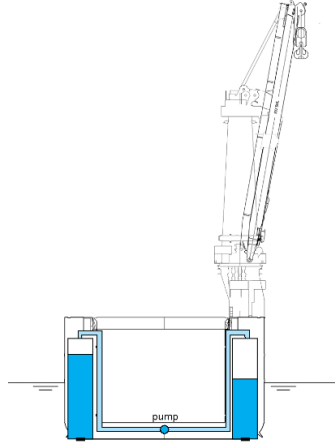
Figure 2.5 Visual representation of free-flooding tanks on board a J-class vessel

2.3.2   Gyrostabilizers

A gyrostabilizer consists of one or more fast spinning flywheels. The gyroscopic effect this creates is then used to counteract the roll excitation forces and is able to nearly eliminate the roll motions. An example of such a device is shown in Figure 2.6. The performance of a gyrostabilizer is exceptional and can reduce the roll amplitudes up to 95% of the initial amplitudes (Perez & Blanke, 2012). On the downside, this system is expensive, has quite a large weight and size, and puts large stresses on the hull. More recently, the development of this system has been resumed again, mostly for the yacht industry to stabilise roll when at anchor.
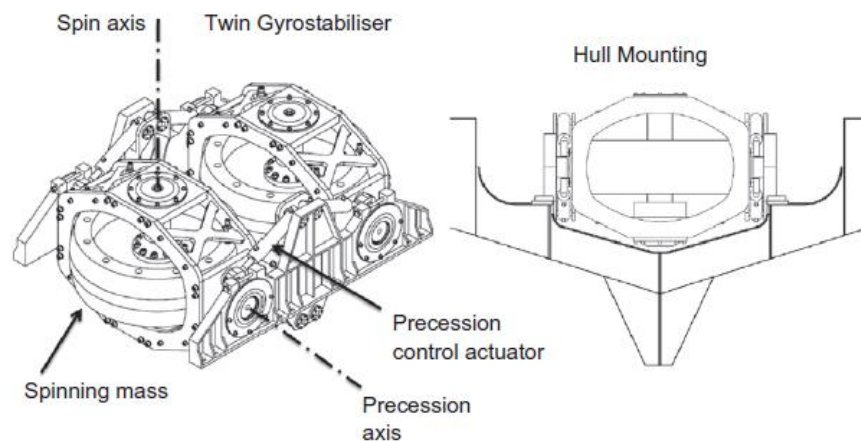
Figure 2.6 Example of a gyrostabilizer and its hull mounting (Perez & Blanke, 2012)

2.3.3   Stabilizer fins

Standard stabilizer fins are controllable hydrofoils mounted on the side of the hull. By actively adjusting the angle of attack of the incoming flowing water, they produce lift to counteract the roll motions of the ship. Since these hydrofoils rely on the incoming flow to produce their lift, these standard stabilizer fins will perform poorly when the vessel is at (near) zero forward speed. To still be able to use these fins, the fins are used more or less as 'paddles' in the water; the fins create a reaction force by moving up and down, which can be used to counter the roll motions of the vessel (Fan, et al., 2009). A visual representation of where these stabilizer fins would be installed on a J-class vessel is given in Figure 2.7.
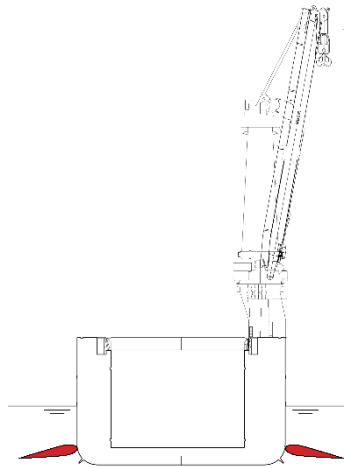
Figure 2.7 Visualization of stabilizer fins (in red) on board a J-class vessel

Stabilizer fins perform quite well during sailing, but are not usable during offshore installations, as they are reliant on the incoming flow. The zero speed fins are mainly applicable for the somewhat smaller vessels, such as yachts and vising vessels. A large heavy lift vessel would need such enormous fins, and with that high powers to paddle them through the water, that this would not be a feasible solution for the offshore industry. Also, the fins extend further than the side of the hull, which might cause problems during installations, as also the subsea structures are over-boarded on the side and they might hit the fins. A solution to this problem would be retractable fins, but then they cannot be used during the offshore installations, which was the reason they were installed in the first place.

2.3.4 Rudder control

Most ships have at least one rudder on board. A rudder can also be used for motion stabilization. The most obvious motion that is induced by a rudder is, of course, yaw. But, it is observed that when a rudder is swung towards a side, the vessel initially heels towards the same side due to the weight of the rudder (van Amerongen, et al., 1990). The yaw rate of a vessel is, at that moment, still (nearly) zero, and the heading changes are nearly zero when quickly moving the rudder from one side to another. This roll effect is greatly enlarged by the lift created by the angle of the incoming water. Thus, the efficiency of the roll reduction (mainly) related to the forward speed. At zero speed this system is not quite as efficient (Millan, et al., 2007).

2.3.5 Solid mass displacement

One might remember the 'Up Is Down' scene of the movie (Pirates of the Caribbean - At World's End, 2007) [1]. Of course, this is not scientifically underlined here, but the concept is clear: Move a weight from one side to the other, periodically, and a roll moment is induced. This concept is actually the basis of every roll reduction system, active or passive, underlining the fact that the displaced weight could be anything between water and human beings. A more common concept on board a ship would be, for instance, a weight block on a track that is driven by a motor, located on the aft of the vessel.

In a survey done by the David Taylor Research Center in the United States this system is also mentioned as translating a solid weight. The stabilizing power of this system is proportional to the weight. It is recommended that the weight is between 0.5 and 2% of the total displacement of the vessel, although not larger than 5% (Smith & Thomas III, 1990). The main advantage of this type of system, is that it has no free surface effect, compared to a ballast system using fluids. According to (Smith & Thomas III, 1990) a well-designed system will also take up less space compared to ballasting tanks. Furthermore, Huisman has developed a vessel which makes use of a similar system (Huisman, 2016).

---

[1] The scene can be viewed on Youtube via https://www.youtube.com/watch?v=sNj8mJq65i4

2.4 Selection of recommended roll induction system

All the mentioned active roll reduction systems have their advantages and disadvantages. The system for this project will have to comply with two main requirements. First, the system must be able to work at (nearly) zero forward speed, as it will be the case during offshore installation. Second, the system may not take up the area needed for the installation or cargo. These requirements are combined in Table 2.1, together with the applicability of the system for the solution of the problem.

System	Zero speed requirement	Area requirement	Feasible?
Roll reduction tanks	Yes	Yes	**Yes**
Stabilizer fins	Yes	No	**No**
Gyrostabilizer	Yes	Yes	**Yes**
Rudder control	No	Yes	**No**
Solid mass	Yes	Yes	**Yes**

Table 2.1 Fulfilment of requirements of active roll reduction systems

The results from Table 2.1 show that the RRTs, the gyrostabilizer, and the solid mass displacement systems are feasible for this project. The stabilizer fins do not comply with the area requirement, and the rudder control does not comply with the speed requirement. Note that the standard stabilizer fins also don't comply with the speed requirement.

As a final requirement, the costs of (new) systems are always of importance. The gyrostabilizer is, especially compared with the RRTs, very costly. Therefore, the choice for the recommended system is either the active roll reduction tanks, or the solid mass displacement. The final choice depends on the functionality, costs, available space, and many more other parameters, though.

The Simulink model will be built based on both the solid mass displacement, as well as a very simplified version of the ballast tanks. In case of the ballast systems, the pipe and pump systems are not modelled. The reason for this is that the different options for a ballasting tank system are far too extensive. One can think of different pipe diameters for the cross-flooding pipes, different pump types, different sizes in tank width, height, etc. The solid mass will have a fixed weight and is placed at a fixed height in reference with the vessel's COG, and can be displaced transversely only. In Chapter 3 a more extensive explanation of the system is given.

3 Underlying Principles Computer Model

A computer model is, simply said, a mathematical representation of reality. To build such a model, several underlying principles and equations must be determined, along with some simplifications. This chapter explains the basic lay-out of the computer model, elucidates the underlying theories and clarifies the assumptions made to build it.

3.1 Summary of assumptions & simplifications

Throughout this chapter several assumptions and simplifications are made. For convenience, a summary of the simplifications and assumptions in advance. Throughout the chapter, these will be explained.

- No forward vessel speed
- Ideal fluid
- Low wave steepness
- Unidirectional wave profiles
- Harmonic waves
- Mass of the vessel (and all on board) is constant
- Payload fixed in the crane tip
- Sloshing in ballast tanks is negligible
- Constant acceleration and deceleration of the ballast

3.2 Wave theory

The waves induce forces on the vessel. To investigate the resulting motions of the vessel due to waves, the waves must be described by mathematics as done by potential theory. To make use of potential theory, some assumptions and requirements are in order:

- Ideal fluid (inviscid, irrotational, incompressible and without surface tension)
- Small wave steepness $(2\zeta_a/\lambda)$
- Fulfil the Laplace equation
- Fulfil seabed boundary condition (no-leak condition)
- Fulfil free surface dynamic boundary condition
- Fulfil free surface kinematic boundary condition

The complete derivation of the full velocity potential of the waves is described in chapter 5 of (Journée & Massie, 2001). The final resulting velocity potential is given in equation (3.1).

$$\Phi_w(x, z, t) = \frac{\zeta_a g}{\omega} \cdot \frac{\cosh\big(k(h + z)\big)}{\cosh(kh)} \cdot \sin(kx - \omega t) \tag{3.1}$$

In which:

- Φ_w = wave velocity potential
- ζ_a = wave amplitude
- g = gravitational acceleration
- $k = 2\pi/\lambda$ = wave number
- λ = wave length
- h = water depth
- z = z-coordinate
- $\omega = 2\pi/T$ = circular wave frequency
- T = wave period
- t = time
- x = x-coordinate

Based on the velocity potential displacements, velocities and accelerations of water particles can be calculated, as well as pressure and wave energy, which are necessary for the calculations of the ship motions.

3.2.1 Regular waves

To analyse a complex and irregular wave system, first regular, harmonic waves will be explained. This is the basis for the description of irregular wave patterns later. The harmonic elevation of the water surface at a certain location (x, y) for a vessel in a wave heading μ at zero vessel speed, is defined by equation (3.2).

$$\zeta = \zeta_a \cos(\omega t - kx \cos(\mu) - ky \sin(\mu)) \tag{3.2}$$

The wave heading is 0° for following waves, 90° for waves coming from starboard, 180° for head waves and 270° for waves coming in from portside. The wave elevation at the COG can be described by equation (3.3).

$$\zeta = \zeta_a \cos(\omega t) \tag{3.3}$$

3.2.2 Irregular waves

The wave elevation as described by equation (3.3) is a harmonic, or regular wave. In reality, the surface elevation can become very irregular. Even so, it still is possible to describe a very irregular sea by a summation of a finite number N of harmonic wave components, each with its own amplitude, circular frequency, length and direction. This is called the superposition principle, given in equation (3.4).

$$\zeta(t) = \sum_{n=1}^{N} \zeta_{a_n} \cos(\omega_n t + \varepsilon_n) \text{ for } n = 1 \ldots N \tag{3.4}$$

In which:

- ζ_{a_n} = wave amplitude of wave component n
- ω_n = circular wave frequency of wave component n
- ε_n = phase shift of wave component n

3.2.2.1 *Fourier analysis*

Irregular waves lend themselves to be analysed using Fourier analysis, as it is considered a summation of multiple sinusoidal waves. The Fourier analysis will yield a set of wave amplitudes ζ_{a_n} and ε_n, belonging to its own circular wave frequency ω_n.

3.2.3 Wave statistics

As the waves become more irregular, it becomes more difficult to obtain usable information from it. Based on time traces of irregular wave patterns, statistical analysis can be performed. This time trace must be of sufficient length in time to obtain reliable statistics. As a rule of thumb the time trace must be at least a 100 times the length of the longest wave period in the wave pattern. The following statistical information can be obtained from a time trace:

- Average wave period $\bar{T}$, or average zero up-crossing period
- Mean wave height $\bar{H}$
- Significant wave height H_s
- Maximum wave height H_{max}
- Standard deviation of the wave height σ
- Normal wave amplitude distribution
- Rayleigh wave amplitude distribution

A short explanation of the statistics is given in the following sub-paragraphs.

3.2.3.1 *Standard deviation*

The standard deviation, or Root Mean Square (RMS), value follows from equation (3.5). In this equation n represents the instant wave elevation of a discretized time trace of the wave elevation. The RMS value is related to the significant wave height according to equation (3.6).

$$\sigma = \sqrt{\frac{1}{N-1} \sum_{n=1}^{N} \zeta_n^2} \text{ for } n = 1 \ldots N \tag{3.5}$$

$$H_s = 4 \cdot \sigma \tag{3.6}$$

3.2.3.2 *Normal wave amplitude distribution*

If the time trace of the wave elevation is sufficiently long, the discretized wave elevation fits a normal distribution. This distribution is given in equation (3.7), in which σ is the standard deviation and x the variable that is distributed, usually the wave elevation ζ. The mean value of this distribution is zero.

$$f(x) = \frac{1}{\sigma\sqrt{2\pi}} \cdot \exp\left\{-\left(\frac{x}{\sigma\sqrt{2}}\right)^2\right\} \tag{3.7}$$

Based on this wave amplitude distribution, the probability P of exceeding a wave elevation of a certain value a can be calculated according to equation (3.8).

$$P\{\zeta > a\} = \int_a^\infty f(x) \cdot dx = \frac{1}{\sigma\sqrt{2\pi}} \cdot \int_a^\infty \exp\left\{-\left(\frac{x}{\sigma\sqrt{2}}\right)^2\right\} \cdot dx \tag{3.8}$$

3.2.3.3 *Rayleigh wave amplitude distribution*

If the frequency range of a time trace is not too large, which is often the case for waves, the frequency spectrum can be said to be narrow banded. If the water elevation is normal distributed, the wave amplitude statistics are Rayleigh distributed. The Rayleigh distribution is given in equation (3.9).

$$f(x) = \frac{x}{\sigma^2} \cdot \exp\left\{-\left(\frac{x}{\sigma\sqrt{2}}\right)^2\right\} \tag{3.9}$$

The probability of the amplitude exceeding a certain value becomes as given in equation (3.10).

$$P\{\zeta_a > a\} = \int_a^\infty f(x) \cdot dx = \frac{1}{\sigma^2} \cdot \int_a^\infty x \cdot \exp\left\{-\left(\frac{x}{\sigma\sqrt{2}}\right)^2\right\} \cdot dx \tag{3.10}$$

3.2.4 Wave spectra

By means of Fourier analysis, a wave energy $S_\zeta(\omega_n)$ spectrum can be defined according to equation (3.11) with the obtained values for ζ_{a_n}.

$$S_\zeta(\omega_n) \cdot d\omega = \frac{1}{2}\zeta_{a_n}^2 \tag{3.11}$$

Based on the obtained wave energy spectrum, some variables can be obtained using the integral in equation (3.12). Here, m denotes a moment, and n the n-th order moments.

$$m_{n\zeta} = \int_0^\infty \omega^n \cdot S_\zeta(\omega) \cdot d\omega \tag{3.12}$$

The most important values that can be obtained by this equation are:

- $\sigma_\zeta = \sqrt{m_{0\zeta}}$ = RMS of the surface elevation
- $H_s = 4 \cdot \sqrt{m_{0\zeta}}$ = significant wave height
- $T_p = 2\pi \cdot \sqrt{m_{0\zeta}/m_{2\zeta}}$ = mean zero-crossing wave period, or peak period

One of the most commonly known standardised wave spectra is the JONSWAP wave spectrum. This is based on extensive measurements performed in the North Sea. Analysis of the obtained data yielded a formulation for the wave energy spectrum as described by equation (3.13).

$$S_\zeta(\omega) = \frac{320 \cdot H_s^2}{T_p^4} \cdot \omega^{-5} \cdot \exp\left\{-\frac{1950}{T_p^4} \cdot \omega^{-4}\right\} \cdot \gamma^A \tag{3.13}$$

In which:

- γ = Peakedness factor (standard 3.3)
- A = $\exp\left\{-\left(\frac{(\omega/\omega_p - 1)}{\sigma\sqrt{2}}\right)^2\right\}$
- ω_p = $2\pi/T_p$
- σ = Step function of ω: $\begin{cases} \sigma = 0.07 \text{ if } \omega < \omega_p \\ \sigma = 0.09 \text{ if } \omega > \omega_p \end{cases}$

As mentioned earlier, a sea usually consists of waves coming from multiple directions. This is called directional spreading, and can be incorporated in the wave spectrum. For simplicity of the computer model this is not taken into account, and it is assumed that only unidirectional waves occur.

3.3 Ship motion theory

As mentioned in Chapter 1, the resulting motions of a vessel consist of three translations and three rotations. These six motions of and about the coordinate system located in the ship's COG are defined by equations (3.14) to (3.19).

$$x(t) = x_a \cdot \cos(\omega t + \varepsilon_{x\zeta}) \tag{3.14}$$

$$y(t) = y_a \cdot \cos(\omega t + \varepsilon_{y\zeta}) \tag{3.15}$$

$$z(t) = z_a \cdot \cos(\omega t + \varepsilon_{z\zeta}) \tag{3.16}$$

$$\phi(t) = \phi_a \cdot \cos(\omega t + \varepsilon_{\phi\zeta}) \tag{3.17}$$

$$\theta(t) = \theta_a \cdot \cos(\omega t + \varepsilon_{\theta\zeta}) \tag{3.18}$$

$$\psi(t) = \psi_a \cdot \cos(\omega t + \varepsilon_{\psi\zeta}) \tag{3.19}$$

In these equations, the symbols mean the following:

- $x_a, y_a, z_a, \phi_a, \theta_a, \psi_a$ = amplitude of the motion
- $\varepsilon_{x\zeta}, \varepsilon_{y\zeta}, \varepsilon_{z\zeta}, \varepsilon_{\phi\zeta}, \varepsilon_{\theta\zeta}, \varepsilon_{\psi\zeta}$ = phase shift of the motion

The phase shifts of the motions are with respect to the harmonic wave elevation, as described by equation (3.3). The equations describe the displacement along the axes, and the rotation about the axes. By taking the time derivatives of the equations, the velocities and accelerations are found. In the case of heave, this is described by equation (3.20) and (3.21).

$$\dot{z}(t) = \frac{d}{dt}\left(z_a \cdot \cos(\omega t + \varepsilon_{z\zeta})\right) = -z_a \cdot \omega \cdot \sin(\omega t + \varepsilon_{z\zeta}) \tag{3.20}$$

$$\ddot{z}(t) = \frac{d^2}{dt^2}\left(z_a \cdot \cos(\omega t + \varepsilon_{z\zeta})\right) = -z_a \cdot \omega^2 \cdot \cos(\omega t + \varepsilon_{z\zeta}) \tag{3.21}$$

3.3.1 Motions of an eccentric point

If the motions of the vessel's COG are known, the motions of any other point away from the COG can be calculated using superposition. For this, the angles of rotation about the axes are assumed to be small in order to apply linearization such that:

$$\sin(\phi) \approx \phi \tag{3.22}$$

$$\cos(\phi) \approx 1 \tag{3.23}$$

The motions of a point P at (x_p, y_p, z_p) can be determined according to the transformation matrix given in equation (3.24). If this point P would be the location of the tip of the crane, the resulting expanded equation for the heave amplitude of the crane tip would become as given in equation (3.25).

$$\begin{bmatrix} x_p(t) \\ y_p(t) \\ z_p(t) \end{bmatrix} = \begin{bmatrix} 1 & -\psi(t) & \theta(t) \\ \psi(t) & 1 & -\phi(t) \\ -\theta(t) & \phi(t) & 1 \end{bmatrix} \cdot \begin{bmatrix} x_p \\ y_p \\ z_p \end{bmatrix} \tag{3.24}$$

$$z_{aCT} \cdot \cos(\omega t + \varepsilon_{zCT}) = z_a \cdot \cos(\omega t + \varepsilon_{z\zeta}) - x_p \cdot \theta_a \cdot \cos(\omega t + \varepsilon_{\theta\zeta}) + y_p \cdot \phi_a \cdot \cos(\omega t + \varepsilon_{\phi\zeta}) \tag{3.25}$$

Based on equation (3.25), the amplitude and phase shift of the heave motion of the crane tip can be calculated according to the equations (3.26) and (3.27). For the full derivation towards these equations is referred to chapter 6 of (Journée & Massie, 2001).

$$z_{aCT} = \sqrt{(z_{aCT} \cdot \sin(\varepsilon_{zCT}))^2 + (z_{aCT} \cdot \cos(\varepsilon_{zCT}))^2} \tag{3.26}$$

$$\varepsilon_{zCT} = \tan^{-1}\left(\frac{z_{aCT} \cdot \sin(\varepsilon_{zCT})}{z_{aCT} \cdot \cos(\varepsilon_{zCT})}\right) \tag{3.27}$$

In which:

- z_{aCT} = heave amplitude of the eccentric crane tip
- ε_{zCT} = phase shift of the heave motion w.r.t. the harmonic wave elevation at the vessel's COG

3.3.2 Coupled equation of motion

The complete response of a vessel in water subjected to waves are a summation of all the motions that occur. The full set of equations of motion follows from Newton's second law. For translations, this is represented by equation (3.28), and for rotations this is represented by equation (3.29).

$$\vec{F} = \frac{d}{dt}(m\vec{U}) \tag{3.28}$$

$$\vec{M} = \frac{d}{dt}(\vec{H}) \tag{3.29}$$

In which:

- $\vec{F}$ = resulting external forces acting in the COG
- $\vec{M}$ = resulting external moments acting about the COG
- m = mass of the body
- $\vec{U}$ = velocity of the COG
- $\vec{H}$ = angular momentum about the COG

Based on Newton's second law for forces and moments, the complete 6DOF coupled equation of motion (EOM) of a vessel in waves is represented by equation (3.30).

$$[M + A(\omega)] \cdot \ddot{x}_i + [B](\omega) \cdot \dot{x}_i + [C] \cdot x_i = F_i \tag{3.30}$$

In which:

- $[M]$ = mass matrix of the body
- $[A(\omega)]$ = frequency dependent added mass matrix
- $[B(\omega)]$ = frequency dependent damping matrix
- $[C]$ = hydrostatic restoring matrix
- $\ddot{x}_i, \dot{x}_i, x_i$ = acceleration, velocity, and displacement of the body in direction i
- F_i = sum of forces or moments on the body in direction i

The components of the added mass matrix $[A(\omega)]$ and the damping matrix $[B(\omega)]$ are frequency dependent, and can be obtained using potential theory software such as Ansys AQWA. Chapter 7 in (Journee) gives the full derivations and equations to obtain the coefficients of these matrices.

For a ship that has symmetry about the x-axis and the COG located at the origin of the coordinate system, the mass matrix $[M]$ is defined by:

$$[M] = \begin{bmatrix} m & 0 & 0 & 0 & 0 & 0 \\ 0 & m & 0 & 0 & 0 & 0 \\ 0 & 0 & m & 0 & 0 & 0 \\ 0 & 0 & 0 & I_{xx} & 0 & I_{xz} \\ 0 & 0 & 0 & 0 & I_{yy} & 0 \\ 0 & 0 & 0 & I_{zx} & 0 & I_{zz} \end{bmatrix} \tag{3.31}$$

In this matrix:

- m = mass of the vessel
- $I_{ii} = k_{ii}^2 \cdot m$ = mass moment of inertia about the ith axis ($i = x, y, z$)

The component I_{xz} and I_{zx} is the mass moment of inertia for roll-yaw coupling. This can be considered zero if a vessel has fore-aft symmetry, or otherwise can be neglected because it is very small.

The hydrodynamic restoring matrix $[C]$ is defined as:

$$[C] = \begin{bmatrix} 0 & 0 & 0 & 0 & 0 & 0 \\ 0 & 0 & 0 & 0 & 0 & 0 \\ 0 & 0 & c_{33} & 0 & c_{35} & 0 \\ 0 & 0 & 0 & c_{44} & 0 & 0 \\ 0 & 0 & c_{53} & 0 & c_{55} & 0 \\ 0 & 0 & 0 & 0 & 0 & 0 \end{bmatrix} \tag{3.32}$$

Only the motions heave, roll and pitch have a hydrostatic restoring coefficient. The values for these coefficients can be determined using the equations (3.33) to (3.36).

$$c_{33} = \rho g \cdot A_{WL} \tag{3.33}$$

$$c_{44} = \rho g \nabla \cdot \overline{GM}_T \tag{3.34}$$

$$c_{55} = \rho g \nabla \cdot \overline{GM}_L \tag{3.35}$$

$$c_{35} = c_{53} = \rho g \cdot S_{WL} \tag{3.36}$$

In which:

- A_{WL} = waterline area
- $\overline{GM}_T$ = transverse metacentric height
- $\overline{GM}_L$ = longitudinal metacentric height
- S_{WL} = first order moment of the waterline

3.3.3 Roll damping

The damping matrix that is obtained by Ansys AQWA. This, however, is only the potential damping. The so-called viscous damping is not included in this, but this has a significant contribution to the roll damping of the vessels. During model tests performed at MARIN in 2013 (van Essen, et al., 2013), the linear and quadratic roll damping was obtained for the model by means of curve fitting. The potential damping is subtracted from the results to obtain the viscous roll damping terms, listed in Table 3.1.

Linear viscous roll damping	$B_{44}^{(1)}$	18,480 kNm/rad/s
Quadratic viscous roll damping	$B_{44}^{(2)}$	593,011 kNm/rad/s²

Table 3.1 Viscous damping terms obtained from MARIN model tests

According to (Journée & Massie, 2001), the additional roll damping has a highly non-linear behaviour. This can be linearized by means of an equivalent linear damping coefficient $B^{(eq)}$, according to:

$$B_{44}^{(eq)} = B_{44}^{(1)} + \frac{8}{3\pi} \cdot \omega \cdot \phi_a \cdot B_{44}^{(2)} \tag{3.37}$$

This now becomes a function of both the wave frequency and the roll amplitude, which can be included in the model.

3.4 Load behaviour

If a load is suspended from deck and under the influence of the environment, it will most likely start to move in all kinds of directions. In Figure 3.1 these influences are illustrated in three different categories: A, B and C.

The influences on the motions of a load from category A are mainly the motions of the vessel. These motions of course are influenced by waves, wind, current, etc. and cause the tip of the crane from which the load hangs to move. The motions in surge and sway direction will most likely not influence the motions of the load due to the inertia of the mass in water. This can be illustrated by the following example: If the ship were to move 2 meters in surge direction, and the load were to hang 500 m below the crane tip if it were to hang straight downward, the upward displacement due to the surge motions will be only 0.4 cm. Even if the load were to hang 'only' 100 meters below the crane tip, this upward displacement would only be 2 cm, thus it is fair to say that both surge and sway will not influence the motion of the load, if it is assumed that the load will remain in its x- and y-position due to the inertia.
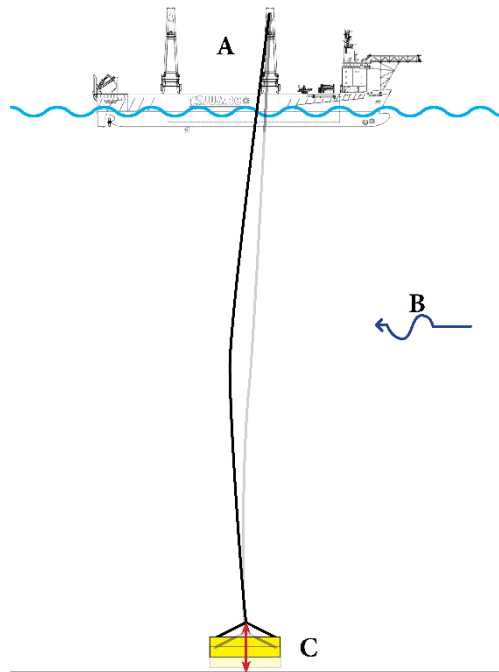

Figure 3.1 Influences on the motions of a heavy load

Heave on the other hand will influence the motions of the load. If it is assumed that the cable will not elongate when it is under a stretching force, and the crane tip would heave 2 meters, the load will also heave 2 meters. Of course, the cable does not behave infinitely stiff, but more like a 'spring'. Again, due to the inertia of the load, the cable will be elongated due to the heave motion of the crane tip, resulting in a phase lag of the heave motion of the load. This phase lag is dependent on the spring stiffness of the cable, which again is dependent on its cross-sectional area and the length of the cable. This also means it varies during the lowering of the load, because the length changes during this process. Note that if the phase lag would be exactly opposite to the crane tip motion, the load would resonate and the heave amplitudes may become much larger than those of the crane tip, which may result in very high forces in the cable and on the connection points!

Category B influences are mainly influences on the cable. In the first place, the cable will be 'pushed' out of its neutral position due to current. On top of that, when a cable, or any object, is subsided in current vortices will occur on the backside of it. These vortices shed alternately on both sides of the cable, creating a lifting force. Due to these alternating vortices, the lifting force also alternates, creating an oscillation of the cable. This is visualized in Figure 3.2. The current in the ocean has a depth profile, which means that the current speeds will not be uniform over the entire depth of the water. This creates variation in the lifting forces along the length of the cable. This again will result in different oscillation amplitudes. At some points the amplitude may become very large because of resonation, and at other points the amplitude might be close to zero. This causes the cable to not hang straight down, but usually in a more bend profile, like displayed in Figure 3.1.
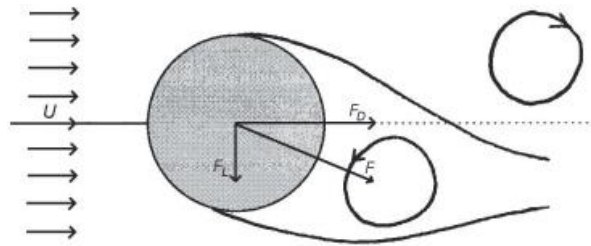
Figure 3.2 Current induced vortex shedding

These oscillations will cause the cable to harmonically 'decrease' in length. It will not actually shorten, but when a line is bent, the distance between the ends approaches each other, which is what happens also in this case. This 'shortening' results in a heaving motion of the load.

The last category, C, that influences the motions of the load, is the load itself. Its weight influences the motions of the cable, because a heavier load will have a higher inertia and will be more likely to move less than a lighter load will. Also, the so-called porosity is of influence. It is more difficult to move a horizontal completely flat plate up in down the water than the same plate oriented vertically. When a load is a very densely packed module, this will need more forces to move, than a very open template. The last part that may have a very large influence, is the proximity of the sea bed. This may create very large added mass problems, and several studies have been executed to describe this phenomenon.

These influences combined make it that the mathematical description of the load behaviour is very complex. Due to this complexity, the load in the crane is modelled as fixed, located in the tip of the crane. The influence of the load is that it causes a shift in GM.

3.5   Ballasting system
The entire system is based on the balance between forces and moments. The moment that is created by the ballasting system is called the restoring moment M_r. There are two possible ways of ballasting, as mentioned in Chapter 1, and these both have a slightly different solving approach in the Simulink model. This paragraph explains both systems.

3.5.1   Restoring moment solid mass
The solid mass displacement system is the simplest of both ballasting systems. The moment that is induced by this system is described by equation (3.38).

$$M_r = mg \cdot d \tag{3.38}$$

In this equation, M_r represents the moment caused by this system, mg equals the force caused by the weight of the solid mass, and d the (vertical) distance between the centre of the solid mass and the COG of the ship. Furthermore, the height of this system in comparison with the ship's COG is of influence on the restoring moment. If the mass is placed at a certain distance off-centre above the COG, and induces a roll angle, the arm between both COGs increases as the roll angle increases. If the mass was placed lower than the vessel's COG, this arm decreases with increasing roll angle, and, if placed at the same height, the arm remains equal. This can be verified by looking at equation (3.39).

$$d' = \cos\left(\mathrm{atan}\left(\frac{h}{d}\right) - \phi\right) \cdot \sqrt{h^2 + d^2} \tag{3.39}$$

Here, h is the height of the solid mass above the ship's COG. A negative h represents the mass being above the COG. If looked at the difference between a mass being placed 4 meters above or below the COG, and 8 meters off-centre, under a roll angle of 5 degrees, the new arm d' increases from 8 meters to 8.32 meters, and decreases to 7.62 meters, respectively. The system is visualized in Figure 3.3.
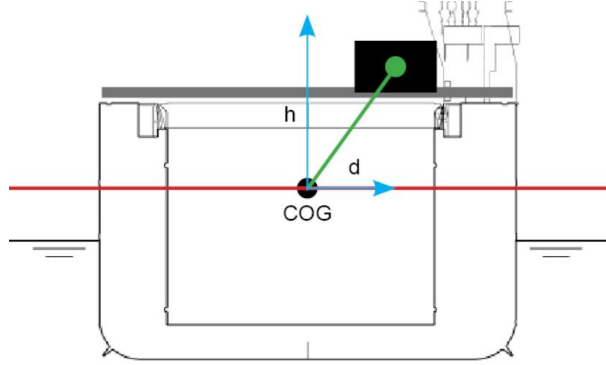
Figure 3.3 Coordinates of the COG of the solid mass ballast

3.5.2 Restoring moment ballasting tanks

This moment is based on the amount of water that is situated in the tanks times the distance the mass is located away from the centre of gravity of the vessel. Again, equation (3.38) applies, where m now equals the mass of the ballast water. The length of the arm varies while the ballast water is moving from side to side, and can be calculated using equation (3.40).

$$d' = \frac{d_{ps} \cdot A_{ps} + d_{sb} \cdot A_{sb}}{A_{ps} + A_{sb}} \tag{3.40}$$

In which the values d_{ps} and d_{sb} represent the vertical arm between the COG of the vessel and the COG of the water mass in the portside and starboard tank, respectively. The values A_{ps} and A_{sb} represent the filled area of the tanks, calculated by the fill height times the tank width.

Furthermore, the height of the water's COG is of influence, and can be determined using equation (3.41).

$$h' = \frac{h_{ps} \cdot A_{ps} + h_{sb} \cdot A_{sb}}{A_{ps} + A_{sb}} \tag{3.41}$$

The influence of the roll motion on the righting arm d' can again be calculated with equation (3.40).

The coordinates and arms are visualized in Figure 3.4 and Figure 3.5.
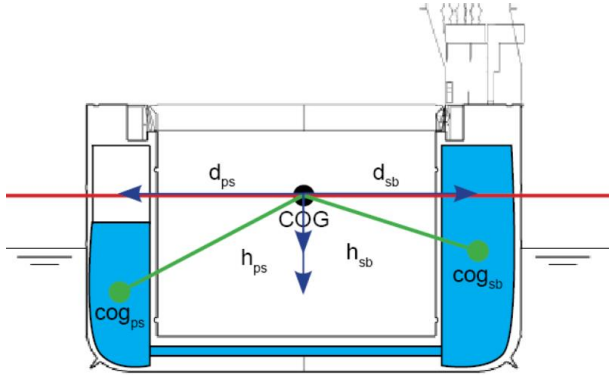
Figure 3.4 Definition of the coordinates of the COGs in the water ballast
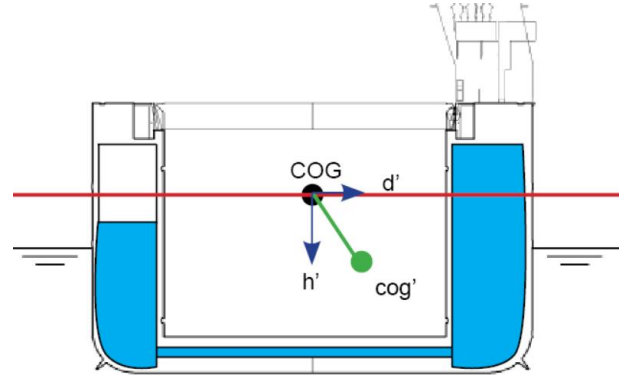
Figure 3.5 Coordinates of the total COG of the water ballast

3.5.3 Heeling angle

The heeling angle of a vessel due to the shifting of weight can be determined by equation (3.42).

$$\phi = \cos^{-1}\left(\frac{\rho\nabla \cdot \overline{GN_\phi} \cdot \sin(\phi)}{p \cdot d}\right) \rightarrow \tan(\phi) = \frac{p \cdot d}{\rho\nabla \cdot \overline{GN_\phi}} \tag{3.42}$$

In which p is the weight of the ballast, c the distance the weight has moved, $\rho\nabla$ the total displacement of the vessel and $\overline{GN_\phi}$ calculated using equation (3.43).

$$\overline{GN_\phi} = \overline{KB} + \overline{BN_\phi} - \overline{KG} \tag{3.43}$$

In which $\overline{KB}$ and $\overline{KG}$ represent the distance between the vessel's keel and its buoyance point and COG, respectively, furthermore equation (3.44) must be used to correct the value for $\overline{BM}$ for the roll motions.

$$\overline{BN_\phi} = \overline{BM} \cdot \left(1 + \frac{1}{2}\tan^2(\phi)\right) = \frac{I_T}{\nabla} \cdot \left(1 + \frac{1}{2}\tan^2(\phi)\right) \tag{3.44}$$

3.5.4 Ballast system dimensioning

Using the abovementioned equations, a first estimate can be made with respect to the necessary amount of ballast weight. If a maximum roll angle of 10° is to be induced, with a GM of 2.6 m, and a maximum moving distance of the ballast of approximately 12 m off centre, then the amount of weight necessary equals approximately 865 tons. If the maximum roll angle is reduced to 5°, this weight decreases to approximately 430 tons. The choice is made to set the mass to 450 tons, as roll angles larger than 5° are not favoured during offshore installations. This will be able to create a roll motion of approximately 5.5°. Using these estimates, both ballast systems can be dimensioned. Note that these are not the final dimensions, but a first try. Of course, the parameters can be optimized in a later stage, however this is out of the scope of this project.

3.5.4.1 Solid mass

The dimensions of a solid mass are straightforward, because it is equal to that of the estimated necessary mass, being 450 tons. Furthermore, the choice is made to place the mass on deck height, approximately 6.5 meters above the COG of the vessel. In the chosen coordinate system, this means it has a z-coordinate of -6.5 meters. It can have a maximum offset from the centreline of ± 12 meters. The properties of the solid mass ballast system are listed in Table 3.2.

Property	Value
Mass	450 t
Vertical offset	-6.5 m
Horizontal offset (maximum)	$\pm$ 12.0 m

Table 3.2 Properties solid mass ballast system

3.5.4.2 Ballast tanks

The dimensioning of the ballast tanks system is a little less straightforward, and subject to much more design choices in comparison with the solid mass system. In Table 3.3 the chosen properties of the initial system are listed.

Property	Portside	Starboard
Tank width	4.3 m	5.2 m
Fill height (maximum)	7.8 m	6.4 m
Tank length	15.0 m	15.0 m
Total volume	500 m^3	500 m^3
Horizontal offset of the cog	-11.1 m	10.65 m
Vertical offset (fully filled)	8.7 m	9.4 m
Vertical offset (10% filled)	12.2 m	12.3 m

Table 3.3 Properties ballast tank system

The width of the side tanks is different from each other in a J-class vessel. This is kept the same way, as altering it would mean large constructional alterations. Furthermore, a ballast tank of 500 m^3 might seem unrealistic, but this could of course be split into separate smaller tanks. Due to practical reasons, each tank will need to have at least a 10% fill in the tank, thus the movable amount is 450 m^3 of water. If assumed that the water has a specific density of 1,000 m^3/kg, this resembles 450 tons, equal to the solid mass system. Furthermore, due to the small width of the tanks with respect to the vessel, sloshing effects are neglected in the model.

3.5.4.3 Ballast speeds

To model the ballast systems, the ballast is said to be able to move at a constant velocity in transverse direction. Realistically, the ballast can only move at a maximum velocity of approximately 2 m/s, as higher velocities will require too much (extra) power. Furthermore, ballast water requires pumps to displace the water. These have their limitations in capacity. To investigate the necessity of higher velocities, the choice is made that the solid mass averaged velocities are 1 and 2 m/s, and the ballast tanks averaged velocities are 0.2 and 1 m/s. The acceleration time for the ballast to reach full speed is 0.5 s, thus the accelerations are 2, 4 and 0.4 m/s^2. The acceleration is kept constant. It is expected that higher velocities will respond more accurately.

3.5.4.4 Inertial influences

Displacing a large, eccentrically located mass, especially accelerating and deceleration a large mass, will have an influence on the motions of the vessel. When the mass changes direction, this causes an impulse in the opposite direction, creating a short extra moment about the x-axis. If the centre of gravity of this mass has a large offset in z-direction, this moment is even larger.

The impulse J that occurs due to the change of direction of the mass can be calculated using equation (3.45).

$$J = F \cdot t = m \cdot \Delta v \tag{3.45}$$

In this equation, Δv is the change in velocity in a certain period. If the impulse is divided by the time this occurs in, and multiplied with the vertical offset of the mass with respect to the COG, the occurring extra inertial moment M_i can be determined:

$$F_i = \frac{J}{t} \rightarrow M_i = \frac{J \cdot z}{t} \tag{3.46}$$

If we assume that the duration of the change in direction takes approximately 1 second, the occurring moments for the different velocities and systems become as large as listed in Table 3.4. Because the accelerations are constant in the model, the moment caused by acceleration or deceleration is constant. When the velocity of the mass does not increase or decrease, the impulse equals zero.

Ballast system	Velocity	M_i
Solid mass	± 1.0 m/s	± 5,850 kNm
	± 2.0 m/s	± 11,700 kNm
Ballast tanks	± 1.0 m/s	± 9,585 kNm
	± 0.2 m/s	± 1,917 kNm

Table 3.4 Inertial moments due to velocity changes in ballast mass displacement

In case of the solid mass system, the mass is placed above the COG. If the mass is changed in direction, the impulse is directed outward, in this case creating an even larger roll moment. The ballast water tanks have their COG below the vessel's COG, causing the impulse to reduce the roll moment.

3.5.5 Power consumption

To move a mass, power is necessary. To accelerate a mass, an even larger amount of power is necessary. If a ballasting system would be incorporated in a Jumbo vessel, it is also of importance to have an estimate of what the amount of power necessary to employ such a system. For this, an estimation for all four ballast systems is done.

3.5.5.1 *Solid mass system*

The equation for the power consumption estimation P for the solid mass system is given in equation (1.2).

$$P = \frac{F \cdot a}{t} \tag{3.47}$$

This is a very much simplified calculation for the necessary power, as it does not incorporate the inclination of the vessel due to roll and the extra power necessary to overcome the extra addition of gravity. To include this in the equation, the following equation is used:

$$P = \frac{(1 + \sin(\phi))Fa}{t} \tag{3.48}$$

The simulations have an acceleration time to the maximum velocity of 0.5 s, this means that the accelerations become 2 and 4 m/s². The estimated power to accelerate the ballast from 0 to its maximum ballast velocity is listed in Table 3.5, under a maximum inclination of 5°.

3.5.5.2 *Ballast tank system*

To make an estimation of the necessary power to transfer and accelerate the water in the ballast tanks, some assumptions must be made, as the configurations are also of influence on the necessary power. To determine the power, it must be known what the pipe length between the ballast tanks is, as well as the diameter, and the amount of bends it has in it. For the power estimation, the length used between the pipes is equal to 17 m. The diameter of one pipe is equal to 0.5 m. To reach the transverse velocities of 1 m/s and 0.2 m/s of the COG of the ballast, the total flow rate must equal 25,8 m³/s and 5.4 m³/s, respectively. To distribute the flow, there will be 5 pumps to displace the water.

These assumptions are necessary to determine the head loss the pump must overcome. The head loss due to pipe friction can be calculated using the following equation:

$$\Delta h_{pipe} = f_D \cdot \frac{1}{2g} \cdot \frac{V^2}{D} \cdot L \tag{3.49}$$

In this equation, f_D represents the Darcy friction coefficient, which is in term dependent on the flow velocity in the pipe and the Reynolds number Re. The Reynolds number can be calculated using equation (3.50).

$$Re = \frac{V \cdot D}{\nu} \tag{3.50}$$

In this equation, ν represents the kinematic viscosity of water. The Reynolds number for both cases equal $2.51 \cdot 10^6$ and $5.26 \cdot 10^5$. Furthermore, the Darcy friction coefficient can be calculated using the Darcy-Weisbach equation:

$$\frac{1}{\sqrt{f_D}} = -2.00 \log \left(\frac{\varepsilon/D}{3.7} + \frac{2.51}{Re\sqrt{f_D}} \right) \tag{3.51}$$

Where ε represents the pipe roughness. For steel, this is approximately 0.0045 mm. With the friction coefficient known, the head losses of the pipes can be calculated. The friction coefficient becomes 0.0423 and 0.0471, respectively, resulting in a head loss of 0.48 and 0.11 m.

Furthermore, head losses occur due to the sudden expansion or contraction Δh_{io} of the pipe flowing into the tank. These head losses can be calculated using equation (3.52), using the values 0.5 for the inlet coefficient and 1.05 for the outlet coefficient.

$$\Delta h_{io} = (K_i + K_o) \cdot \frac{V^2}{2g} \tag{3.52}$$

The total head loss is a summation of the above two calculate head losses. The equation for the power consumption estimation for the ballast system is as follows:

$$P = \rho \cdot Q \cdot g \cdot h \tag{3.53}$$

In this equation, ρ is the density of water, Q is the mass flow rate in cubic meters per second, g the gravitational acceleration and h the head loss that the pump must overcome. Note that this equation is for one flow line, and must be multiplied by five to acquire the total necessary power for the pumps. The total required power for the pumps is listed in Table 3.5. The required power for the ballast tank system is significantly lower than for the solid mass system. The required power is very much dependent on the diameter of the pipes, if a smaller diameter would be chosen, the required power will go up fast, as this causes an increase in the flow velocity which is squared in the equations.

Ballast system	Velocity	P
Solid mass	1.0 m/s	2,000 kW
	2.0 m/s	4,000 kW
Ballast tanks	1.0 m/s	985 kW
	0.2 m/s	34 kW

Table 3.5 Total estimated required power

3.6 Control System

The control system verifies whether the crane tip amplitude is too large, and based on this it calculates whether the displacement of the ballast must be accelerated, decelerated or kept at the same velocity.

3.6.1 PID controller

A Proportional-Integral-Derivative controller, or PID controller, is a control loop feedback system. This type of controller is very common in control systems. It continuously calculates an error value $e(t)$ as an offset between a desired value, and the measured values. In this case, this represents the vertical displacement of the tip of the crane with respect to its original coordinate.

Next, it calculates the correction needed, based on a proportional term K_p, an integral term K_i and a derivative term K_d, hence the name. Equation (3.54) describes the PID controller process:

$$u(t) = K_p e(t) + K_i \int_0^t e(\tau) d\tau + K_d \frac{de(t)}{dt} \tag{3.54}$$

The output value $u(t)$ is the control variable, in this case the vertical location of the ballast system with respect to the vessel's COG.

The three different terms represent the following:

- The proportional term K_p accounts for the present error values
- The integral term K_i accounts for the past error values
- The derivative term K_d accounts for the possible error values in the future

3.6.2 Calculations

The control system needs to calculate what the amount of roll must be, and what that means for the ballast system. Based on the offset of the crane tip in vertical direction, the necessary roll angle ϕ_n can be calculated according to equation (3.55).

$$\phi_n(t) = \alpha - \beta(t) = \tan^{-1}\left(\frac{z}{y}\right) - \sin^{-1}\left(\frac{z - z_{ct}(t)}{\sqrt{y^2 + z^2}}\right) \tag{3.55}$$

In which:

- $\phi_n(t)$ = calculated necessary roll angle at time t
- α = original angle between y-axis and the crane tip (constant value)
- $\beta(t)$ = new angle between the COG z-axis and the crane tip, at time t
- y, z = y- and z-coordinate of the crane tip
- $z_{ct}(t)$ = vertical displacement of the crane tip at time t

For clarification, the different parameters are visualized in Figure 3.6.
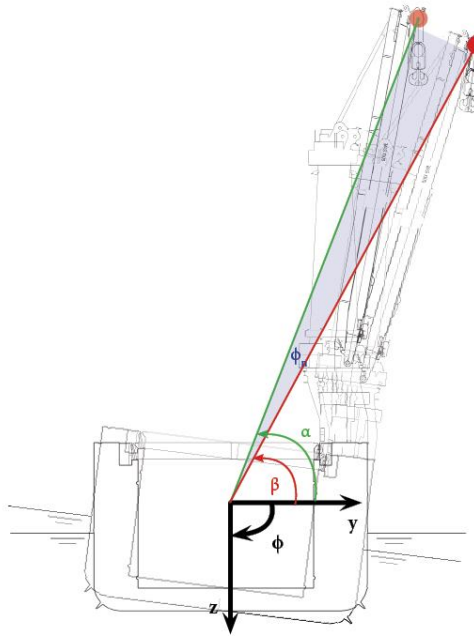
Figure 3.6 Definition of the variables α, β and ϕ_n

The next step is now to determine the arm that is necessary to create the calculated roll angle, according to equation (1.2)

$$\tan(\phi_n(t)) = \frac{p \cdot c(t)}{\rho \nabla \cdot \overline{GN_\phi}} \rightarrow c_n(t) = \frac{\tan(\phi_n(t)) \cdot \rho \nabla \cdot \overline{GN_\phi}}{p} \tag{3.56}$$

Based on the necessary arm c_n, and the current ballast arm, the control system determines if the ballast velocity must increase, decrease, or remain the same.

4 Validation of the Simulink model

In 2012, Jumbo has performed model tests in the Sea Keeping and Manoeuvring Basin of MARIN. The goal of these model tests was to investigate the use of an ART, in combination with a suspended load in the crane. These tests were performed in regular waves as well as in JONSWAP wave spectra, for cases with and without forward speed. In total a few dozen tests were performed, with varying settings. One of these test cases can be used for the validation, the (unscaled) settings of this model test are listed in Table 4.1. For the validation of the Simulink model, a new AQWA analysis is performed with different vessel parameters, amongst which a smaller draught and larger radius of gyration about the x-axis, k_{xx}.

Parameter	Value
Test number	204001
H_s	1.75 m
T_p	12 s
μ	90°
GM	2.19 m
T	7.0 m
k_{xx}	11.26 m

Table 4.1 Relevant MARIN test case

The test case has a JONSWAP wave spectrum mimicked in the tank. During the tank test, the 1:38 scaled model is kept in place by means of a soft mooring system. The measurement systems measure, amongst others, the motions of the model in 6DOF, as well as the wave elevation at two locations. Based on these measurements, several parameters can be calculated. The most important parameters that can be determined, are the RAO values for the vessel motions. This can be done by means of equation (1.2).

$$\frac{x_i}{\zeta_a}(\omega) = \sqrt{\frac{S_{x_i}(\omega)}{S_\zeta(\omega)}} \tag{4.1}$$

In which:

$\frac{x_i}{\zeta_a}(\omega)$ = RAO for motion x_i
$S_{x_i}(\omega)$ = Spectral density of motion x_i
$S_\zeta(\omega)$ = Spectral density of the wave elevation

By means of Fourier analysis of the simulated motions of the vessel without the ballast system, a comparison between the results from Simulink and the towing tank tests at MARIN can be made.

The model used by MARIN and the model available for the Simulink simulations are made as similar as possible, although there are a few small differences between them. The main difference is the displacement of the Simulink model, which is approximately 1.5% larger than that of the scaled MARIN model. This is caused by the simplifications that are made in the AQWA model. Furthermore, the Simulink model has no bilge keels and no rudders, but is compensated for this by means of an equivalent roll damping term, as explained in Chapter 3. It is expected that there will be a small difference between the results of the Simulink model and the MARIN model.

4.1 Fourier analysis

The plotted motions of the Simulink model can be described by a finite number of harmonic components according to equation (4.2).

$$x(t) = x_0 + \sum_{n=1}^{N} x_n \cos(\omega_n t + \varepsilon_n) \tag{4.2}$$

In which:

x_n = the nth amplitude of the harmonic component for the motion
ε_n = the phase angle of the nth harmonic component
ω_n = the angular frequency of the nth harmonic component

The next step is to perform a Fourier transformation of the Fourier series, resulting in equation (4.3).

$$X_T(\omega) = \int_{-T}^{T} x(t) \cdot e^{-i\omega t} dt \qquad (4.3)$$

The final step is computing the spectral density using the Fourier transform. With the obtained spectral density and the JONSWAP spectrum the RAOs can be calculated for the ship motions, using equation (4.4).

$$S_x(\omega) = \lim_{T\to\infty} \frac{1}{2\pi T} |X_T(\omega)|^2 \qquad (4.4)$$

Unfortunately, Matlab is unable to approximate the time series from the simulations with enough Fourier terms. The R^2-value for the Fourier series is less than 0.2, which means the fit is far from accurate. Therefore, the RAOs cannot be calculated from the time series from the Simulink simulation. During the model tests performed by MARIN a few tests in regular waves were performed. However, these were performed with the ART in service, thus are not suitable for comparison with the Simulink model. The next best possible solution to compare the data, is by looking at the time traces of the motions heave, roll and pitch from the MARIN data, and the matching Simulink data, and their statistics.

4.2 Fast Fourier Transform

Matlab has a built-in function called Fast Fourier Transform. This function computes the discrete Fourier transform of a vector a fast Fourier transform (FFT) algorithm. The input of the function is the (evenly spaced) time trace of a signal, for example the heave amplitude of the vessel. This function $Y = \mathrm{fft}(X)$ is defined in Matlab as follows:

$$Y(k) = \sum_{j=1}^{n} X(j) \cdot W_n^{(j-1)(k-1)} \qquad (4.5)$$

In which:

$$W_n = e^{-2\pi i/n} \qquad (4.6)$$

In these equations, n is the length of the input vector. This function will be used for the validation of the Simulink model in comparison with the MARIN tests.

4.3 Results

In, the computed RAOs from the time traces are given in Figure 4.1 to Figure 4.3. Furthermore, the computed RAOs are superposed to the heave motion of the crane tip, shown in Figure 4.4.

4.3.1 RAOs of the COG

From Figure 4.1, it can be seen that both the heave RAO computed from the MARIN tests is very similar to that of the Simulink model. The heave RAO in the very low wave frequency range, between 0 and 0.25 rad/s, is slightly higher during the MARIN tests, but otherwise nearly equal. When looking at roll, it can be seen that the Simulink model has a larger RAO in the region between 0 and 0.3 rad/s. Furthermore, the peak of the Simulink model is higher than that of the MARIN model. Otherwise again the RAO is equal to that of the MARIN tests. The difference in the lower frequency region can be explained by the lack of bilge keels, rudders, and other appendices that are on the MARIN model, but not on the Simulink model. The difference in peak height can be explained by the linearization of the roll damping as described in chapter 3. With higher roll amplitudes, the equivalent roll damping increases, in turn causing a decreasing roll amplitude. Initially, the determination of the equivalent roll damping term is an iterative process, but as the roll amplitude is not varied anymore with the linearization, the roll damping is underestimated if the amplitudes become larger, as is the case around the roll Eigen frequency.

In the case of pitch, see Figure 4.3, there is a larger offset between the MARIN model and the Simulink results. The Simulink results show a smaller response in comparison to the MARIN model over the full wave frequency range, especially in the lower wave frequency region.

4.3.2 Heave RAO of the crane tip

With the composed RAOs from the MARIN and the Simulink results, the RAO for heave of the crane tip can be calculated. This is plotted in Figure 4.4. The plot shows that the RAO from the Simulink model is very similar to the RAO calculated from the MARIN results.
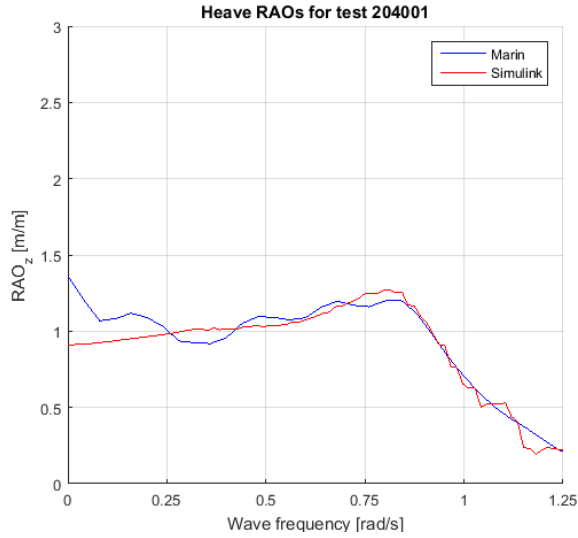
Figure 4.1 Computed heave RAO
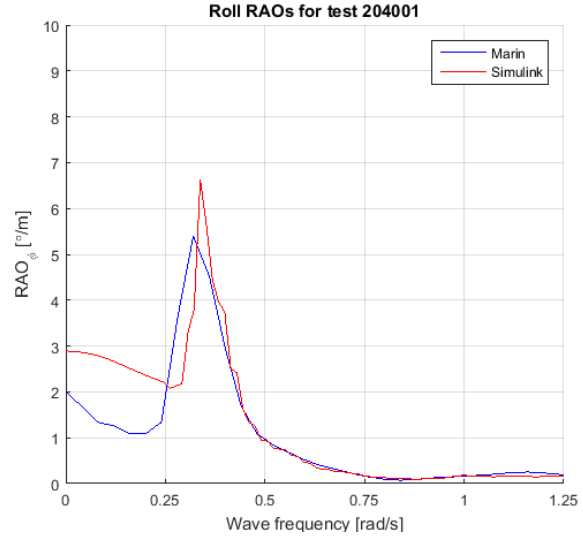
Figure 4.2 Computed roll RAO
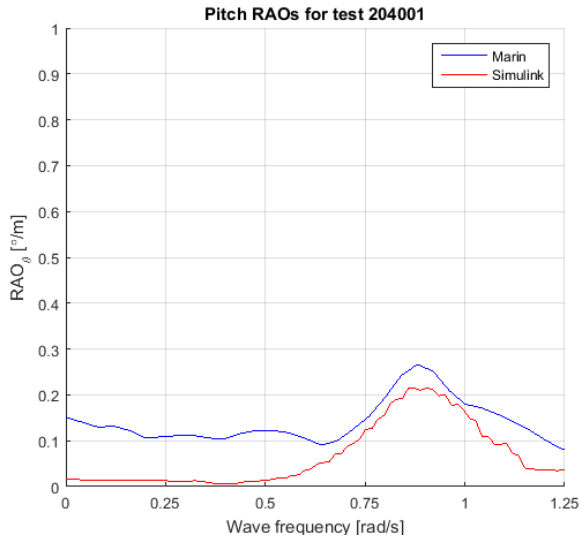
Figure 4.3 Computed pitch RAO
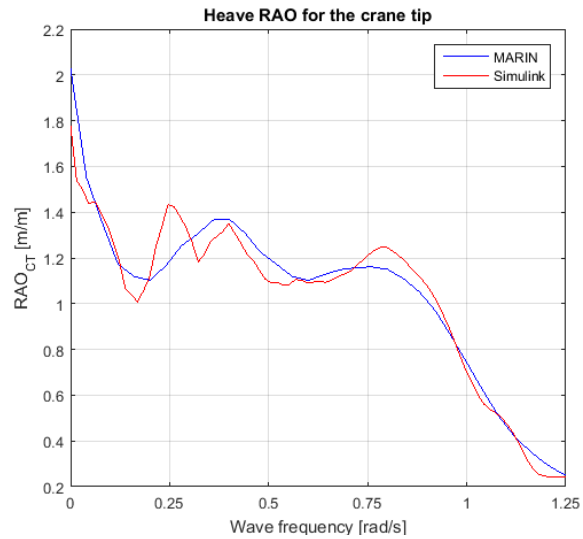
Figure 4.4 Computed heave RAO for the crane tip

4.4 Conclusion

Based on the processed MARIN and Simulink results, it can be concluded that the Simulink model is validated for the wave spectrum with a significant wave height of 1.75 m, a peak period of 12 s, and a wave heading of 90°, with equal parameters for the vessel as used during the MARIN model tests. There are some offsets between the computed RAOs of the vessel's COG, which can be explained. Especially the pitch RAO calculated from the Simulink data is significantly smaller than that of the MARIN data. However, this is acceptable due to the small contribution in the heave amplitude of the crane tip. The conservative roll amplitude in the lower wave frequency region is also acceptable when looking at the computed crane tip heave RAO in Figure 4.4, as these RAOs are approximately equal to one another.

The validation is only performed for vessel motions without the use of an active ballast system, which is only half of the Simulink model. It is proposed to perform model tests including an active ballast system to also validate the ballasting part of the Simulink model. A proposal for this can be found in Appendix B.

5 Simulation results

In this chapter the results of the Simulink model will be presented, analysed and discussed. In the first paragraph an overview of the variations between the different simulations is given. The next paragraph describes the regular wave simulation results, followed by the JONSWAP wave simulations in the third paragraph.

5.1 Simulations

The Simulink model was used to simulate the motions of the vessel in several types of sea. The model was subjected to simulations both with, and without a ballasting system activated. As such, the results can be compared to one another. The following paragraphs first explain the test cases that were performed, followed by the results of the different cases. The results are split up between the different wave profiles.

5.1.1 Test case variations

During a simulation in the Simulink model, several options are varied: the waves in which the vessel is located, and the ballasting system that is used for the compensation of the heave of the crane tip. One simulation lasts 1,500 (virtual) seconds.

5.1.1.1 *Waves*

Out on the ocean, a vessel may encounter all sorts of waves. This varies quite a lot depending on the location of the operational area of the vessel. Variations throughout the simulations in the wave profiles are wave height, wave period/length and wave heading.

Regular wave

The regular waves that are used during the simulations has an amplitude of 1.0 m. Furthermore, the wave heading is varied in steps of $45°$ starting from $0°$ until $315°$. Lastly, the regular waves are changed in wave frequency, starting at 0.1 rad/s until 0.4 rad/s, as Jumbo experiences most difficulties with swell waves.

JONSWAP wave spectrum

The JONSWAP wave spectrum is varied in the same manner for the wave heading as is done for the regular wave patterns. Furthermore, the significant wave height is varied from 0.5 m until 2.5 m, in steps of 0.5 m. The peak frequency is varied from 16 to 19 s.

5.1.1.2 *Ballasting system*

There are two types of ballasting systems; the solid mass and the ballast tank systems. The simulations for the both systems are done as described in Chapter 3. For convenience, some abbreviations are used throughout this chapter: S1 and S2 stands for the solid mass system at maximum velocity number one and two, 1 and 2 m/s, respectively, where T1 and T2 stands for the ballast tank system at maximum velocity number one and two, 1 and 0.2 m/s respectively.

5.1.2 Representation of the results

The (unprocessed) output of the Simulink model for one separate simulation consists of, amongst others, the following:

- Vessel motions
- Crane tip motions
- Ballast system
- Wave elevation

The simulation model has much more data that can be extracted from a simulation, for instance accelerations, wave forces, drift forces, etc., but for this project is resided to the above output.

5.2 Regular wave results

In total 128 different simulation settings exist, combining the different settings: four wave frequencies, four ballast system settings and eight wave headings. To represent the results in a clear manner, the RAO for heave of the crane tip is plotted for the different wave frequencies, split up per wave heading, shown in Figure 5.1. In this figure, the uncompensated heave amplitude divided by the wave amplitude for the crane tip is plotted (red), as well as the solid mass ballast systems, with their maximum velocity of 1 and 2 m/s (blue and green, respectively), and the ballast tank system, with their maximum velocity of 1 and 0.2 m/s (magenta and cyan, respectively). Furthermore, the decrease in the RAO value per ballast system are tabulated per wave frequency in Table 5.1 to Table 5.4. The decrease is calculated using equation (5.1).

$$\text{decrease} = \frac{RAO|_C - RAO|_U}{RAO|_U} \cdot 100\% \qquad (5.1)$$

In which $RAO|_U$ is the uncompensated RAO, and $RAO|_C$ the compensated RAO.

In the following sub-paragraphs the influence of the wave heading, and frequency, as well as the ballast system will be discussed based on these results.
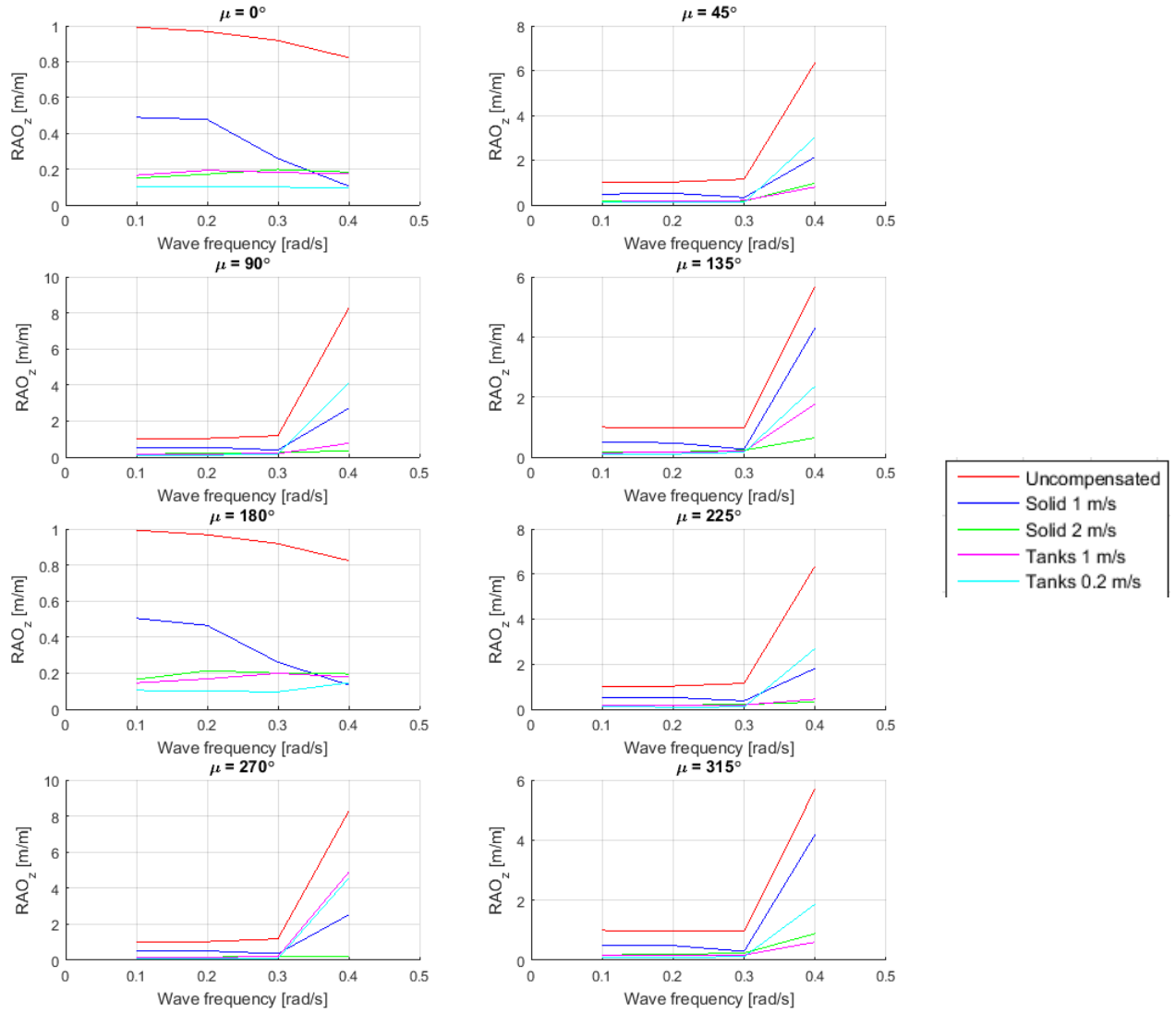
Figure 5.1 Heave RAOs of the crane tip for the different ballasting systems

μ	S1	S2	T1	T2
0°	-50.8%	-84.9%	-83.3%	-89.9%
45°	-51.7%	-84.9%	-85.6%	-89.7%
90°	-49.5%	-83.0%	-85.3%	-89.9%
135°	-50.5%	-82.5%	-86.2%	-89.8%
180°	-49.2%	-83.3%	-85.3%	-89.5%
225°	-47.4%	-84.9%	-83.5%	-89.6%
270°	-49.9%	-84.4%	-86.1%	-89.7%
315°	-48.4%	-82.2%	-83.0%	-89.4%

Table 5.1 Decrease in crane tip heave RAO for ω = 0.1 rad/s

μ	S1	S2	T1	T2
0°	-71.8%	-78.4%	-80.2%	-89.1%
45°	-71.1%	-84.9%	-82.6%	-90.7%
90°	-67.1%	-79.7%	-83.5%	-84.9%
135°	-72.7%	-76.4%	-80.0%	-83.3%
180°	-71.6%	-78.1%	-78.3%	-89.5%
225°	-67.3%	-81.2%	-83.4%	-91.4%
270°	-69.0%	-80.9%	-82.7%	-91.6%
315°	-69.0%	-75.0%	-81.6%	-87.7%

Table 5.3 Decrease in crane tip heave RAO for ω = 0.3 rad/s

μ	S1	S2	T1	T2
0°	-50.7%	-82.3%	-80.0%	-89.7%
45°	-49.2%	-81.1%	-84.6%	-89.8%
90°	-47.1%	-80.5%	-83.3%	-89.8%
135°	-51.4%	-82.6%	-82.6%	-89.4%
180°	-52.0%	-77.9%	-82.6%	-89.6%
225°	-49.3%	-82.2%	-85.0%	-90.6%
270°	-50.2%	-83.4%	-83.8%	-90.4%
315°	-50.1%	-79.3%	-83.1%	-90.0%

Table 5.2 Decrease in crane tip heave RAO for ω = 0.2 rad/s

μ	S1	S2	T1	T2
0°	-87.2%	-77.7%	-79.0%	-88.7%
45°	-66.3%	-84.8%	-87.4%	-52.4%
90°	-67.2%	-95.7%	-90.7%	-50.1%
135°	-24.4%	-88.7%	-68.9%	-58.4%
180°	-83.7%	-76.2%	-78.3%	-82.2%
225°	-71.5%	-95.0%	-93.0%	-57.6%
270°	-69.6%	-97.2%	-41.0%	-45.0%
315°	-26.7%	-84.4%	-89.4%	-67.3%

Table 5.4 Decrease in crane tip heave RAO for ω = 0.4 rad/s

5.2.1 Influence of wave parameters

The uncompensated heave RAO of the tip of the crane is approximately 1 for all wave headings in combination with a wave frequency of 0.3 rad/s or smaller. The wave heading becomes of importance as soon as the wave frequency is around 0.4 rad/s, as this is near the roll Eigen frequency of the vessel. From Figure 5.1 it can be noted that for the wave frequency of 0.4 rad/s the crane tip heave RAO can become very large for waves not being following or head waves. This is due to the fact that the heave motion of the crane tip consists of heave, roll and pitch. With following and head waves, the vessel will not roll, but when the waves come from either side, the contribution of roll will increase greatly, especially around the Eigen frequency.

Another point of attention is the difference in results between waves coming from portside or starboard. The cause of the RAOs not being equal for symmetric waves (for instance a wave heading of 135° and 225°), is the location of the tip of the crane. This location has an offset in all three directions, causing the plots being different from each other.

5.2.2 Influence of the ballast system

All applied simulated ballast systems cause a reduction in the crane tip heave amplitude in comparison with an uncompensated simulation. There are a few things to discuss based on the plots in Figure 5.1 and the decreases listed in the tables. Looking at the range between 0.1 and 0.3 rad/s, the S1 system performs least of all fours system settings. This is the case for all wave headings. Furthermore, for the same wave frequency range, the T2 system performs best with the largest decreases.

ω	S1	S2	T1	T2
0.1 rad/s	-49.7%	-83.8%	-84.8%	-89.7%
0.2 rad/s	-50.0%	-81.2%	-83.1%	-89.9%
0.3 rad/s	-69.9%	-79.3%	-81.6%	-88.5%
0.4 rad/s	-62.1%	-87.5%	-78.4%	-62.7%

Table 5.5 Averaged decrease over all wave headings, per ballast system

The wave frequency close to the roll Eigen frequency is a bit more unclear as to which system and setting is performing least and best, looking at Table 5.4. At first glance, the S2 system seems to perform best, and either the S1 system or the T2 system seem to perform least. Taking the average total percentage of each system results in an average decrease of 87.5% for the first mentioned, and an average decrease of 62.1% and 62.7% for the second mentioned systems, respectively. The average decreases, per wave frequency per system, are listed in Table 5.5. The T1 system has an average decrease of 78.4%. Averaging the decreases over all frequencies and headings gives the decreases as listed in Table 5.6.

System	Average decrease	Ranking
S1	-56.5%	4
S2	-82.9%	1
T1	-82.0%	3
T2	-82.7%	2

Table 5.6 Averaged decrease in heave RAO for all ballast systems

Summarizing the results of the regular wave simulations:

- All systems cause a decrease in heave amplitude
- For ω = 0.1 – 0.3 rad/s, the S1 system performs least of all
- For ω = 0.1 – 0.3 rad/s, the T2 system performs best of all
- For ω = 0.4 rad/s, the S1 system is the least performing system
- For ω = 0.4 rad/s, the S2 system is the best performing system
- Overall, the S2 system, and both T1 and T2 systems perform approximately and equally well with a decrease between 82 and 83%

5.2.3 Processing the results

From the results of the regular wave simulations, several influences will be discussed, or require elucidation. The location of the COG of the ballast has an influence on the performance of a ballasting system, as well as the velocity. Furthermore, these influences are also discussed for a different wave amplitude.

5.2.3.1 Location of the COG of the ballast

As shown in Table 5.6, the S1 system performs least of all systems, where the T1 system performs much better. This can be explained by the location of the COG of the ballast with respect to the COG of the vessel and the impulse caused by the acceleration and deceleration of the ballast.

The solid mass is placed above the COG of the vessel, where the ballast water is below the vessel's COG. The impulse of deceleration is directed outward, independently from if it is travelling towards portside or starboard side. This impulse causes a roll moment. In case of the solid mass, this impulse increases the roll moment, where in case of the ballast tanks, this impulse the roll moment

decreases. The latter is convenient, as when the mass must decelerate, the roll moment should also decrease, therefore the ballast tank system performs better at the same maximum velocity than the solid mass system.

5.2.3.2 *Ballast velocity*

Both ballast systems are simulated at two different (maximum) ballasting velocities. The result in decrease differs between the two velocities, for both systems. However, in case of the solid mass system, the faster system performs better, where in case of the ballast tank system the slower system performs better, on average. The better performance of both velocities can be explained by a combination of the responsiveness of the system, the moment caused by the impulse, and the location of the COG of the ballast.

The solid mass system performs better at higher velocities. This is mainly caused by the responsiveness of the system; the system responds to the calculations of control system, determining the necessary ballast arm. Because the system is a responding system, it always has a lag between where the ballast's COG should be and where it currently is located. Logically, the faster system can reach the necessary ballast location quicker than the slower system. This causes the system to have to accelerate less, and travel at constant speed more, resulting in less extra roll moments caused by the impulse of acceleration or deceleration.

In the case of the solid mass system, the differences between the two maximum velocities is much smaller: the slower system only performs an averaged 0.7% better than the faster system. This is caused by the impulse from acceleration and deceleration, combined with the location of the COG of the ballast.

Firstly, the impulse caused by the change in velocity is five times larger for the faster system. In case of acceleration, the impulse causes an increase of the roll moment, and vice versa for deceleration. The roll moment caused by the impulse is of very large contribution to the total roll moment. At smaller ballast arms (less than 2 m), the impulse of the faster system actually counters the ballast moment caused by the weight, creating an opposite effect to the property of being at the calculated ballast location faster than the slower system. This last property however is the reason why the faster system performs better than the slower system at a wave frequency of 0.4 rad/s, as shown in Table 5.5.

5.2.3.3 *Wave amplitude*

The heave motion of the crane tip consists, as mentioned, from the motion heave, roll and pitch. The results are for a wave amplitude of 1 m. To show the influence of the wave amplitude, the simulations were also performed for a wave amplitude of 2 m. The roll RAO for larger wave amplitudes will cause a large roll amplitude, causing larger vertical amplitudes at the crane tip. The averaged results are listed in Table 5.7.

System	Average decrease	Ranking
S1	-50.0%	4
S2	-82.9%	1
T1	-75.0%	2
T2	-61.7%	3

Table 5.7 Averaged decreases over all wave headings, per wave frequency, and total, per system, for ζ_a = 2 m

The ballasting still results in decreases of the heave amplitude, but now the performance of the different system changes in comparison with the performances for a wave amplitude of 1 m.

The same explanation can be given for the better performance of the faster solid mass system, in comparison with the slower solid mass system: the ballast can reach the necessary location sooner. The difference between the performances of the two velocities of the ballast tank system can be explained in the same manner: the ballast must reach a certain offset with respect to the centreline of the vessel, within a certain time. This offset has increased due to the larger wave amplitudes, and now the slower system can't reach the calculated offset anymore, as it is simply not fast enough. The ballast tank system still performs better than the solid mass system, when at the same velocity, as explained in the previous paragraph.

5.3 JONSWAP wave spectrum results

The total amount of simulations for JONSWAP wave profiles is a summation of four peak periods, five significant wave heights, four ballast system speed settings and eight wave, thus 640 simulations. The results of the JONSWAP simulations are a bit more extensive, therefore not all results are plotted and listed in this chapter. In this chapter, the results for a significant wave height of 1 m are given. The results for the other values of H_s are processed in a similar manner and given in Appendix D.

To visualize and evaluate the results of the simulations with a JONSWAP wave spectrum, the significant heave amplitude of the crane tip is calculated for each simulation. This is done using equation (5.2) and (1.2). For this, first the spectrum of the heave motion must be determined from the results of the simulations. This is done using FFT. The results are plotted in Figure 5.2.

$$H_{s,z_{CT}} = 4 \cdot \sqrt{m_{0z_{CT}}} \qquad (5.2)$$

$$m_{0z_{CT}} = \int\limits_0^\infty S_{z_{CT}}(\omega)d\omega \qquad (5.3)$$

In which:

- $H_{s,z_{CT}}$ = significant heave amplitude of the crane tip
- $m_{0z_{CT}}$ = first order moment of the spectral density
- $S_{z_{CT}}$ = spectral density of the heave amplitude of the crane tip

Furthermore, the decrease in significant heave amplitude are listed in Table 5.8 to Table 5.11, per peak period, and the averaged decreases overall are listed in Table 5.12.
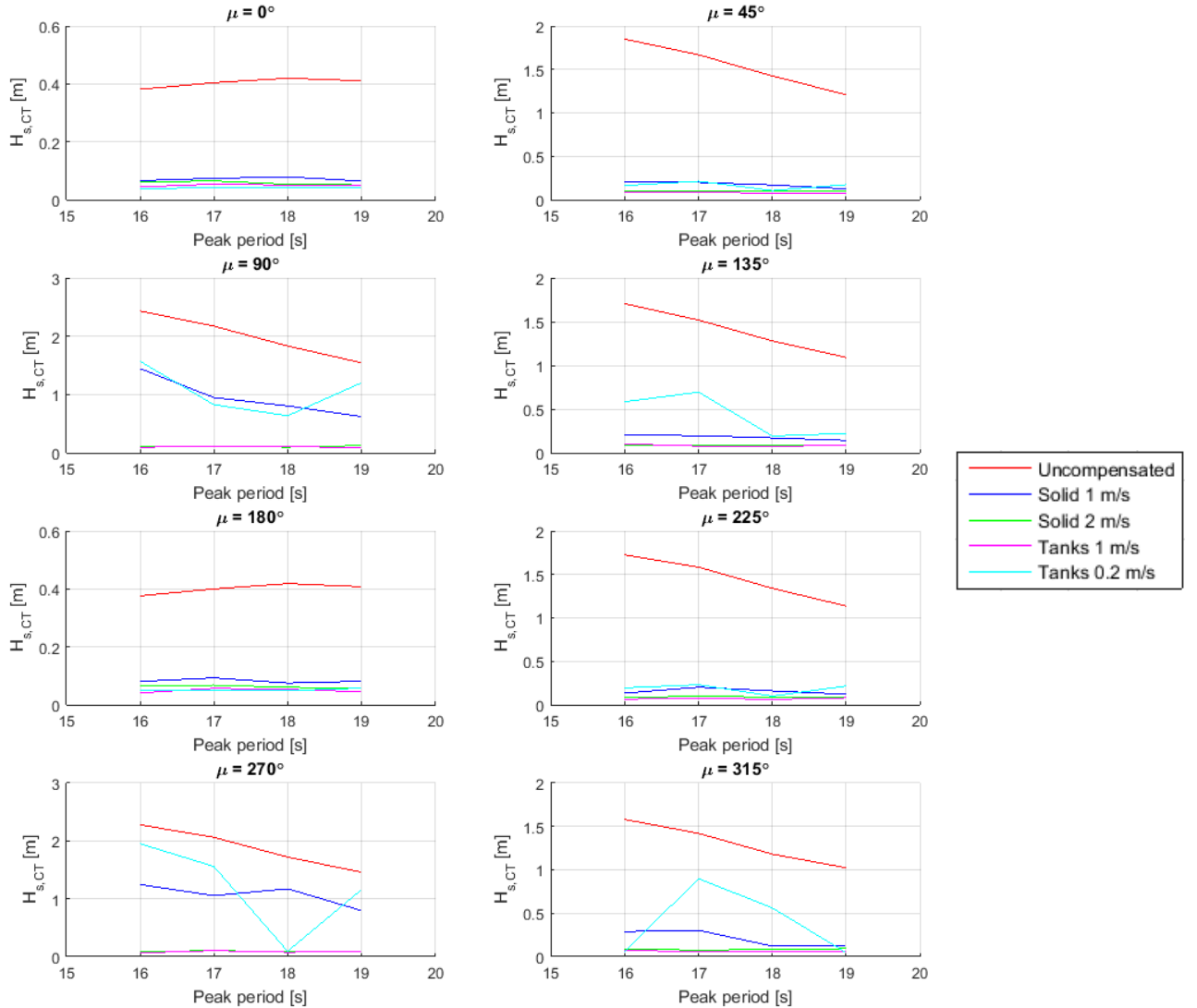
Figure 5.2 Significant crane tip heave amplitudes for the different ballast systems

5.3.1   Influence of wave parameters

The peak period of 16 s is very close to the Eigen period of roll of the vessel. The significant heave amplitudes of the crane tip are the largest for this peak period, when the waves are incoming from portside or starboard. With following of head waves, the significant heave amplitudes are steady for all peak periods. Waves with a direction of 90° or 270° result in the largest significant heave amplitude, due to the rolling of the vessel. Furthermore, the offset of the crane tip on all three axes causes the difference between symmetrical waves about the x-axis.

5.3.2   Influence of the ballast system

All four ballast systems result in a decrease of the significant heave amplitude of the crane tip for all peak periods and wave headings.

μ	S1	S2	T1	T2
0°	-82.7%	-84.1%	-88.4%	-89.8%
45°	-89.0%	-94.4%	-95.5%	-91.2%
90°	-40.6%	-95.1%	-96.1%	-35.5%
135°	-88.2%	-94.9%	-94.0%	-65.7%
180°	-78.5%	-82.4%	-89.2%	-86.9%
225°	-92.2%	-95.2%	-96.3%	-88.7%
270°	-45.3%	-96.2%	-97.1%	-14.4%
315°	-81.7%	-94.5%	-95.3%	-96.0%

Table 5.8 Decrease in significant crane tip heave amplitude for T_p = 16 s

μ	S1	S2	T1	T2
0°	-81.2%	-87.3%	-88.0%	-90.1%
45°	-88.1%	-93.3%	-94.5%	-92.6%
90°	-56.1%	-94.7%	-94.3%	-65.3%
135°	-86.7%	-92.9%	-94.3%	-85.0%
180°	-82.1%	-85.6%	-87.4%	-88.5%
225°	-88.1%	-93.4%	-95.4%	-92.5%
270°	-31.8%	-95.1%	-95.5%	-94.6%
315°	-89.8%	-93.0%	-94.5%	-52.4%

Table 5.10 Decrease in significant crane tip heave amplitude for T_p = 18 s

μ	S1	S2	T1	T2
0°	-81.8%	-83.9%	-86.6%	-90.0%
45°	-88.1%	-94.4%	-95.2%	-87.3%
90°	-56.4%	-94.9%	-94.6%	-62.0%
135°	-87.1%	-94.2%	-94.9%	-54.3%
180°	-76.8%	-83.1%	-85.9%	-87.3%
225°	-87.3%	-93.7%	-95.3%	-85.5%
270°	-48.9%	-94.9%	-94.9%	-24.4%
315°	-78.6%	-94.6%	-96.1%	-36.8%

Table 5.9 Decrease in significant crane tip heave amplitude for T_p = 17 s

μ	S1	S2	T1	T2
0°	-84.3%	-87.5%	-88.1%	-90.3%
45°	-89.7%	-91.3%	-93.9%	-85.6%
90°	-59.7%	-91.9%	-94.1%	-22.3%
135°	-86.9%	-92.6%	-91.9%	-79.7%
180°	-80.1%	-86.1%	-89.0%	-86.0%
225°	-89.4%	-92.2%	-93.0%	-81.0%
270°	-45.3%	-93.2%	-93.6%	-20.8%
315°	-87.8%	-90.9%	-93.8%	-95.5%

Table 5.11 Decrease in significant crane tip heave amplitude for T_p = 19 s

System	Average decrease	Ranking
S1	-75.9%	3
S2	-91.6%	2
T1	-93.0%	1
T2	-72.4%	4

Table 5.12 Averaged decrease in significant heave amplitude for all ballast systems

5.3.3   Processing the results

The influences on the results of the JONSWAP wave simulations will be elucidated and discussed here. As was the case for regular waves, the location of the COG of the ballast is of influence in the performance of the ballasting. The same holds for the ballasting velocity. Lastly, the results of different significant wave heights will be discussed.

5.3.3.1   *Location of the COG of the ballast*

The influences of the height of the COG of the ballast is compared by looking at the results from the S1 system and the T1 system. From the simulations with regular waves it already became clear that the height of the COG with respect to the vessel's COG is of great importance, due to the sign of the moment caused by the impulse of the acceleration and deceleration of the mass. From the results of the JONSWAP simulations this again becomes clear, looking at the averaged decrease of significant heave amplitude listed in Table 5.12. The averaged decrease over all peak periods and wave directions for the solid mass system is approximately 76%, where the averaged decrease of the ballast tank system is 93%, again showing the influence of the additional roll moment caused by the impulse.

5.3.3.2 *Ballast velocity*

The influence of the maximum velocity of the ballast system is investigated by looking at equal systems, at two different maximum velocities again. From the averaged results given in Table 5.12 it can be read that if the system is faster, its performance increases, as was also shown from the regular wave simulation results.

5.3.3.3 *Different significant wave heights*

As was mentioned in the introduction of the chapter, the simulations were also performed for significant wave heights of 0.5, 1.5, 2.0 and 2.5 m. In Appendix D the plots similar to Figure 5.2 are given for these results, as well as the tabulated results. All the averaged decreases over all peak periods and wave directions are listed in Table 5.13.

H_s	S1	S2	T1	T2
0.5 m	-81.7%	-88.3%	-90.8%	-86.3%
1.0 m	-75.9%	-91.6%	-93.0%	-72.4%
1.5 m	-65.6%	-92.9%	-93.3%	-65.4%
2.0 m	-57.9%	-93.4%	-92.7%	-58.7%
2.5 m	-53.7%	-93.6%	-88.3%	-57.7%

Table 5.13 Summary of all averaged decreases for the JONSWAP simulations

The application of any ballast system results in a decrease of the heave amplitude. The differences in the decreases are explained in the previous paragraphs. The trend of the better performance of the T1 system in comparison to the S1 system remains and becomes larger as the significant wave height becomes larger. Furthermore, the trend in the higher maximum ballasting velocities outperforming the slower systems, also remains.

6 Conclusion & Recommendations

Based on the results displayed in the previous chapter, conclusions can be drawn. These conclusions concern the type of ballast system, the velocity of the ballasting, and the implementability of a ballasting system. This is concluded with a final conclusion as to which of the simulated systems is most viable for continued research and finally implementation on a Jumbo vessel. Furthermore, the results will be discussed in the second paragraph, and recommendations will be made in the last paragraph of the chapter.

6.1 Type of ballast system

From the comparison between the results of both the regular wave simulations, as the results of the JONSWAP wave simulations with both ballasting systems at equal maximum ballasting velocity, it can be concluded that the ballast tank system performs better than the solid mass system. This is explained by a combination of the impulse due to acceleration and deceleration, and the vertical location of the COG of the ballast in comparison to the vertical location of the COG of the vessel. In the case of the solid mass, which is located at deck height, the impulse caused a negative effect on the necessary roll moment, where the ballast tanks, which a COG located below the vessel's COG, has a positive effect on the necessary roll moment. From this it can be concluded that the ballast tank system is the more interesting option, at equal ballasting velocities, due to the location of its COG.

6.2 Ballast velocity

It is too simple to conclude that a faster system always gives a better performance. Based on the results given in the previous chapter, the regular wave simulations showed that in the case of the solid mass system for both the wave amplitude of 1 and 2 m, as for all significant wave heights in the JONSWAP simulations. On the other hand, the faster ballast tank system performed slightly better but for the regular waves with an amplitude of 1 m. The cause of this is the impulse caused by acceleration; it is too large in the faster ballast tank system, causing it to cancel the roll moment by the offset of the COG of the mass and even causes it to be opposite to what it is calculated to be. On the other hand, in all other cases, the faster system performs better than the slower system. Furthermore, with increasing wave amplitude or significant wave height, the faster systems remain fairly stable in performance, whereas the slower systems have a decreasing performance.

6.3 Overall performance

The JONSWAP simulations are the more realistic results. Therefore, the overall performance of the ballasting systems from the JONSWAP simulations is used for this conclusion. Based on the [Table …], it can be concluded that the S2 and T1 systems perform equal, as do the S1 and T2 systems. The first two systems result in an overall averaged decrease of 92% for all wave directions, peak periods and significant wave heights, where the second two systems result in an overall averaged decrease of 68%. All four systems cause a significant decrease in significant heave amplitude of the crane tip, but the S2 and T1 systems have best overall averaged performance.

6.4 Implementability of a ballasting system

The implementability of a system concerns the physical possibilities in implementing a ballasting system on board a Jumbo vessel. This means whether mayor changes must be made to the ship, as well as estimated power consumption of the ballast system implemented.

In the case of the ballast tank systems, Jumbo vessels are equipped with ballast tanks, as well as pumps to transfer water from one side to the other. Currently, the pumps do not have sufficient capacity to transfer the ballast water at the velocities and accelerations as simulated. This means that the pump and pipe system must undergo an upgrade to facilitate this. Depending on the maximum velocity, the pumps and pipes must become larger. Depending on the number of pumps, also fuel and electricity routing must be upgraded to implement such a system. But, because the tanks are already there, the reduction of available workspace will remain quite small. Furthermore, engineers on board the vessel will not have to extend their knowledge on new systems too much, as pumps are already a very common system on board the vessel.

In the case of the solid mass ballast system, available deck space must be reduced to locate the system. A solid mass with a weight of 450 tonnes which travels from portside to starboard side, including a system that drives the mass, will have a footprint on the deck, which cannot be used for anything else. On the plus-side, if the system would be built up from modules, it could be placed on deck, and removed if not necessary. Furthermore, the deck strength of the ship must be increased, as the current deck strength is not sufficient to carry such a large load. For a solid mass ballast system, a full system must be engineered, including the training of the engineers on board to handle the solid mass driving system.

In terms of power requirements, the faster a system is, the more power it requires. Furthermore, accelerating a very large mass requires a lot of power, as was shown in Chapter 3. The S1 and S2 systems require almost two and four times as much power compared to the T1 system. The T2 system barely requires any power, this is caused by the low flow velocities in the pipes. Of course, these estimates are based on assumptions in terms of the configuration of the systems.

To conclude on the implementability of the ballast systems, it will take less rigorous changes to implement the ballast tank system, than it would take to implement the solid mass system. In terms of power consumption, the most favourable option is also the ballast tank system.

6.5 Most viable system

The above conclusions are listed in Table 6.1, and sorted in performance. The final row gives a summation of these numbers. The system with the lowest number is the most viable system.

	S1	S2	T1	T2
COG	3	3	1	1
Velocity	3	1	1	3
Performance	3	1	1	3
Implementable	3	3	1	1
Power	3	4	2	1
Total	15	12	6	9

Table 6.1 Total performance of all systems

The main conclusion of this research, is that the application of an active ballasting system will contribute greatly to the workability of a Jumbo vessel. By reducing the crane tip heave amplitude, a Jumbo vessel will have larger windows of opportunity to work in. Based on the results from Table 6.1, the most viable system for the compensation of the heave amplitude of the crane tip, is the T1 system. This system proves best at nearly all points listed in the table.

6.6 Discussion of the results

A computer model is a representation of reality. In this case, several simplifications were made to create the model, which of course influence the results obtained from it. The simplifications have been listed in Chapter 3. The results of the computer simulations, and the influences of simplifications and the lack of several parameters, will be discussed here.

First, during deep water offshore installations, there are a lot of different parameters that influence the motions of a load. One of these motions is the heaving of the crane tip. For this research, the load is projected to be at the crane tip, ruling out all other influences other than the ship motions. In reality, a load hanging several hundreds of meters below the crane tip will swing and heave by itself, causing a pulling force on the crane tip, influencing the ship motions again. The reduction of the heaving of the crane tip thus only is part of the solution to reduce the heaving of the load in deep water.

Then, a JONSWAP spectrum is a mathematically description of a sea state. During the simulations, only a one-dimensional wave spectrum is used, but a sea state consists not just from waves coming from one direction, but multiple. It is possible to obtain results with directional spreading, but the choice was made only to use unidirectional wave spectra, for ease of processing.

Furthermore, the results have been validated by means of model tests done by MARIN. The MARIN model however could only be used to validate the Simulink model without the ballasting systems implemented, and not the ballasted part of the model. The validation showed that the motions of the MARIN model and the Simulink model resembled quite well, so it is assumed that the implementation of a similar ballasting system as used during the simulations on the MARIN model, will also give a good resemblance. This however, is not validated.

Finally, the control system of the Simulink model is not tuned. It calculates the error in offset in y-direction of the ballast's COG, and determines if the ballast should accelerate, decelerate, or remain at equal velocity. It does this at 20 Hz with linear acceleration. The values for the controller have not been tuned, as the update frequency of 20 Hz was the largest possible for the computer on which the simulations were performed. The results from the simulations were promising at these settings, but for a more realistic model, the control system should be tuned more properly.

6.7   Recommendations

The results of the simulation of the implementation of an active ballast system seem quite promising for the Jumbo vessels. The heave motion of the tip of the crane can be compensated quite well for the performed cases. The left-over heaving amplitude can, if such were to be necessary, be further reduces by for instance the passive heave compensator that Jumbo already has at its disposal. The simulation however is not entirely sufficient yet, as was discussed in the previous paragraph. Thus, based on the discussion of the results, several recommendations can be made for further research.

The first recommendation would be to implement load behaviour into the Simulink model. The interaction between load motions and vessel motions could be of great contribution to the performance of an active ballasting system.

Furthermore, it would be recommended to expand the simulated ballast systems to more realistic and detailed ballast systems. Based on the conclusion that all ballasting systems cause an averaged decrease of the crane tip heave amplitude, and the T1 system being the best performing, it is recommended to investigate into configurations for this system, and modelling these realistically into the Simulink model. Also it would be interesting to investigate the maximum velocity of the ballast, as well as the acceleration of the ballast, as doubling the ballast velocity and acceleration does not double the performance of the system. This again can be combined with implementing a more realistic ballast system in the model.

Another recommendation is the execution of dedicated model tests in order to validate the performance of the ballast system. During the research the intention was set to perform such tests. Due to unforeseen circumstances and setbacks, the tests that were performed were not usable for the validation of either the concept of an active ballast system, or the validation of the Simulink model (either with or without the ballasting system). However, a proposal for executing the tests is added in Appendix B, and these are recommended to be performed.

The control system of the Simulink model is not optimal, yet. It is recommended to further investigate in the tuning of the control system, especially if realistic ballast configurations will be modelled.

Lastly, the Simulink model is already quite insightful. It would be recommended to further expand the model, as it could be an interesting tool for Jumbo to investigate the motions for specific locations of which the wave data is known, even if the ballasting system were not to be implemented at all.

References

Abdel Gawad, A. F., Ragab, S. A., Nayfeh, A. H. & Mook, D. T., 2001. Roll stabilization by anti-roll passive tanks. *Ocean Engineering,* Volume 28, pp. 457-469.

Cerda Salzmann, D. J., 2010. *PhD Thesis: Development of the access system for wind turbines,* Delft: Delft University of Technology.

Cummins, W., 1962. *The impulse response function and ship motions.* Hamburg, Department of the Navy.

Do, K. D. & Pan, J., 2008. Nonlinear control of an active heave compensation system. *Ocean Engineering,* Volume 35, pp. 558-571.

Driscoll, F., Nahon, M. & Lueck, R., 1998. A comparison between ship-mounted and cage-mounted passive heave compensation systems. *OCEANS 1998,* Volume 3, pp. 1449-1454.

Duarte, T., Alves, M., Jonkman, J. & Sarmento, A., 2013. *State-space realization of the wave-radiation force within FAST,* Nantes, France: National Renewable Energy Laboratory.

Fan, W., Hongzhang, J. & Zhigang, Q., 2009. Modeling for active fin stabilizers at zero speed. *Ocean Engineering,* Volume 36, pp. 1425-1437.

Fossen, T. I. & Smogeli, O. N., 2004. Nonlinear time-domain strip theory formulation for low-speed manoeurvring and station keeping. *Modeling, Identificatino and Control,* 25(4), pp. 201-221.

Goeman, A., 1998. *De bepaling van zwaartepuntsligging en massatraagheidsmomenten van een scheepsmodel. Report 1142,* Delft: Delft University of Techonology.

Halse, K. H., Aesoy, V. & Sporsheim, O., 2012. *An active roll reductin system using free flooding tanks controlled by vacuum pumps.* St. Petersburg, Russia, Aalesund University College.

Harenberg, P., 2016. *MSc Thesis: Developing the optimal design solution for Jumbo to increase the offshore stability of a heave crane lift vessel,* Delft: Delft University of Technology.

Hatleskog, J. & Dunnigan, M., 2007. Active heave crown compensation sub-system. *OCEANS 2007 - Europe,* pp. 1-6.

Hejn, K. & Rosenkvist, J. P., 2008. *Thesis: Headtracking using a Wiimote,* Copenhagen: University of Copenhagen.

Holden, C. & Fossen, T. I., 2012. A nonlinear 7-DOF model for U-tanks of arbitrary shape. *Ocean Engineering,* Volume 45, pp. 22-37.

Huisman, 2016. *Wind Turbine Shuttle.* Schiedam: s.n.

Ibrahim, R. & Grace, I., 2010. Modeling of ship roll dynamics and its coupling with heave and pitch. *Mathematical Problems in Engineering,* Volume 2010.

Jensen, F., Kuperman, W., Porter, M. & Schmidt, H., 2011. *Computational Ocean Acoustics.* 8 ed. New York: Springer.

Journée, J. & Massie, W., 2001. *Offshore Hydromechanics.* 1 ed. Delft: Delft University of Technology.

Journée, J. & Naaijen, P., 2008. *Hydromechanics 2. Part 1 Introduction Ship Motions and Manoeuvring.* Delft: Technical University of Delft.

Korde, U. A., 1998. Active heave compensation on drill-ships in irregular waves. *Ocean Engineering,* pp. 541-561.

Koshkouei, A. J. & Nowak, L., 2012. Stabilisation of ship roll motion via switched controllers. *Ocean Engineering,* Volume 49, pp. 66-75.

Liu, Q., Tang, Y., Huang, C. & Xie, C., 2015. Study on a mechanical semi-active heave compensation system of drill string for use on a Floating Drilling Platform.

Marzoek, O. A. & Nayfeh, A. H., 2009. Control of ship roll using passive and active anti-roll tanks. *Ocean Engineering,* Volume 36, pp. 661-671.

Mehling, M., 2006. *Thesis: Implementation of a low cost marker based infrared optical trackin system,* Stuttgart: Fachhochschule Stuttgart.

Millan, J., Thistle, S., Thornhill, E. & Stredulinsky, D., 2007. *Roll reduction control system characteristics of a vessel equipped with Z-drives.* Ottawa, National Research Council Canada.

Moaleji, R. & Greig, A., 2006. *Roll reduction of ships using anti-roll n-tanks,* London: University College London.

Moaleji, R. & Greig, A. R., 2007. On the development of ship anti-roll tanks. *Ocean Engineering,* pp. 103-121.

Perez, T. & Blanke, M., 2012. Ship roll damping control. *Annual Reviews in Control,* Volume 36, pp. 129-147.

Perez, T., Smogeli, O., Fossen, T. & Sorensen, A., 2005. *An overview of the Marine Systems Simulator (MSS): A Simulink toolbox for marine control systems,* Trondheim, Norway: Norwegian University of Science and Technology.

Phairoh, T. & Huang, J.-K., 2007. Adaptive ship roll mitigation by using a U-tube tank. *Ocean Engineering,* pp. 403-415.

Phairoh, T. & Huan, J.-K., 2005. Modeling and analysis of ship roll tank stimulator systems. *Ocean Engineering,* Volume 32, pp. 1037-1053.

Pirates of the Caribbean - At World's End. 2007. [Film] Directed by Gore Verbinski. Unites States: Walt Disney Studios Motion Pictures.

Robichaux, L. & Hatleskog, J., 1993. *Semi-active heave compensation system for marine vessels.* US, Patent No. 5209302.

Saari, H. & Djemai, M., 2012. Ship motion control using multi-controller structure. *Ocean Engineering,* Volume 55, pp. 184-190.

Sharif, M., Roberts, G. & Sutton, R., 1996. Final experimental results of full scale fin/rudder roll stabilisaton sea trials. *Control Engineering Practice,* 4(3), pp. 377-384.

Skandali, D., n.d. *MSc Thesis: Identification of response amplitude operators for ships based on full scale measurements,* s.l.: s.n.

Smith, T. & Thomas III, W., 1990. *A survey of ship motion reduction devices,* Bethesda, Maryland: David Taylor Research Center.

Smogeli, O. N., Perez, T., Fossen, T. I. & Sorensen, A. J., 2005. *The Marine Systems Simulator State-Space model representation for dynamically positioned surface vessels,* Trondheim: Norwegian University of Science and Technology.

Taskar, B. U. et al., 2014. CFD aided modelling of anti-rolling tanks towards more accurate ship dynamics. *Ocean Engineering,* Volume 92, pp. 296-303.

van Amerongen, J., van der Klugt, P. & van Nauta Lemke, H., 1990. Rudder roll stabilization for ships. *Automatica,* Volume 26, pp. 679-690.

van der Logt, M., 2014. *Thesis: Active heave compensator,* Breda: Avans Hogeschool Breda.

van Essen, S., Abeil, B. & Dallinga, R., 2013. *J1800-Class Heavy Lift Vessel (134m); Seakeeping tests, volume 1 - Summary, discussion and conclusion,* Wageningen: MARIN.

van Heijst, J., 2015. *MSc Thesis: Improvement of the workability of monohull heavy lift vessels during lifting operations by reducing roll motion,* Delft: Technical University of Delft.

van Schalkwijk, J., 2015. *MSc Thesis: Increasing the workability for offshore lifting operations by reducing the roll motion,* Delft: Technical University of Delft.

van Slooten, M., 2014. *MSc Thesis: Mathematical modelling of free-flooding anti-roll tanks,* Delft: Delft University of Technology.

Wijaya, A. P., Naaijen, P., Andonowati & van Groesen, E., 2015. Reconstruction and future prediction of the sea surface from radar observations. *Ocean Engineering,* Volume 106, pp. 261-270.

Woodacre, J., Bauer, R. & Irani, R., 2015. A review of vertical motion heave compensation systems. *Ocean Engineering,* Volume 104, pp. 140-154.

List of figures & tables

Figures

Tables

Appendix A
Specifications *Fairplayer*

DP2 Heavy Lift Crane Vessel
FAIRPLAYER

A multi-functional dynamic positioned Heavy Lift Crane Vessel (HLCV) well suited to the offshore requirements of the Energy Industry worldwide.

Length	144.1 m
Breadth	26.7 m
Depth	14.1 m
Accommodation	80 POB
Helideck	Sikorsky S-92
Transit Speed	17 Knots
Mast Cranes	2 x 900 Te
Depth rating	3,000 m

CAPABILITIES

Quayside-to-Seabed

Offering versatility, high transit speed, stability and the ability to work in deep-water and harsh offshore environments, the Fairplayer provides cost effective transport and installation solutions. An exceptionally large, flush working deck and a multi-level cargo hold enables the Fairplayer to add modular components to suit specific project requirements and to integrate all offshore activities from "Quayside-to-Seabed". This unique method saves multiple resources, critical time, complex logistics and offshore interfaces.

Fast Economical Transit and High Workability

The Fairplayer is a large vessel with motion characteristics that allows safe working in the harshest offshore environments. The high freeboard and dock walls protect crew and cargo in harsh weather conditions. A key attribute of Fairplayer is its fast and economical transit speed, saving time and cost to operate in remote logistically challenging locations. On location, its method to lift all components from its own deck ensures maximum safety, installation control and workability.

Dual- Crane Deepwater Heavy Lifting

Fairplayer is equipped with two mast cranes with a Safe Working Load (SWL) of 900Te each. The dual cranes provide tandem heavy lift capacity, dual crane upending capability as well as deep-water lowering capability.

The integrated deep-water deployment systems allow direct lowering and accurate positioning of subsea structures in water depths up to 3,000 m.

Large Main Deck and adjustable Cargo Hold

The main deck has an exceptionally large working area of 3,100 m² and offers a loading capacity of 12 Te/m². The adjustable tween deck has an area of 1,700 m² and offers a loading capacity of 7 Te/m² and the lower hold area of 1,400 m² has a loading capacity of 12 Te/m².

Dynamic Positioning (DP) System

The Fairplayer is fitted with a fully redundant Kongsberg SDP 21 Dynamic Positioning System with six independent reference systems, enabling her to maintain its position during all offshore installation activities.
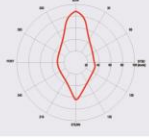
ROV and LARS

During subsea operations the Fairplayer is fitted with two (2) Work Class ROV systems (150HP), launched over the side (starboard and/or portside) with a Launch And Recovery System (LARS) rated to 3,000m depth.

Accommodation/Helideck

The modern living quarters are equipped to accommodate up to 80 persons. All quarters have heating and air-conditioning facilities. The life-saving and fire-fighting equipment are according to the latest class and SOLAS requirements. The helicopter deck is certified for 12,8 Te take-off weight (Sikorsky S-92 Class - CAP 437)

SPECIFICATIONS

General

Call sign	PHPU
IMO no.	9371579
Built	2008
Flag	The Netherlands
Port of Registry	Rotterdam
Classification	Lloyd's Register+ 100A1,
	Strengthened for Heavy Cargos
	LMC, UMS, CG, LI, DP (AA), IWS

Principal Dimensions/Tonnage

Length o.a.	144.1 m
Length b.p.p	133.8 m
Breadth moulded	26.7 m
Depth to Main Deck	14.1 m
Draft (bottom keel)	6.0 m / 8.1 m
Displacement (at 7.5m)	20,120 Te
Deadweight (at 7.5m)	10,700 Te
GRT	15,027 Te
NRT	5,244 Te

Main Deck/Cargo Hold	Area	Strength
Main Deck	3,100 m²	9-12 Te/m²
Tween Deck	1,700 m²	7 Te/m²
Lower Hold/Tank top	1,400 m²	12 Te/m²

Power Plant

Main Engines	2 x MAK 9M 32C 4,500 kW
Auxiliary Engines	2 x Caterpillar 3516B 1,824 kW/ea
Shaft Generators	2 x AEM SE 630 M4 3,000 kW/ea
Emergency Generator	1 x 465 kW

Propulsion Plant

Stern Main Thrusters	2 x Wartsila CPP
Bow Tunnel Thrusters	2 x Wartsila 1,500 kW
Retractable Azimuth Thrusters	1 x Wartsila 1,700 kW

Service Speed

Transit average	17 Knots
Economical	14 Knots

Dynamic Positioning System

DP System	Kongsberg SDP 21
Reference Systems	2 x Seatex 116cm DGPS
	1 x Veripos Verify DGPS
	1 x HiPAP 501
	1 x LTW (tautwire system)
	RADius/Fanbeam

Cranage

Cranes/Type	Huisman Mast Cranes
	2 x 900 Te Revolving
Heavy Lift Capacity	1,000 Te (Offshore)
	1,800 Te (Calm Water/Harbor)
Subsea Lift Capacity	1,000 Te at 1,000 m water depth
	660 Te at 1,500 m water depth
	280 Te at 2,000 m water depth
	200 Te at 3,000 m water depth
Heave Compensation	Passive Heave Compensators
	project specific/tailor made
Ancillary Lifting	Auxiliary Hoists: 2 x 37,5 Te
	Travel Trolley
	Sling Handling Hoists: 2 x 10 Te
	Tugger Winches: 2 x 25 Te / crane
	(constant tension)
	1 x 700 Te Fly-Jib

Capacities

Fuel Oil	1,340 Te I.F.O/290 Te M.G.O
Fresh water	200 Te

Accommodation/Helideck

Accommodation	up to 80 persons (incl. hospital)
	13 x single cabins,
	33 x double cabins
Helideck	12.8 Te (Sikorsky S-92-CAP437)

GENERAL ARRANGEMENT
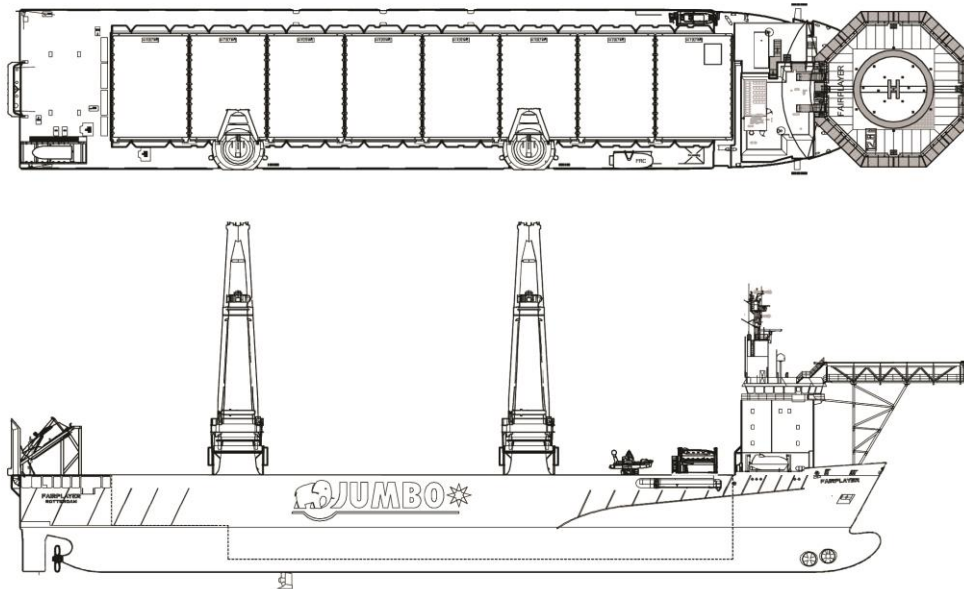
LOAD AND CLEARANCE CURVES
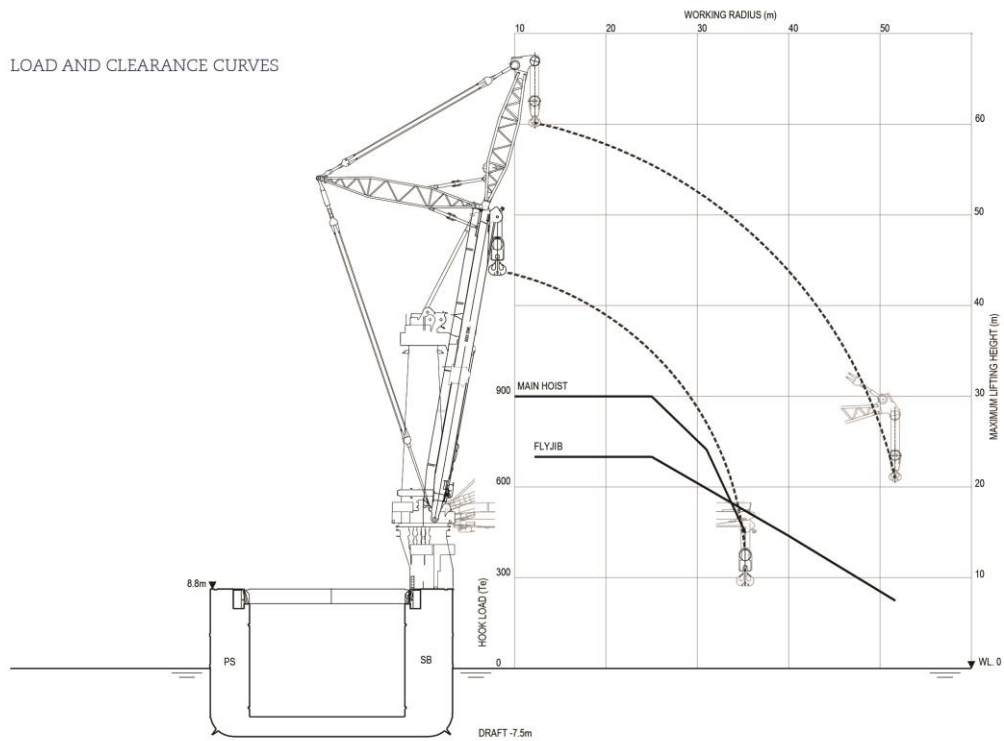
HAVENSTRAAT 23
3115 HC SCHIEDAM
THE NETHERLANDS
PHONE +31 10 79 00 300
INFO@JUMBOMARITIME.NL

Appendix B
Underlying principles of proposed model tests

To verify if the system is working, and compare the results of the computer calculations with reality, physical model tests will need to be performed. This chapter describes the lay-out of the tests, the preparations and the execution. In Appendix C, a proposed description of the tests to be performed can be found.

B.1   Goal

There are a few goals set for the model tests:

- Measure the ship motions with and without the ballasting system activated
- Measure the motions and the expected decrease of the tip of the crane
- Compare the results of the model tests with the results of the computer simulations, with and without the ballasting system activated

B.2   Model test lay-out

The physical test set-up consists of three different parts: the test facility, the actual model, and the necessary measurement equipment. Each part is described in the following sub-paragraphs.

B.2.1   Test facility

Located at the RDM Campus is the Innovations Dock. Within these halls several smaller and larger companies are housed, mainly working on prototypes of sorts of things. Also located within the Innovation Docks, is the Aqualab. The Aqualab is a hydrodynamic laboratory, where research is done for both civil and maritime projects. The specifications of the Aqualab are listed in Table B.1.

Parameter	Value
Length	20 m
Width	10 m
Depth	0.7 m
Wave frequency range	0 – 2 Hz
Maximum wave amplitude	0.15 cm
Maximum wave length	7.00 m

Table B.1 Specifications of the Aqualab

The Aqualab has, apart from what is mentioned in Table B.1 on the wave making capabilities and wave height measurement systems, no other facilities. This means that motion measurement equipment, as well as fixation equipment (such as anchors) all need to be brought to the facility.

B.2.2   Test model

The model that is used for the physical tests consists of two parts: the scaled model of the ship, and the ballast system. Figure B.1 shows the scaled model already mounted with infrared LEDs and the (front) mooring lines in the Aqualab.

B.2.2.1   Scaled model

To perform the tests in the abovementioned Aqualab, a scaled model of the *Fairplayer* is needed. Jumbo has its own scaled model at a scale of 1:38, but this model is too large to be used in the Aqualab. Therefore, a new model is built at a scale of 1:100. The specifications of the model, as it is built, is listed in Table B.2.

Parameter	Value
Scale	1:100
Length	144.1 cm
Width	26.5 cm
Depth	18.5 cm
Actual weight	3.54 kg
Actual draught	1.5 cm
Necessary draught	7.4 cm
Necessary weight	19.78 kg

Table B.2 Specification of the scaled model

The material that is used to for the model, so-called EPS250, has a very low density: only 40 kg/m³. Therefor the weight of the model is not equally scaled, and extra weights are necessary. The necessary weight of the model to reach a draught of 7.4 centimetres, is approximately 19.8 kg. More on this in the Preparations paragraph.

Figure B.1 Scaled model

B.2.2.2 Ballast system

To verify the system that is tested using Simulink, a system must be created that simulates the ballast system. There are several possibilities to do this:

- Build a scaled version of an actual ballast system
- Build a surrogate ballasting system, for instance a moving weight

Initially, a small robot is developed. In short, the essence of the ballast system is that is moves a weight from portside to the starboard side and vice versa, depending on where the weight – according to the control system – is necessary. The robot that is developed to simulate this, is simply a small cart of a certain weight that rides from one side to the other, listening to a small, programmed computer. It is shown in Figure B.2.

The robot is driven by two motor, and controlled by a small computer. Furthermore the robot has an ultrasonic sensor, which can measure the distance between the robot and an object. The weight of the robot is 0.78 kg. It communicates through Bluetooth with the computer.

B.2.3 Measurement equipment

To measure the motions of the model, measurement equipment is necessary. These measurements are both needed for the results of the tests, but also during the test itself, as the motions are determining the response of the ballast system. As this is not readily available in the Aqualab, it needs to be developed.

Figure B.2 Robot mBot Ranger[2]

For this system, eight infrared LEDs are mounted on known positions on the model; four pointing towards portside, and four pointing forward. Furthermore, at a distance two times two infrared cameras are mounted to track the position of the LEDs. As infrared cameras are rather expensive, for this project so-called Wiimotes are used. These are used for the Nintendo Wii, and have an infrared camera located in them which can track the position of up to four infrared LEDs. The Wiimotes are connected to a computer through a Bluetooth connection, and located at a known distance up front of the model and port from the model. The initial locations of the

---

[2] https://www.kiwi-electronics.nl/robotics/robot-kits/makeblock-mbot/mbot-ranger-transformable-stem-educational-robot-kit

LEDs are known by the computer, thus by processing the offset of the LEDs measured by the Wiimotes, the computer can calculate how the model is moving.

Furthermore, 'on-board' is also a 9DOF sensor located: a 3-axis gyroscope, a 3-axis accelerometer and a 3-axis compass in it, hence the 9DOF. This sensor is capable, after some scripting, to determine the amount of roll, pitch and yaw the model makes. This data is again send to the laptop for processing, using the Bluetooth connection.

B.2.4   Control system

During the model tests, there are several computers and sensors that need to work together. The components of the control system are:

- Computer running the control program (Matlab based)
- Wiimotes measuring the locations of the infrared LEDs on the model, transferring the data to the computer by means of Bluetooth communication
- Control and output of the robot and its sensors

The flow of information is visualized in Figure B.3.

As can be noted, the systems are split up into 'onshore' and 'offshore' systems. The offshore systems are located on the model; the onshore systems are not. Furthermore, the infrared LEDs are a separate 'system' on board the model. These LEDs do not need specific information, they simply need to emit infrared light, thus have their own power supply.

B.2.4.1   Onshore systems

The onshore systems consist of the Wiimotes and the control program. The latter is actually the computer used for all the calculations and data processing. As mentioned before, the Wiimotes register the locations of the IR LEDs, and send this information to the computer. The control program then uses this data to calculate what the motions of the vessel and crane tip are, and what the response of the robot must be.

B.2.4.2   Offshore systems

The robot, IR LEDs and the 9DOF sensor are located offshore. The IR LEDs are not really a system, as it needs no controlling.
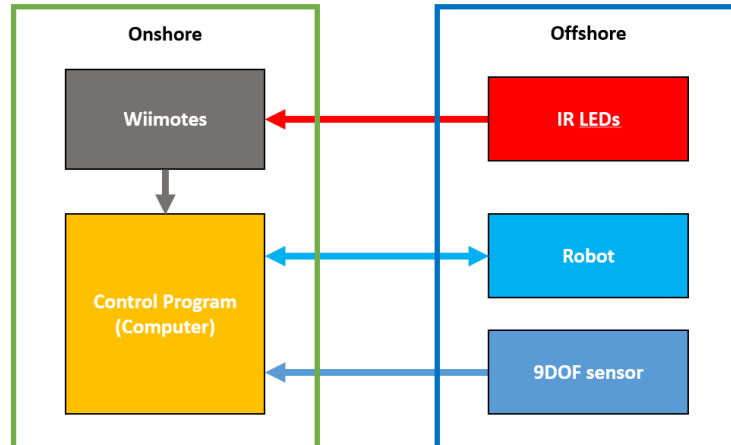
Figure B.3 Information flow of the control system

The robot is controlled by an Arduino based computer, and is programmed using the language C++. This is a fairly simple programming language, and as there are many enthusiasts of this programmable computer all over the world, there is much information available online. Using existing projects and pre-installed libraries as references, the programming of the robot is done. This can be explained fairly easy as the robot only has to listen to what the computer tells it, and execute this. This means it has four options: go forward or go backward, and increase or decrease speed.

The 9DOF sensor sends its data to the computer. This data consists of the measured data, the accelerations in and about all three axis, and the magnetic forces in all three axis directions, as well as processed data, the roll, pitch and yaw angle.

B.2.4.3   Control program

The control program that is needed for the model test, is in fact a slightly altered version of the initial Simulink model. Based on the flowchart in Figure B.3, it can be seen that the input data of the control system is both the data coming from the infrared cameras, as well as measurements from the 9DOF sensor.

Using this information, the control program determines what the orientation of the model is, as well as the offset of the crane tip in vertical direction. This is compared with the previous orientations and offsets to determine if the offset has increased or decreased. Based on these calculations, the control program determines the roll moment needed to compensate the vertical crane tip offset, and again compares this with the previous calculated roll moments.

Next, two scenarios can occur: the moment has increased or the moment has decreased. In the first case the robot must continue moving towards the previously determined side, and in the second case the robot must stop and move in opposite direction. Furthermore, the control program determines if the robot must increase or decrease its speed. This is the output of the control system for the robot.

B.2.5 Full test lay-out

The full test lay-out consists of the model, the ballast system and the measurement equipment, positioned in the test facility. A 3D sketch of the lay-out is shown in Figure B.4.

The ballast system is positioned on the model, at deck height. The cart is put in a wooden container like construction. This is done so that when the model or cart moves to fast, it cannot roll off the model.

The model is positioned inside the towing tank, and is kept in place by means of a four-point spring mooring system. It has two mooring lines attached on the bow, and two on the aft. These lines are spread out to four mounting points on the bottom of the tank. The force on the model caused by the pulling forces of the mooring lines, needs to be known. This can be calculated using equation (B.1)

$$F = k \cdot u \tag{B.1}$$

In which F is the force in Newton, k is the spring constant in Newton per meter, and u is the elongation in meters. The value for k is unknown, but can be determined by putting a weight on the end of the mooring line and measuring the amount it is lengthened by the weight. The value for k of the mooring system is equal to 31.66 N/m.
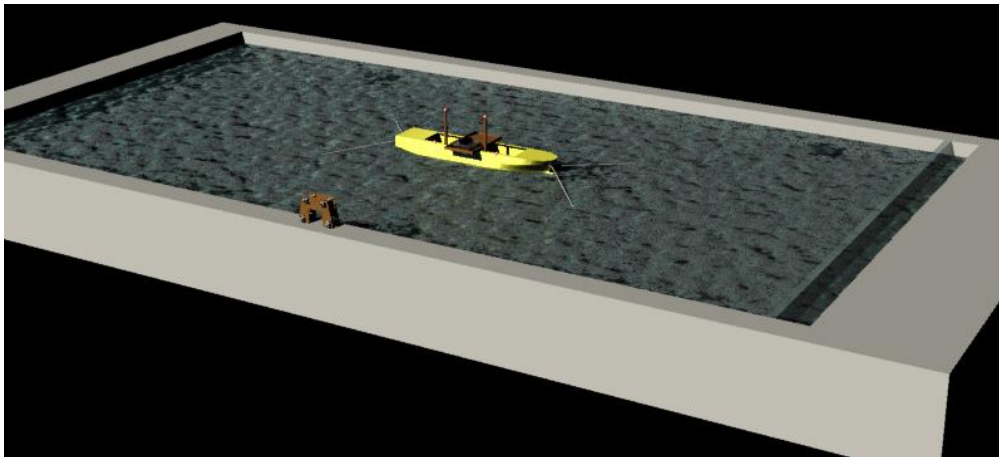
Figure B.4 3D rendering of the complete test set-up

B.3 Preparations

In order to make sure that the model and ballast system work as is to be expected, and equal to the full scale vessel, several calibrations and validations need to be performed beforehand. One can think of determining where the actual COG of the model is located, but also the amount of filtering that is necessary to filter out noise, and implementing damping in the control system of the motor.

B.3.1 Model calibration

3D drawings are provided for a milling-machine, which then produces the model. This milling-machine has a milling-error of approximately 0.1 mm, which means it is rather accurate. Based on this accurate milling, the location of the COG of the model can be estimated quite accurately from the 3D drawings.

Sadly, this is not entirely true for the physical model. To make the model more durable, waterproof and less sensitive to impact, a coating is applied on the outer side. This increases the weight of the model with approximately 75%. As it is unknown how thick the layer is at each outer area of the model, it makes the estimate of the COG a very inaccurate. Thus, the location of the COG of the model needs to be determined by other means. This can be done by using a 'traagheidstafel', possibly translated to 'inertia table', which will be used from now on as the name of this device.

Location of the COG

The location of the COG can be determined with an inertia table. A sketch of such a table is shown in Figure B.5. The numbers in the figure represent the following:

1. The hang-off point (pivot point)
2. The table
3. Springs
4. The foundation
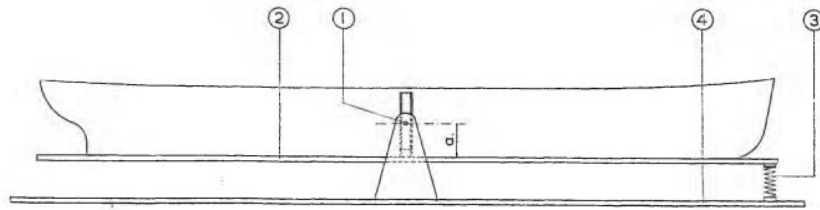
Figure B.5 Sketch of an inertia table

The procedure to determine and verify the location of the COG in height and lengthwise is as follows:

1. The table is hung from the hang-off point at a certain height (a). This resembles the (intended) KG of the model. Also, the springs (3) is set to this length.
2. The springs are detached. The empty table now should hang perfectly horizontal, which can be verified by a level tool. Any offsets can be compensated by a small clump weight.
3. The height of the end of the table above the foundation (4) is measured.
4. A dedicated small weight is placed on the pin, and the amount the table end sags is measured. After this, the weight is removed again.
5. The model is placed on the table, along with the weights and systems that will be on the model during the tests.
6. The model is positioned in such a way that the lengthwise estimated location of the COG is located at the point of rotation, the hang-off point. This will cause the table to hang perfectly horizontal again. Furthermore, the centreline of the model should be parallel to that of the table.
7. If the model does not hang perfectly horizontal, weights must be relocated until it does.
8. The dedicated clump weight is put on the pin again, and the amount of sagging of the end of the table is measured again. If this is equal to the measurement without the model, the estimated height, distance a, is correct and the height KG is determined.

With the location of the COG set, and the assumption that the transverse location of the COG is at the centreline, it can be determined how much weight is necessary and at which location, to decrease or increase the height of the COG. This again can be done by making use of the inertia table.

The location of the centre of gravity is set to the values in Table B.3.

Parameter	Value
Distance above base	12.3 cm
Distance from aft	66.6 cm
Distance off-centre	0.00 cm

Table B.3 Location of the COG of the model

B.3.1.1   Axes of inertia

Apart from the location of the COG of a model, several other parameters must be equal, scaled down, to the full-scale model. The behaviour of the model will be similar to the full-scale vessel, if also the radii of gyration, and thus the mass moments of inertia, are scaled properly. The moments about the y- and z-axis are determined 'dry', the moment about the x-axis is determined in the water ('wet'). The procedures are described here. These scaled properties must be according to Table B.4.

Parameter	Value
k_{xx}	10.9 cm
I_{xx}	2.11 kg.m^2
k_{yy}	36.2 cm
I_{yy}	7.01 kg.m^2
k_{zz}	36.0 cm
I_{zz}	6.97 kg.m^2

Table B.4 Scaled radii and mass moments of inertia

Transverse mass moment of inertia about the x-axis, I_{xx}

The transverse mass moment of inertia is determined in the water. The steps to obtain the value are:

1. The model is put in the towing tank sideways. This is done so that the generated waves by the model will not reflect on the tank-wall, and influence the results.
2. The model is brought in oscillation (the model starts rolling).
3. The oscillation time is measured.

Now the radius of gyration about the x-axis can be determined according to equation (B.2).

$$(k_{xx} + a_{xx}) = \frac{T_\phi \cdot \sqrt{g \cdot GM}}{2\pi}$$
(B.2)

In this equation:

- $k_{xx} + a_{xx}$ [m]   = radius of gyration about the x-axis, including the added mass
- GM [m]   = metacentric height of the model
- T_ϕ [s]   = measured oscillation time

With the determined value for k_{xx}, the value for I_{xx} can be determined according to equation (B.3).

$$I_{xx} = k_{xx}^2 \cdot m$$
(B.3)

In this equation, m represents the total mass of the model.

Longitudinal mass moment of inertia about the y-axis, I_{yy}

After the determination of the COG using the inertia table, the determination of the longitudinal mass moment of inertia can be determined, also using the table. This is done as follows:

1. The springs are reattached to the table ends.
2. The table is brought into oscillation (the model starts pitching).
3. The oscillation time is measured.

With the measured oscillation time now the longitudinal mass moment of inertia can be determined. This can either be done by reading from a graph determined by prof. ir. J.Gerritsma (Goeman, 1998) or by using the following empirical equation given by equation (B.4).

$$I_{yy} = (T^2 - 0.435) \cdot (a + 2.23) \cdot g$$
(B.4)

In this equation:

- I_{yy} [kg.m^2]   = longitudinal mass moment of inertia about the y-axis
- T   [s]   = measured oscillation time
- a   [m]   = height of the pivot point
- g   [m/s^2]   = gravity

If the result is too small, this can be corrected by placing some of the ballast weights further away from the COG, without shifting the weight in height. If the result is too high, logic dictates that the opposite must be done to correct this.

Longitudinal mass moment of inertia about the z-axis, I_{zz}

With the known lengthwise location of the COG and its height, the value of I_{zz} can be determined and altered if necessary. This is done by following the next steps:

1. The model is hung up on two thin wires, where the distance between one wire and the COG is equal to the distance between the other wire and the COG.
2. The model is brought into oscillation about the z-axis (the model make a yaw motion).
3. The oscillation time is measured.

With the measured oscillation time and the following equation, the longitudinal mass moment of inertia can be determined using equation(B.5).

$$I_{zz} = \frac{m \cdot d \cdot T^2 \cdot g}{4\pi^2 \cdot l}$$
(B.5)

In this equation:

- I_{zz} [kg.m^2]   = longitudinal mass moment of inertia about the z-axis
- m   [kg]   = total mass of the model
- T   [s]   = measured oscillation time
- l   [m]   = length of the wires from which the model is hung

B.3.1.2 *Metacentric height*

With the height of the COG known, the metacentric height of the model can be determined by means of an inclining test. This is done in the water, and according to the following steps:

1. The model is put in the water and ballasted such that it is not trimmed lengthwise, not listing to either portside or starboard side, and at the desired draught.
2. A small clump weight is transversely moved from the centreline over a certain distance.
3. The occurring list is measured.

With the measured list, and the known weight and shifted distance the metacentric height can be determined according to equation (B.6).

$$GM = \frac{p \cdot c}{m \cdot \tan(\phi)}$$ (B.6)

In this equation:

- GM   [m]   = metacentric height
- p   [kg]   = shifted clump weight
- c   [m]   = distance over which the weight is shifted
- ϕ [deg]   = occurring list after the shift of the weight

The value of GM should be scaled properly to the desired GM of the full scale ship. If it is too large, this means that COG in height is too small, thus some ballast should be moved up. Thus, this test is also to check the height of the COG. The value for the transverse GM should be 2.37 cm.

B.3.2 Ballast system calibration

There are two parts of the robot that must be calibrated: the speed of the motor, and the echolocation sensor.

The robot returns the distance between itself and the edge back to the computer. This is the feedback on where it is located with respect to the centre of the model. To calibrate this, the robot is set at known distances from a wall. The output of the echolocation sensor is measured for one minute, and averaged. This then is compared with the actual distance, and the offset is accounted for. The amount of noise is very low, less than 2%, and is therefore not compensated for with a filter.

The speed can be regulated by setting the RPM of the motor. The maximum RPM is approximately 180 when loaded. To determine what the actual speed is, related to the RPM of the motor, the robot is asked to move at certain RPMs for 1, 2 and 3 seconds. This results in speeds between 5 and 30 cm/s, for different motor settings.

B.3.3 Measurement system calibration

The last part of the set-up that needs calibration, is the measurement equipment. These are the 9DOF sensor, the Wiimotes, and the wave probe.

B.3.3.1 *9DOF sensor (offshore measurement system)*

The sensor measures 9 different parameters:

- Acceleration in x-, y- and z-direction (translation)
- Acceleration about the x-, y- and z-direction (rotation)
- Magnetism in the x-, y- and z-direction (compass)

If the sensor is held, and kept, still, it will measure where North is, as well as the gravitational accelerations. By reading and storing the data for a certain amount of time, while the sensor is left undisturbed, the mean value of the output can be determined. Also, the variation in the output (the 'shakiness' of the sensor) can be determined, as well as the offset of the mean in comparison with the known location of North and the gravitational acceleration. By repeating this several times, and in several positions, the sensitivity of the sensor can be determined.

The sensor itself is very sensitive and rather 'noisy', and therefore requires a digital filter over the data. For this, a low-pass filter is applied. These types of filters typically provide a smoother form of the signal, removing the short-term fluctuations from it. Matlab has several filter designs in its Signal Processing Toolbox. To not overcomplicate the design, this Toolbox is used for the filtering.

B.3.3.2   Infrared cameras

Each infrared camera that is used during the experiments, measures the positions of four infrared LEDs on board of the model. In total, four cameras are used to track four LEDs. To determine how these cameras measure distances, per camera one LED is set at a known distance from the Wiimote. The Wiimote is asked to measure the location of the LED for one minute. Next the LED is moved a known distance, and the measurement is repeated. This is then processed to verify if the location remains still, and to calculate what the known displacement and the measured displacement ratio is. This is done for each Wiimote, for multiple displacements.

B.3.3.3   Wave probe

The calibration of the wave probe is fairly simple. It is placed in still water. The current measurement now is set to zero, as the wave amplitude is zero at this point. The wave probe is now mounted a known amount lower, or higher, and the wave amplitude is measured again. This must be equal to the amount the probe is lowered, or raised. If this is not the case, the scale must be altered until it does.

B.3.4   Aqualab

During the tests it is necessary to keep track of the wave characteristics, such as the length and height. For this, a measurement device is necessary. The data accumulated from such a measurement system is not necessary to perform the tests, but is necessary for the comparison and validation of the computer simulations later on. The Aqualab has a wave probe available for this, including a computer that processes this data at 60 Hz.

B.4 Execution

In order to validate the made computer simulation model, and the system, several tests are performed. The parameters of influence on the ship motions that can be changed during the tests are the wave length and -height, and the heading of the model. Furthermore, the depth of the water can be varied, but since the depth is already quite shallow (approximately 70 meters at full scale) this will not be done during these model tests.

Each intended test is performed with and without the ballast system activated, and repeated for (at least) four times. Each test will also be executed over a time period of two minutes minimal, after (visual) stabilization of the motions.

B.4.1   Waves

The waves can be varied in both length and height. The main influence of the wave height is the amount of energy that is available to convert into ship motions. The maximum wave height that can be created in the Aqualab is approximately 15 centimetres. This, of course, is far too high for the model as this means that the waves will be 15 meters at full scale. The wave heights that will be used during the model tests are of smaller scale. During the tests the wave height will be varied between 1 and 4 centimetres. This corresponds with a wave height of 1 to 4 meters at full scale.

The wave length is a more complicated parameter to vary. Depending on the wave length, the wave period or -frequency can be determined. This can be done by using the equations (B.7) to (B.9).

$$\omega = \sqrt{k \cdot g \cdot \tanh(kh)} \tag{B.7}$$

$$k = \frac{2\pi}{\lambda} \tag{B.8}$$

$$T = \frac{2\pi}{\omega} \tag{B.9}$$

The results of the wave frequencies and -periods at full scale are listed in Table B.5. The scaled wave frequencies and -periods for the Aqualab are listed in Table B.6, for a water depth of 70 centimetres. Based on the wave characteristics at full scale, the most important wave characteristics can be determined for the scaled model test.

Wavelength	Wave frequency	Wave period
100 m	0.785 rad/s	8.004 s
200 m	0.548 rad/s	11.558 s
300 m	0.430 rad/s	14.621 s
400 m	0.351 rad/s	17.892 s
500 m	0.295 rad/s	21.294 s
600 m	0.253 rad/s	24.798 s
700 m	0.221 rad/s	28.374 s

Table B.5 Unscaled wave characteristics

Wavelength	Wave frequency	Wave period
1 m	7.850 rad/s	0.800 s
2 m	5.484 rad/s	1.146 s
3 m	4.297 rad/s	1.146 s
4 m	3.512 rad/s	1.789 s
5 m	2.951 rad/s	2.129 s
6 m	2.534 rad/s	2.480 s
7 m	2.214 rad/s	2.837 s

Table B.6 Wave characteristics in the Aqualab

There are some wave frequencies that cause resonance for the motions heave, roll and pitch. For roll this occurs at a wave period of approximately 14 seconds in beam waves. Pitch has the largest responses in head waves with a period of approximately 10.5 seconds. Heave responses are largest for a wave period of 8.8 seconds in beam waves, and waves with (infinitely) long period in head waves (over 60 seconds).

Based on these known resonance frequencies, the wave lengths can be estimated. These wave lengths, at full scale and scaled down, are listed in Table B.7.

Resonance period	Motion	Resonance frequency	Wave length	Wave length
8.8 s	Heave (μ=90°)	0.714 rad/s	120 m	1.20 m
10.4 s	Pitch (μ=180°)	0.604 rad/s	165 m	1.65 m
13.9 s	Roll (μ=90°)	0.452 rad/s	275 m	2.75 m
60.0 s	Heave (μ=180°)	0.100 rad/s	2000 m	20.0 m

Table B.7 Wave lengths belonging to the resonance wave frequencies

The waves that will be used during the tests, are listed in Table B.8. The test waves will be combinations of the listed characteristics. Note that not all waves are of importance for all headings. A pitch resonance wave in head waves is not particularly interesting in beam waves.

Wave amplitudes	Wave lengths
1 cm	1.00 m
2 cm	1.20 m
3 cm	1.65 m
4 cm	2.00 m
	2.75 m
	3.00 m
	5.00 m
	7.00 m

Table B.8 Test wave characteristics

B.4.2 Heading

Of course it during offshore installations the most comfortable and stable heading will be chosen, when possible. This (usually) is a heading directly into the waves (μ=180°). Unfortunately, it is not always possible to do this, thus other headings must also be able to withstand as much 'weather' as possible. Therefore, four headings are used during the model tests: μ = 0°, 90°, 135° and 180°. As it is expected that for the wave heading of 0° and 180°, the tests for the wave heading of 0° will not be as extensive as for the heading of 180°.

B.4.3 Tracking and measuring

During the tests a lot of data will be accumulated. This is both necessary for the execution of the tests, as well as for the comparison between the physical results, as the computer simulation results. All data will therefore continuously be stored on the computer. To visualize what is happening during the tests, several plots are live tracking some of the data and results.

B.4.4 Schedule

To execute all tests, a schedule is set up. The Aqualab is available for five days. The full checklist of activities that are intended to be done per day, is listed in Appendix C.

Appendix C
Proposed model tests

This appendix describes the proposed tests and checks for the validation of both the Simulink model, and the ballasting system. This checklist is a guideline, and, of course, may be deviated from if necessary. The test proposal's intended location of the Aqualab at the RDM campus in Rotterdam, but can also be performed elsewhere. In that case, some tests may be unnecessary or need to be changed slightly.

Each test will be performed at least two times, for as long as the wave pattern allows it. Tests will be performed with both the ballasting system switched on and off. There are several tests that should be performed before the actual model tests. These consist of validation of the measurement systems and the model itself.

C.1 Calibration tests
The following components need to be tested beforehand to verify the correctness of them:

- Model
- Waves
- Wave probe
- Motion tracking sensors
- 9DOF motion sensor
- Mooring lines

Per component, the validation tests will be explained. Not all need to be performed in the water, but needless to say it is preferable.

C.1.1 Model
As described in Chapter 4, quite some parameters need to be set to cause the behaviour of the model to be similar to the unscaled vessel. These parameters are the location of the COG and the radii of inertia. The description as how to set these parameters is given in Chapter 4, and thus will not be repeated here.

C.1.2 Waves
During the first test period of this research, the conclusion was drawn that the settings of the wave maker did not produce the same waves as the settings. The frequency of the wave maker equals the frequency of the waves, but the amplitude not. Therefore, for the fill height at that time, per wave frequency (in Hz) was tested with multiple amplitudes for the wave maker. The wave probe measured the average wave height over 6 waves (after the measurement was started), and from this the relation between the amplitude of the wave maker and the wave amplitude was derived. At that time, the tank was filled up to 69 cm. For this depth, the relations in Figure C. and Table C. hold. As the RMS values of the relations all are approximately 1, these relations hold very well.

It is recommended to redo these validation tests, especially if the water depth in the tank is slightly different from the initial 69 centimetres. Based on the established relations the final settings for the tests can be determined. Furthermore, the frequencies that are proposed during the next model tests differ from those used during the previous set of tests.

To create new relations between the wave maker amplitude and the resulting wave amplitude, new tests must be performed. These are listed in Table C.. Based on the measured wave amplitudes, the relations as shown in Table C. and Figure C. can be obtained.

C.1.3 Wave probe
There are two wave probes available at the Aqualab. These all are connected to a computer, which can read and convert the measured voltage data to readable values. The wave probes, if possible both, are placed in the tank at known locations (with respect to the model). The wave probe is put at a certain height, and the voltage that is read from the probe is set to be 'zero' for this value. Now the probe can be lowered (or raised) by 5 centimetres, which again is read by the computer. If the computer reads out the same value that the probe is lowered or raised, the measurement device is set correctly. Otherwise, a small change must be made in the program, to correct the offset again.
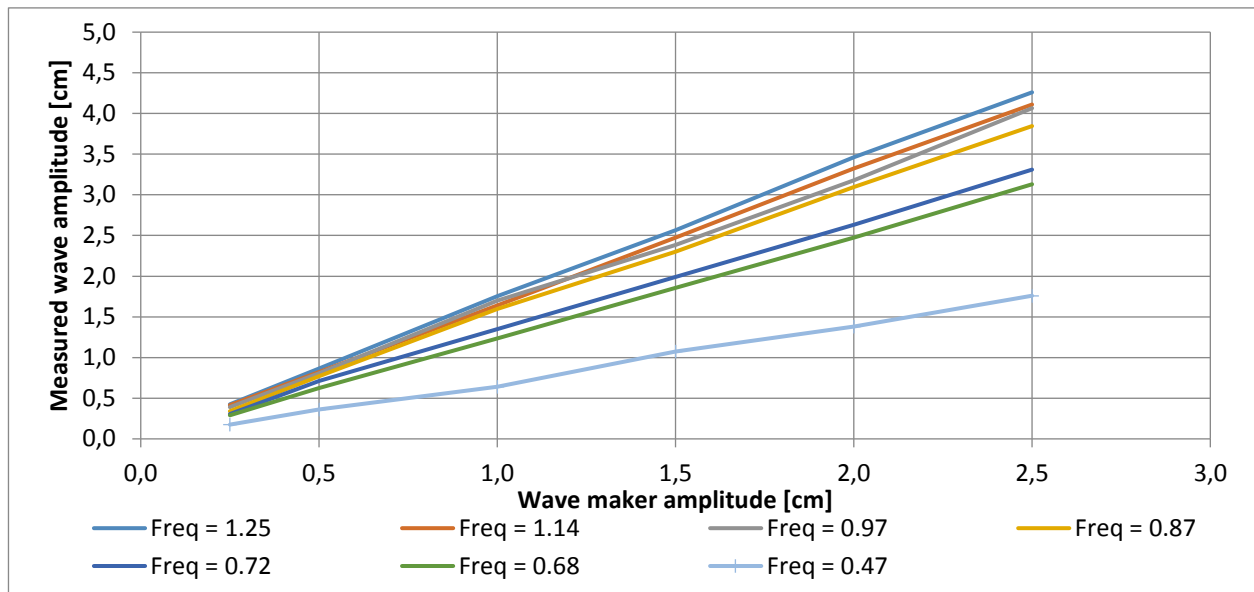
Figure C.1 Relation between the wave maker -, and the wave amplitude

Scaled wave		Linear relation	
Hz	**m**	**Equation**	**RMS**
1.25	**1.00**	$\zeta_a = 1.7078 \cdot \zeta_{WM} + 0.0157$	0.9997
1.14	**1.20**	$\zeta_a = 1.6510 \cdot \zeta_{WM} - 0.0017$	0.9999
0.97	**1.65**	$\zeta_a = 1.6101 \cdot \zeta_{WM} + 0.0077$	0.9988
0.87	**2.00**	$\zeta_a = 1.5488 \cdot \zeta_{WM} - 0.0097$	0.9994
0.72	**2.75**	$\zeta_a = 1.3160 \cdot \zeta_{WM} + 0.0160$	0.9995
0.68	**3.00**	$\zeta_a = 1.2532 \cdot \zeta_{WM} - 0.0170$	0.9999
0.47	**5.00**	$\zeta_a = 0.7033 \cdot \zeta_{WM} - 0.0102$	0.9976

Table C.1 Linear equations and RMS of the relation between the wave maker- and wave amplitude

Test no.	Wave maker frequency [Hz]	Wave maker amplitude [cm]
101	0.159	0.25
102		0.50
103		1.00
104		1.50
105		2.50
106	0.318	0.25
107		0.50
108		1.00
109		1.50
110		2.50
111	0.477	0.25
112		0.50
113		1.00
114		1.50
115		2.50
116	0.637	0.25
117		0.50
118		1.00
119		1.50
120		2.50

Table C.2 Test scenarios to obtain the relations between the wave maker -, and the wave amplitude

C.1.4 Motion tracking sensors

The motion tracker sensors consist of infrared LEDs attached to the model, and infrared sensors (Wiimotes) at a distance from the model. To calibrate the sensors correctly, it is required to measure the distance between the sensors and the LEDs, and do calibration measurements. These are listed in Table C.3. With the measured data, the sensors can be calibrated properly.

Test no.	Description of test
001	Take measurements for 1 minute while the model remains in position
002	Take measurements for 1 minute while the model is moved 10 cm forward, the sensors kept in position
003	Take measurements for 1 minute while the model is moved 10 cm aft, the sensors kept in position
004	Take measurements for 1 minute while the model is moved 10 cm to starboard, the sensors kept in position
005	Take measurements for 1 minute while the model is moved 10 cm to portside, the sensors kept in position
006	Take measurements for 1 minute while the model is brought in 5 degrees positive roll, the sensors kept in position
007	Take measurements for 1 minute while the model is brought in 5 degrees negative roll, the sensors kept in position
009	Take measurements for 1 minute while the model is brought in 10 degrees positive yaw, the sensors kept in position
010	Take measurements for 1 minute while the model is brought in 10 degrees negative yaw, the sensors kept in position

Table C.3 Test descriptions for the calibration of the motion trackers and 9DOF sensor

C.1.5 9DOF motion sensor

The calibration tests as mentioned in Table C.3 can also be used for the calibration of the 9DOF sensor.

C.1.6 Mooring lines

The mooring lines are elastic lines with a known spring coefficient. These mooring lines of course have an influence on the motions of the model. The most important thing about the mooring lines, is that they keep the model straight into the waves, thus the mooring points at the bottom must be very precisely located.

C.2 Model tests

Based on calculations done with the Simulink model, several tests cases have been determined to be part of the test programme. Variation is brought in wave amplitude, wave frequency and wave heading. The full programme is listed in Table C.4 to Table C.7. The table lists the unscaled values. The tests are only performed in regular waves, at zero speed. The basin is able to do tests with a JONSWAP spectrum, but there is far too little known of the settings of the wave maker and the resulting wave spectrum to accurately perform tests with this. The scaled wave maker frequencies are listed in Table C.8.

Test no.	Wave conditions			Remarks
	ζ	ω		μ	
	[m]	[rad/s]	[s]	[°]	
201	0,5	0,1	62,8	180	[1]
202	0,5	0,2	31,4		[2]
203	0,5	0,3	20,9		
204	0,5	0,4	15,7		
205	1	0,1	62,8		[1]
206	1	0,2	31,4		[2]
207	1	0,3	20,9		
208	1	0,4	15,7		
209	1,5	0,1	62,8		[1]
210	1,5	0,2	31,4		[2]
211	1,5	0,3	20,9		
212	1,5	0,4	15,7		
213	2,5	0,1	62,8		[1]
214	2,5	0,2	31,4		[2]

Test no.	ζ [m]	ω [rad/s]	[s]	μ [°]	Remarks
215	0,5	0,1	62,8	135	[1]
216	0,5	0,2	31,4		[2]
217	0,5	0,3	20,9		
218	0,5	0,4	15,7		
219	1	0,1	62,8		[1]
220	1	0,2	31,4		[2]
221	1	0,3	20,9		
222	1	0,4	15,7		
223	1,5	0,1	62,8		[1]
224	1,5	0,2	31,4		[2]
225	1,5	0,3	20,9		
226	0,5	0,1	62,8	90	[1]
227	0,5	0,2	31,4		[2]
228	0,5	0,3	20,9		
229	0,5	0,4	15,7		
230	1	0,1	62,8		[1]
231	1	0,2	31,4		[2]
232	1	0,3	20,9		
233	1	0,4	15,7		
234	1,5	0,1	62,8		[1]
235	1,5	0,2	31,4		[2]

Table C.4 Tests without the ballast system activated

Test no.	Wave conditions				Remarks
	ζ	ω		μ	
	[m]	[rad/s]	[s]	[°]	
301	1	0,3	20,9	180	
302	1	0,4	15,7		
305	1,5	0,1	62,8		[1]
306	1,5	0,2	31,4		[2]
307	1,5	0,3	20,9		
308	1,5	0,4	15,7		
309	2,5	0,1	62,8		[1]
310	2,5	0,2	31,4		[2]
311	0,5	0,4	15,7	135	
312	1	0,1	62,8		[1]
313	1	0,2	31,4		[2]
314	1	0,3	20,9		
315	1	0,4	15,7		
316	1,5	0,3	20,9		
317	0,5	0,3	20,9	90	
318	0,5	0,4	15,7		
319	1	0,2	31,4		[2]
320	1	0,3	20,9		
321	1	0,4	15,7		depends on roll amplitude w/o ballast

Table C.5 Tests with a ballast system at unscaled velocity of 1 m/s

Test no.	Wave conditions			Remarks
	ζ	ω		μ	
	[m]	[rad/s]	[s]	[°]	
401	1	0,3	20,9	180	
402	1	0,4	15,7		
403	1,5	0,1	62,8		[1]
404	1,5	0,2	31,4		[2]
405	1,5	0,3	20,9		
406	1,5	0,4	15,7		
407	2,5	0,1	62,8		[1]
408	2,5	0,2	31,4		[2]
409	2,5	0,3	20,9		
410	1	0,2	31,4	135	[1]
411	1	0,4	15,7		[2]
412	1,5	0,1	62,8		
413	1,5	0,2	31,4		[1]
414	1,5	0,3	20,9		[2]
415	0,5	0,4	15,7	90	
416	1	0,4	15,7		
417	1,5	0,1	62,8		[1]
418	1,5	0,3	20,9		

Table C.6 Tests with a ballast system at unscaled velocity of 2 m/s

Test no.	Wave conditions			Remarks
	ζ	ω		μ	
	[m]	[rad/s]	[s]	[°]	
501	1,5	0,3	20,9	180	
502	1,5	0,4	15,7		
503	2,5	0,2	31,4		[2]
504	2,5	0,3	20,9		
505	2,5	0,4	15,7		Depends on the motions in test 502
506	1	0,2	31,4	135	[2]
507	1	0,4	15,7		
508	1,5	0,2	31,4		[2]
509	1,5	0,3	20,9		
510	0,5	0,4	15,7	90	
511	1	0,4	15,7		Depends on the motions in test 510
512	1,5	0,2	31,4		[2]
513	1,5	0,3	20,9		

Table C.7 Tests with a ballast system at unscaled velocity of 3 m/s

[1] Wave with a length of approximately 16 m, possibly not possible in the Aqualab due to reflection
[2] Wave with a length of approximately 8 m, possibly not possible in the Aqualab due to reflection

ω (unscaled) [rad/s]	ω (scaled) [rad/s]	f_{WM} [Hz]	λ (scaled) [m]
0.1	1.0	0.159	16.1
0.2	2.0	0.318	7.8
0.3	3.0	0.477	4.9
0.4	4.0	0.637	3.3

Table C.8 Unscaled and scaled wave frequencies, and corresponding wave maker frequency

Appendix D
JONSWAP simulation results

The JONSWAP simulations were performed for five significant wave heights: 0.5, 1.0, 1.5, 2.0 and 2.5 m. Each was processed to obtain the significant heave amplitude with and without one of four ballast systems activated. This was done for peak periods of 16, 17, 18 and 19s, and eight wave headings. The following sub paragraphs give the plotted results per significant wave heights, as well as the tables containing the decrease in significant heave amplitude.

D.1 JONSWAP results for H_s = 0.5 m

Significant heave amplitude of the crane tip for H_s = 0.5 m
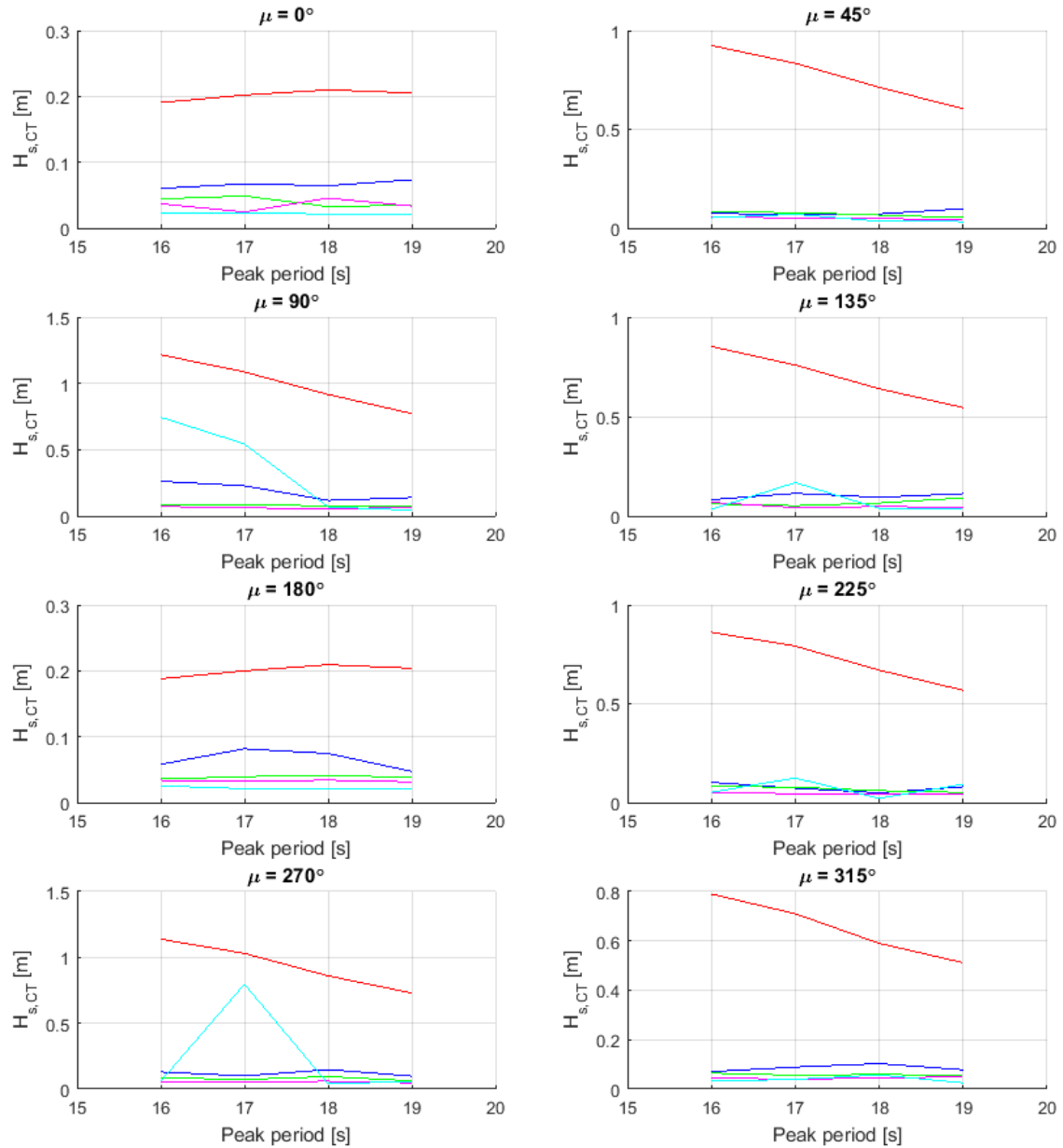
Figure D.1 Significant heave amplitudes for H_s = 0.5m

μ	S1	S2	T1	T2
0°	-68.4%	-76.7%	-80.7%	-88.3%
45°	-91.8%	-91.4%	-93.6%	-94.3%
90°	-78.5%	-93.2%	-94.1%	-38.7%
135°	-90.4%	-92.9%	-92.0%	-96.0%
180°	-69.1%	-81.0%	-82.0%	-86.6%
225°	-88.2%	-90.5%	-94.0%	-93.9%
270°	-88.6%	-92.4%	-95.4%	-94.7%
315°	-91.1%	-91.8%	-94.3%	-96.0%

Table D.1 Decrease in significant crane tip heave amplitude for T_p = 16 s, for H_s = 0.5m

μ	S1	S2	T1	T2
0°	-66.7%	-75.8%	-87.9%	-88.6%
45°	-91.9%	-90.5%	-94.1%	-91.6%
90°	-79.0%	-91.9%	-94.4%	-50.0%
135°	-85.0%	-93.1%	-94.4%	-77.8%
180°	-59.2%	-80.3%	-83.7%	-89.5%
225°	-90.8%	-90.2%	-94.4%	-84.4%
270°	-90.3%	-92.9%	-94.4%	-22.7%
315°	-87.4%	-92.1%	-94.4%	-94.4%

Table D.2 Decrease in significant crane tip heave amplitude for T_p = 17 s, for H_s = 0.5m

μ	S1	S2	T1	T2
0°	-69.3%	-84.5%	-78.3%	-89.8%
45°	-89.9%	-90.7%	-93.4%	-95.1%
90°	-87.2%	-91.9%	-94.0%	-92.6%
135°	-85.3%	-89.8%	-92.6%	-94.0%
180°	-64.4%	-80.1%	-83.7%	-89.6%
225°	-92.6%	-91.0%	-93.5%	-96.9%
270°	-82.8%	-89.0%	-93.0%	-95.3%
315°	-82.5%	-89.9%	-92.3%	-90.3%

Table D.3 Decrease in significant crane tip heave amplitude for T_p = 18 s, for H_s = 0.5m

μ	S1	S2	T1	T2
0°	-64,2%	-83,0%	-83,6%	-89,4%
45°	-83,7%	-91,2%	-92,7%	-94,5%
90°	-82,0%	-91,0%	-91,7%	-94,4%
135°	-79,4%	-83,3%	-91,9%	-93,4%
180°	-76,8%	-81,4%	-84,6%	-89,5%
225°	-86,0%	-91,0%	-93,0%	-83,8%
270°	-86,4%	-91,3%	-93,4%	-91,9%
315°	-84,7%	-89,2%	-90,3%	-95,0%

Table D.4 Decrease in significant crane tip heave amplitude for T_p = 19 s, for H_s = 0.5m

D.2 JONSWAP results for H_s = 1.0 m

Significant heave amplitude of the crane tip for H_s = 1 m

Figure D.2 Significant heave amplitudes for H_s = 1.0m
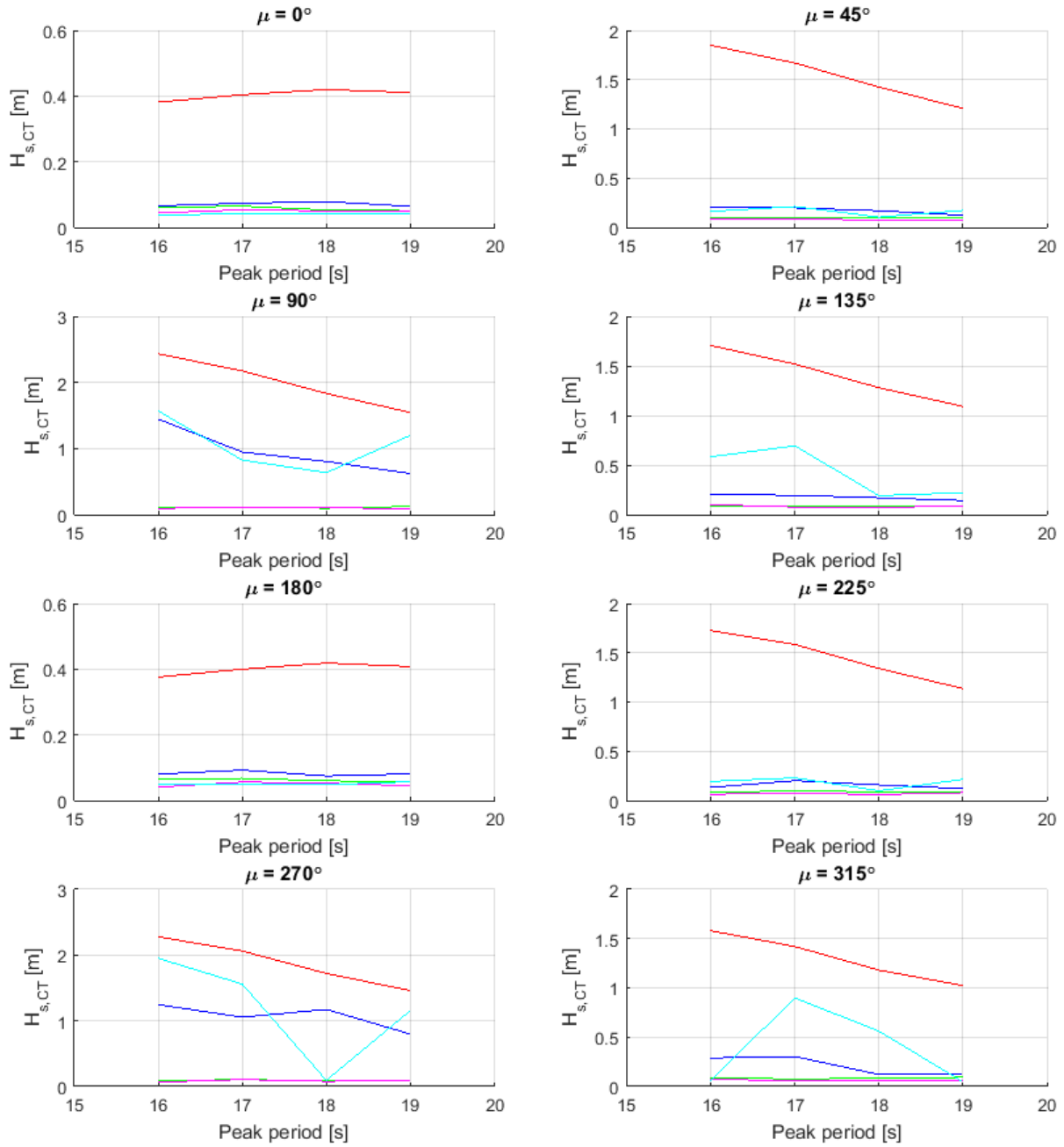
μ	S1	S2	T1	T2
0°	-82.7%	-84.1%	-88.4%	-89.8%
45°	-89.0%	-94.4%	-95.5%	-91.2%
90°	-40.6%	-95.1%	-96.1%	-35.5%
135°	-88.2%	-94.9%	-94.0%	-65.7%
180°	-78.5%	-82.4%	-89.2%	-86.9%
225°	-92.2%	-95.2%	-96.3%	-88.7%
270°	-45.3%	-96.2%	-97.1%	-14.4%
315°	-81.7%	-94.5%	-95.3%	-96.0%

Table D.5 Decrease in significant crane tip heave amplitude for T_p = 16 s, for H_s = 1.0m

μ	S1	S2	T1	T2
0°	-81.8%	-83.9%	-86.6%	-90.0%
45°	-88.1%	-94.4%	-95.2%	-87.3%
90°	-56.4%	-94.9%	-94.6%	-62.0%
135°	-87.1%	-94.2%	-94.9%	-54.3%
180°	-76.8%	-83.1%	-85.9%	-87.3%
225°	-87.3%	-93.7%	-95.3%	-85.5%
270°	-48.9%	-94.9%	-94.9%	-24.4%
315°	-78.6%	-94.6%	-96.1%	-36.8%

Table D.6 Decrease in significant crane tip heave amplitude for T_p = 17 s, for H_s = 1.0m

μ	S1	S2	T1	T2
0°	-81.2%	-87.3%	-88.0%	-90.1%
45°	-88.1%	-93.3%	-94.5%	-92.6%
90°	-56.1%	-94.7%	-94.3%	-65.3%
135°	-86.7%	-92.9%	-94.3%	-85.0%
180°	-82.1%	-85.6%	-87.4%	-88.5%
225°	-88.1%	-93.4%	-95.4%	-92.5%
270°	-31.8%	-95.1%	-95.5%	-94.6%
315°	-89.8%	-93.0%	-94.5%	-52.4%

Table D.7 Decrease in significant crane tip heave amplitude for T_p = 18 s, for H_s = 1.0m

μ	S1	S2	T1	T2
0°	-84.3%	-87.5%	-88.1%	-90.3%
45°	-89.7%	-91.3%	-93.9%	-85.6%
90°	-59.7%	-91.9%	-94.1%	-22.3%
135°	-86.9%	-92.6%	-91.9%	-79.7%
180°	-80.1%	-86.1%	-89.0%	-86.0%
225°	-89.4%	-92.2%	-93.0%	-81.0%
270°	-45.3%	-93.2%	-93.6%	-20.8%
315°	-87.8%	-90.9%	-93.8%	-95.5%

Table D.8 Decrease in significant crane tip heave amplitude for T_p = 19 s, for H_s = 1.0m

D.3 JONSWAP results for H_s = 1.5 m

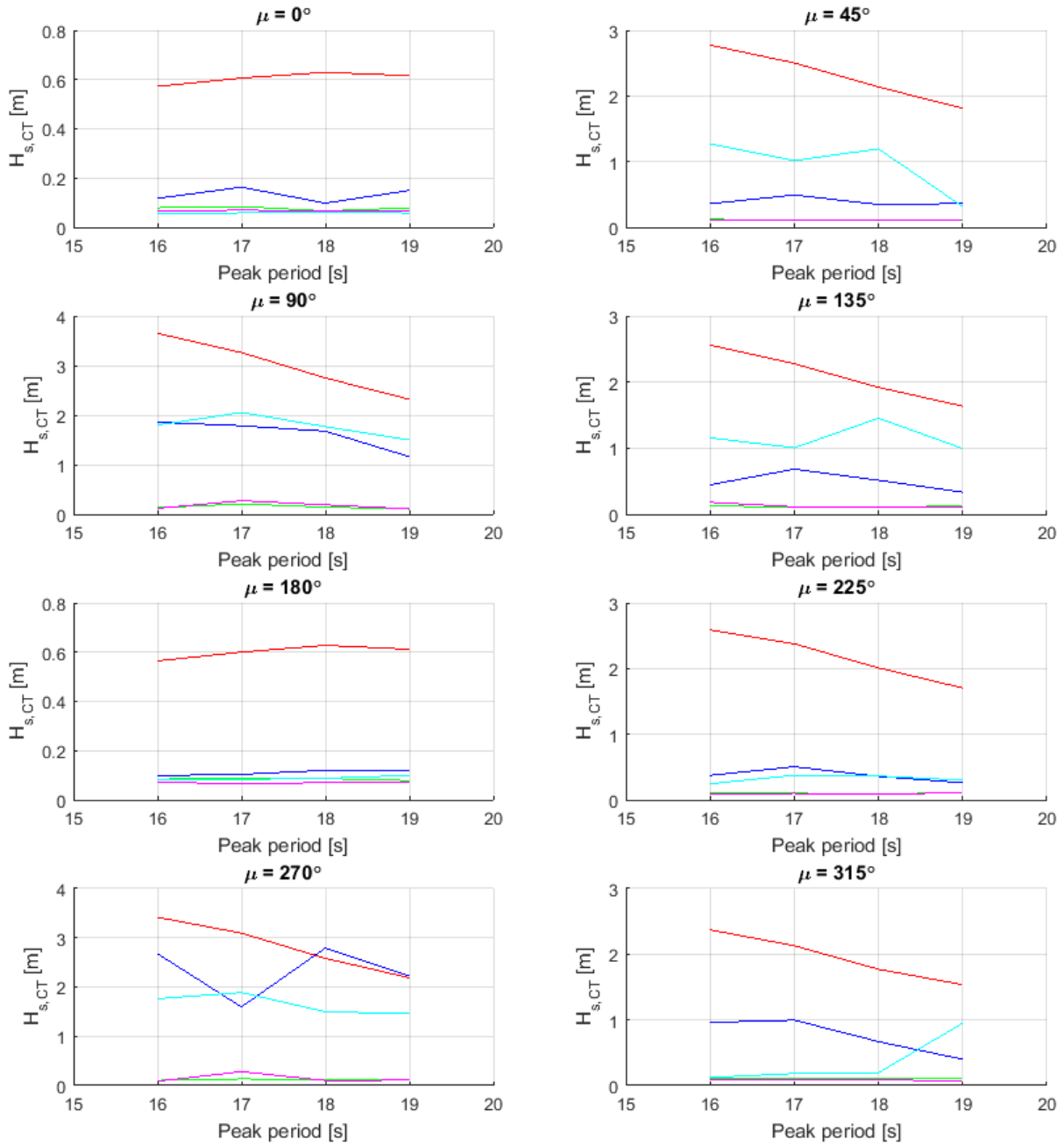

Figure D.3 Significant heave amplitudes for H_s = 1.5m

μ	S1	S2	T1	T2
0°	-79.5%	-86.1%	-88.4%	-90.3%
45°	-87.1%	-95.6%	-95.7%	-54.2%
90°	-49.1%	-96.4%	-96.7%	-50.7%
135°	-82.6%	-95.3%	-92.9%	-54.8%
180°	-82.5%	-85.0%	-87.3%	-85.9%
225°	-85.6%	-95.8%	-96.5%	-90.5%
270°	-21.6%	-96.9%	-97.5%	-48.4%
315°	-59.4%	-95.6%	-96.0%	-94.9%

Table D.9 Decrease in significant crane tip heave amplitude for T_p = 16 s, for H_s = 1.5m

μ	S1	S2	T1	T2
0°	-73.1%	-86.1%	-88.6%	-90.4%
45°	-80.4%	-95.8%	-95.5%	-59.5%
90°	-45.3%	-93.7%	-91.6%	-37.1%
135°	-70.0%	-95.0%	-95.0%	-55.8%
180°	-82.7%	-85.6%	-89.1%	-86.2%
225°	-78.8%	-95.7%	-95.8%	-84.2%
270°	-48.4%	-95.7%	-90.9%	-39.0%
315°	-53.2%	-94.7%	-95.7%	-91.4%

Table D.10 Decrease in significant crane tip heave amplitude for T_p = 17 s, for H_s = 1.5m

μ	S1	S2	T1	T2
0°	-84.4%	-89.5%	-89.4%	-90.5%
45°	-83.8%	-95.1%	-94.8%	-44.1%
90°	-39.1%	-94.8%	-93.1%	-35.7%
135°	-73.2%	-94.3%	-94.0%	-24.3%
180°	-80.9%	-86.2%	-88.8%	-86.0%
225°	-82.2%	-95.6%	-95.9%	-81.9%
270°	8.2%	-95.3%	-96.0%	-42.0%
315°	-62.2%	-94.2%	-95.3%	-89.0%

Table D.11 Decrease in significant crane tip heave amplitude for T_p = 18 s, for H_s = 1.5m

μ	S1	S2	T1	T2
0°	-75.7%	-87.2%	-88.9%	-90.6%
45°	-80.0%	-94.4%	-94.1%	-82.7%
90°	-49.9%	-95.5%	-95.3%	-35.4%
135°	-79.7%	-92.3%	-93.8%	-39.2%
180°	-80.5%	-87.1%	-88.4%	-83.8%
225°	-84.7%	-93.4%	-93.4%	-82.4%
270°	1.5%	-94.7%	-95.1%	-33.3%
315°	-74.0%	-92.7%	-95.2%	-38.1%

Table D.12 Decrease in significant crane tip heave amplitude for T_p = 19 s, for H_s = 1.5m

D.4 JONSWAP results for H_s = 2.0 m
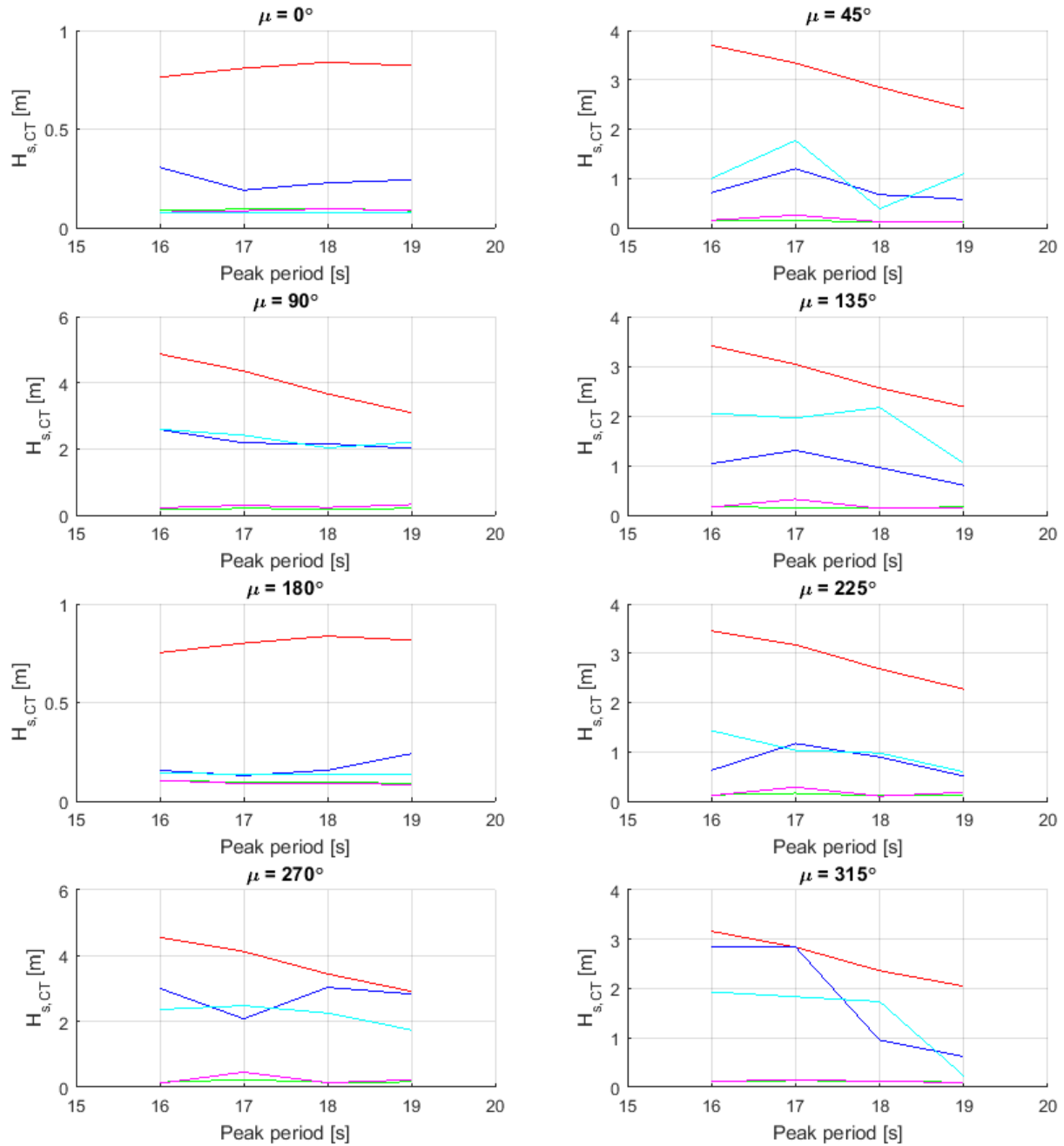

Figure D.4 Significant heave amplitudes for H_s = 2.0m

μ	S1	S2	T1	T2
0°	-59.9%	-88.1%	-89.7%	-90.3%
45°	-80.8%	-96.0%	-95.9%	-73.0%
90°	-46.9%	-96.6%	-95.5%	-46.8%
135°	-69.6%	-95.2%	-95.3%	-39.9%
180°	-79.3%	-86.1%	-86.0%	-80.6%
225°	-81.9%	-96.3%	-96.7%	-58.6%
270°	-34.1%	-96.7%	-97.4%	-48.1%
315°	-9.9%	-96.0%	-96.1%	-38.9%

Table D.13 Decrease in significant crane tip heave amplitude for T_p = 16 s, for H_s = 2.0m

μ	S1	S2	T1	T2
0°	-76.4%	-88.5%	-89.4%	-90.5%
45°	-64.1%	-95.7%	-92.3%	-47.0%
90°	-50.0%	-95.3%	-93.2%	-44.5%
135°	-57.1%	-95.0%	-89.5%	-35.6%
180°	-83.8%	-88.1%	-88.9%	-83.3%
225°	-63.1%	-95.0%	-91.0%	-67.4%
270°	-49.5%	-94.5%	-88.9%	-39.9%
315°	-0.10%	-95.3%	-95.0%	-35.5%

Table D.14 Decrease in significant crane tip heave amplitude for T_p = 17 s, for H_s = 2.0m

μ	S1	S2	T1	T2
0°	-72.9%	-88.2%	-88.6%	-90.6%
45°	-76.4%	-95.9%	-95.7%	-86.5%
90°	-41.3%	-94.9%	-93.7%	-44.5%
135°	-62.6%	-94.5%	-94.8%	-15.4%
180°	-81.3%	-88.6%	-89.0%	-83.9%
225°	-66.7%	-96.0%	-96.2%	-63.6%
270°	-11.9%	-95.6%	-96.0%	-34.6%
315°	-59.7%	-94.5%	-94.7%	-26.5%

Table D.15 Decrease in significant crane tip heave amplitude for T_p = 18 s, for H_s = 2.0m

μ	S1	S2	T1	T2
0°	-70.4%	-89.6%	-89.1%	-90.7%
45°	-76.2%	-94.5%	-95.1%	-54.9%
90°	-34.9%	-93.5%	-89.7%	-28.8%
135°	-72.4%	-92.4%	-93.2%	-52.4%
180°	-70.6%	-88.9%	-89.8%	-83.1%
225°	-77.6%	-94.9%	-92.2%	-73.9%
270°	-2.8%	-94.5%	-92.3%	-40.2%
315°	-69.6%	-95.2%	-95.7%	-88.7%

Table D.16 Decrease in significant crane tip heave amplitude for T_p = 19 s, for H_s = 2.0m

D.5 JONSWAP results for H_s = 2.5 m

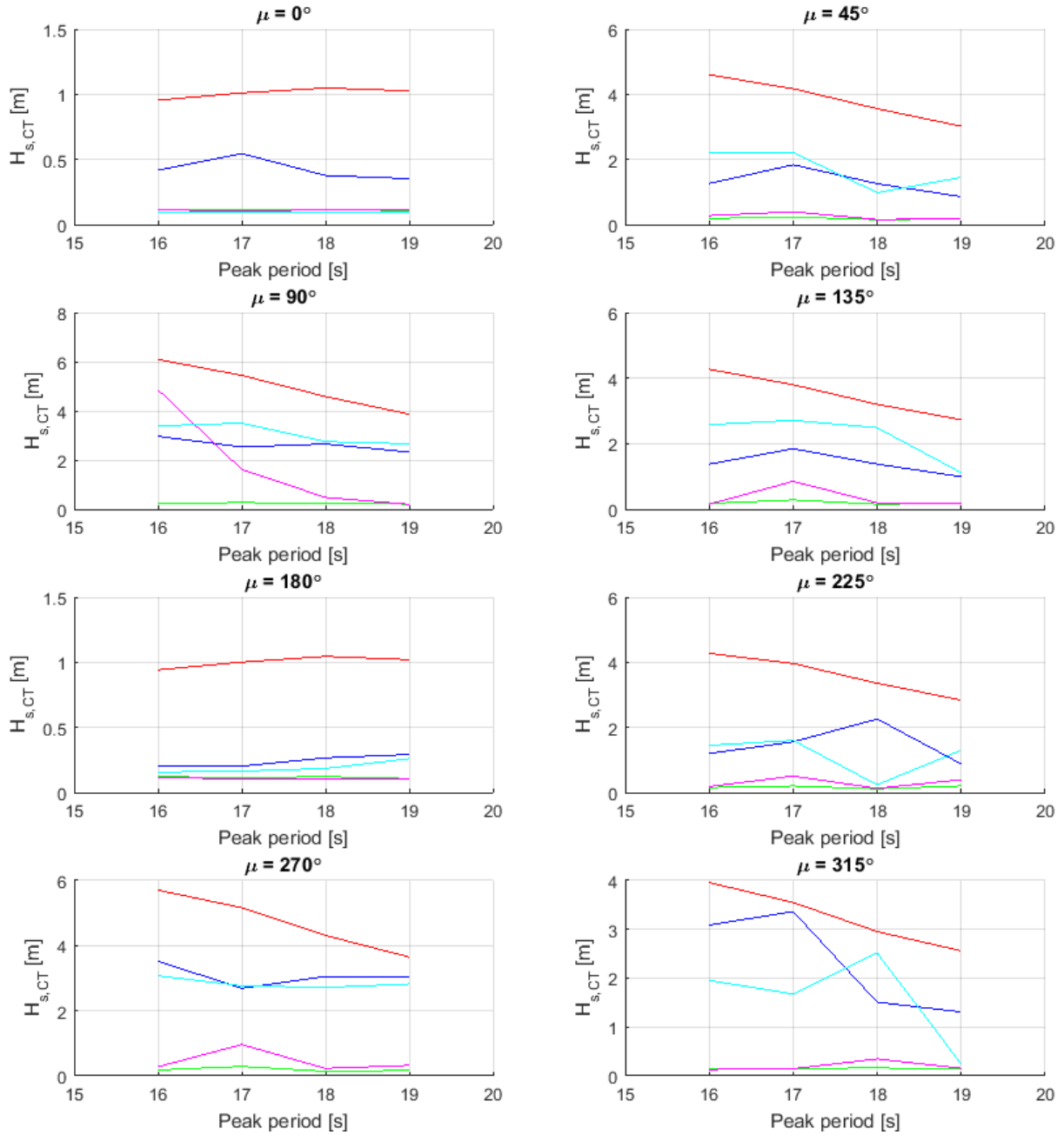

Figure D.5 Significant heave amplitudes for H_s = 2.5m

μ	S1	S2	T1	T2
0°	-56.3%	-88.4%	-88.3%	-90.6%
45°	-72.6%	-95.9%	-94.0%	-52.3%
90°	-51.3%	-96.3%	-20.2%	-44.3%
135°	-67.8%	-95.8%	-96.4%	-39.6%
180°	-78.8%	-87.0%	-87.7%	-83.3%
225°	-72.0%	-96.4%	-95.7%	-66.1%
270°	-38.2%	-96.8%	-95.1%	-46.1%
315°	-22.0%	-96.4%	-96.7%	-50.6%

Table D.17 Decrease in significant crane tip heave amplitude for T_p = 16 s, for H_s = 2.5m

μ	S1	S2	T1	T2
0°	-46.1%	-88.9%	-89.6%	-90.7%
45°	-56.0%	-94.5%	-90.6%	-46.9%
90°	-53.5%	-95.0%	-70.3%	-35.7%
135°	-51.4%	-92.6%	-77.6%	-28.6%
180°	-79.8%	-88.6%	-89.7%	-83.6%
225°	-60.7%	-94.9%	-87.2%	-59.6%
270°	-47.9%	-94.4%	-81.4%	-46.4%
315°	-5.2%	-95.7%	-95.8%	-52.8%

Table D.18 Decrease in significant crane tip heave amplitude for T_p = 17 s, for H_s = 2.5m

μ	S1	S2	T1	T2
0°	-64.1%	-89.1%	-89.3%	-90.7%
45°	-64.7%	-95.8%	-95.7%	-72.5%
90°	-42.1%	-95.0%	-89.6%	-40.0%
135°	-57.0%	-95.2%	-93.9%	-22.3%
180°	-74.6%	-88.3%	-89.7%	-82.3%
225°	-32.7%	-96.7%	-96.2%	-92.9%
270°	-29.2%	-96.8%	-94.7%	-37.0%
315°	-48.9%	-94.5%	-88.2%	-14.8%

Table D.19 Decrease in significant crane tip heave amplitude for T_p = 18 s, for H_s = 2.5m

μ	S1	S2	T1	T2
0°	-65.6%	-89.6%	-89.2%	-90.8%
45°	-71.7%	-94.3%	-94.1%	-52.0%
90°	-39.9%	-94.6%	-94.9%	-31.1%
135°	-63.7%	-93.7%	-92.8%	-59.2%
180°	-71.3%	-89.5%	-89.7%	-74.5%
225°	-69.1%	-92.8%	-86.1%	-54.3%
270°	-16.6%	-95.4%	-91.2%	-22.7%
315°	-48.9%	-94.6%	-93.9%	-90.7%

Table D.20 Decrease in significant crane tip heave amplitude for T_p = 19 s, for H_s = 2.5m